

***SCARF2* and *SNAP29*: Candidate Genes Implicated in the Generation of  
Phenotypic Variability in 22q11.2 Deletion Syndrome**

**Vafa Keser**

Department of Human Genetics  
McGill University, Montreal, Quebec, Canada

December, 2018

A thesis submitted to McGill University in partial fulfillment of the requirements of the degree  
of Doctor of Philosophy

© Vafa Keser 2018

## **DEDICATION**

**To my lovely grandmother Mahiye Salimova who always stood by me**

## **ABSTRACT**

22q11.2 deletion syndrome (22q11.2DS) is the most common contiguous gene syndrome and is characterized by a 3 Mb *de novo* deletion of the chromosome 22q11.2 region in 90% of individuals. Patients are born with a number of congenital birth defects and malformations in various combinations that are different even within the same family where members carry the same deletion. The most common phenotypes seen in patients are facial dysmorphism (>90%), learning disability/mental retardation/developmental delay (90%), motor and/or speech delays (>90%), cardiovascular (50%-75%), palatal and related (75%), hypocalcemia and/or hypoparathyroidism (>60%), psychiatric disorders (60%) and recurrent infections (35%-40%). Additional findings, such as skin conditions, gastrointestinal or renal anomalies, various skeletal abnormalities, ophthalmological findings have also been shown.

The common 3 Mb deletion removes approximately 45 functional genes, including a number of developmentally important genes. Two such genes that contribute to the congenital abnormalities are *SCARF2* and *SNAP29*, which are known to be associated with congenital malformations in human patients without 22q11.2DS. Moreover, unmasking of rare variants in the non-deleted chromosome is associated with the phenotypic spectrum found in subset of the patients with 22q11.2DS. Studies in our and other laboratories showed that 22q11.2 deletion uncovered rare variants in *SCARF2* and *SNAP29* that resulted in manifestations of the recessive disorders Van den Ende-Gupta syndrome (VDEGS) and cerebral dysgenesis, neuropathy, ichthyosis, and keratoderma (CEDNIK), respectively, in 22q11.2DS patients, thus contributing variability in phenotypes in those patients.

Different mouse models have been generated for the 22q11.2DS syntenic region in mouse chromosome 16, however, these only modeled a subset of the abnormalities seen in patients. Importantly, *SCARF2* and *SNAP29* were not included in those models because of the positional change of locations of the genes on the mouse chromosome.

SCARF2 is a member of the scavenger receptor protein family, which are involved in a variety of cellular processes, including pathogen clearance and lipid transport. Although mutations in *SCARF2* are associated with VDEGS, which is characterized by craniofacial and skeletal abnormalities some of which have also found in 22q11.2DS patients, the function of the gene is not clear.

SNAP29 is a member of SNARE family of proteins involved in the maintenance of diverse membrane trafficking pathways. Unfortunately, current mutant mouse lines for *Snap29* only model skin abnormalities of CEDNIK patients. We postulated that deletion of *SNAP29* contributes to the phenotypic spectrum of abnormalities found in a subset of 22q11.2DS patients and aimed to characterize expression of this gene during mouse development and to generate a constitutive knockout mouse model to determine where and when *Snap29* is required for normal development.

In the present study, we describe mRNA expression for *Scarf2* and *Snap29* in different developmental stages in mice. We have generated a novel, constitutive *Snap29* knockout mouse line, and the homozygous *Snap29*<sup>lam1/lam1</sup> (*Snap29*<sup>-/-</sup>) models the craniofacial malformations, skin and motor defects described in CEDNIK and in a subset of patients with 22q11.2DS. Using our *Snap29*<sup>lam1/lam1</sup> mutant mouse line we have uncovered a novel requirement for *Snap29* in male fertility. Unlike previous *Snap29* mouse models, *Snap29*<sup>lam/lam</sup> survived until adulthood,



allowing us to study both neonatal and postnatal phenotypes and to gain insight on the etiology of a subset of abnormalities found in patients with mutations in *SNAP29*.

Our study shows that hemizyosity for *SCARF2* and *SNAP29* might contribute to the phenotypic spectrum of abnormalities found in a subset of 22q11.2DS patients that cannot be explained using previously generated mouse models.

## **RÉSUMÉ**

Le syndrome de délétion 22q11.2 est une maladie congénitale causée par une délétion d'une région de 3Mb du chromosome 22q11.2. Les patients présentent des malformations congénitales variables malgré une délétion commune. Les phénotypes les plus communs retrouvés chez les patients sont les suivants : dimorphisme facial (>90%), retard du développement/ problèmes d'apprentissage/ retard mental (>90%), retard moteur et/ou de langage (>90%), problèmes cardiovasculaires (50-75%), palais anormal (75%), hypocalcémie et/ou hypoparathyroïdisme (>60%), désordres psychiatriques (60%) et infections récurrentes (35-40%). D'autres affections peuvent être présentes mais sont moins communes telles que des problèmes de peau, gastrointestinaux, rénaux, squelettiques et ophtalmologiques.

Cette délétion de 3Mb comprend environ 45 gènes fonctionnels, incluant des gènes importants dans le développement tels que *SCARF2* et *SNAP29*. Il a été démontré que ces deux gènes sont associés aux malformations congénitales chez les patients souffrant du syndrome de délétion 22q11.2. Par ailleurs, des études dans notre laboratoire et d'autres ont démontré que la délétion d'un allèle du chromosome 22q11.2 dévoile des mutations rares de *SCARF2* et *SNAP29*, qui provoquent la manifestation de maladies récessives Van den Ende-Gupta syndrome (VDEGS) et dysgénèse cérébrale, neuropathie, ichtyose, keratoderma (CEDNIK), respectivement. Ceci suggère que ces mutations contribuent à la variabilité phénotypique chez les patients 22q11.2.

Différents modèles animaux ont été générés pour le 22q11.2 qui correspond à une région du chromosome 16 chez la souris, mais ils ne répliquent qu'une partie des anomalies observées chez les patients. De manière importante, aucun des modèles murins existants n'inclue *SCARF2* et *SNAP29*.

*SCARF2* est un membre de la famille de récepteurs scavengers, impliqués dans une multitude de fonctions cellulaires, incluant le transport des lipides et l'enlèvement de pathogènes. Bien qu'il a été rapporté que des mutations dans *SCARF2* sont associées au VDEGS, caractérisé par des anomalies squelettiques et craniofaciales, sa fonction demeure inconnue.

SNAP29 est un membre de la famille de protéines SNARE, impliqué dans la maintenance de différentes voies de transport membranaire. De manière intéressante, les lignées murines connues à ce jour ayant des mutations dans *Snap29* récapitulent seulement les anomalies de la peau observées chez les patients souffrant de CEDNIK. Nous postulons qu'une délétion de *SNAP29* contribue au spectrum d'anomalies phénotypiques observées chez une partie des patients 22q11.2. Notre but est de caractériser l'expression de ce gène au cours du développement embryonnaire chez la souris et de générer un modèle murin muté pour *Snap29*, ce qui nous permettra de déterminer où et quand ce gène est requis au cours du développement normal murin.

Dans ce projet, nous décrivons l'expression génique de *Scarf2* et *Snap29* à différents stades de développement embryonnaire chez la souris. Nous avons généré un nouveau modèle murin avec une délétion de *Snap29*, et nous démontrons que les souris homozygotes (*Snap29*<sup>-/-</sup>) récapitulent les malformations craniofaciales, les anomalies moteurs ainsi que les problèmes de peau décrits chez les patients CEDNIK ainsi que dans un sous-groupe de patients 22q11.2. Grâce à ce nouveau modèle de souris, nous avons décrit un nouveau rôle pour Snap29 dans la fertilité chez les mâles. Contrairement aux modèles murins existants, les souris *Snap29*<sup>-/-</sup> survivent jusqu'à l'âge adulte, nous permettant d'étudier des phénotypes au stade néo-natal et post-natal. De plus, il sera possible d'améliorer notre compréhension de l'étiologie des anomalies phénotypiques observées chez une partie des patients portant des mutations dans *SNAP29*.

Notre étude démontre que l'hemizygosité pour *SCARF2* et *SNAP29* peut contribuer au spectrum phénotypique des anomalies présentes chez un sous-groupe de patients 22q11.2, chose auparavant impossible avec les modèles murins disponibles

## **TABLE OF CONTENTS**

<b>ABSTRACT.....</b>	<b>3</b>
<b>RÉSUMÉ.....</b>	<b>6</b>
<b>LIST OF ABBREVIATIONS.....</b>	<b>13</b>
<b>LIST OF FIGURES .....</b>	<b>18</b>
<b>LIST OF TABLES .....</b>	<b>21</b>
<b>ACKNOWLEDGMENTS .....</b>	<b>22</b>
<b>THESIS FORMAT.....</b>	<b>25</b>
<b>CONTRIBUTIONS OF AUTHORS.....</b>	<b>26</b>
<b>ORIGINAITY AND SIGNIFICANCE.....</b>	<b>27</b>
<b>CHAPTER 1. INTRODUCTION AND LITERATURE REVIEW.....</b>	<b>28</b>
1.1. 22q11.2 deletion syndrome.....	28
1.1.1. Mechanisms/pathophysiology.....	28
1.1.2. Developmental aspects of 22q11.2DS.....	31
1.1.3. Clinical manifestations.....	32
1.1.3.1. Craniofacial findings associated with 22q11.2 deletion syndrome.....	33
1.1.3.2. Brain abnormalities.....	38
1.1.3.3. Cardiovascular abnormalities.....	38
1.1.3.4. Immunodeficiency.....	38
1.1.3.5. Endocrine abnormalities. ....	39
1.1.3.6. Gastrointestinal abnormalities.....	39
1.1.3.7. Risk of malignancy in 22q11.2DS .....	39
1.1.4. Diagnosis.....	42
1.1.5. Genes within the deletion.....	42

1.1.6. Mouse models for 22q11.2DS.....	52
1.1.7. Screening.....	55
1.1.8. Management.....	55
1.1.9. Normal development of structures affected in 22q11.2DS patients: facial structures, brain, reproductive and motor system.....	56
1.1.9.1. Face development.....	56
1.1.9.2. Eyelid development.....	57
1.1.9.3. Ear development.....	57
1.1.9.4. Brain development.....	57
1.1.9.5. Sensorimotor development.....	62
1.1.9.6. Pre and postnatal motor development.....	62
1.1.9.6.1. Motor regulation.....	63
1.1.9.7. Reproductive system development.....	65
1.1.9.7.1. Development of female reproductive system.....	66
1.1.9.7.2. Development of male reproductive system.....	66
1.2. Overview of intracellular trafficking pathways.....	68
1.3. SNARE proteins and their role in membrane fusion.....	69
1.3.1. SNARE proteins mediate synaptic vesicle fusion .....	74
1.3.2. SNARE proteins are required for autophagy.....	74
1.3.3. SNAREs in development.....	75
1.3.4. Diseases associated with SNARE proteins.....	76
1.4. RATIONAL, OBJECTIVES AND HYPOTHESIS.....	77

<b>CHAPTER 2. MATERIALS AND METHODS .....</b>	<b>79</b>
2.1. Animals.....	79
2.2. Embryo collection.....	79
2.3. Cloning and probe generation.....	79
2.4. In situ hybridization .....	80
2.5. Generation of <i>Snap29</i> knockout mice line using CRISPR/Cas9.....	80
2.6. Genotyping.....	81
2.7. Western Blot.....	81
2.8. Hematoxylin and Eosin Staining.....	82
2.9. Skeletal preparations.....	82
2.10. Body and brain measurements .....	82
2.11. Nissl Staining.....	83
2.12. Immunohistochemistry and histological staining for cortex.....	83
2.13. Brdu and Edu injection.....	84
2.14. BrdU and EdU staining.....	84
2.15. Cell counting.....	84
2.16. Magnetic resonance imaging.....	85
2.18. Grips strength measurement.....	85
2.19. Rotarod.....	86
2.20. CatWalk Automated Quantitative Gait Analysis.....	86
2.21. Testis collection and histology.....	87
2.22. Perfusion.....	87
2.23. Transmission Electron Microscopy.....	87
2.24. Statistical analysis.....	87

## CHAPTER 3. RESULTS ..... 89

3.1. Aim 1. Characterize mRNA expression of <i>Scarf2</i> and <i>Snap29</i> during mouse organogenesis.....	89
3.1.1. <i>Scarf2</i> is broadly expressed during mouse embryogenesis with stronger expression in cartilages of different bones.....	89
3.1.2. <i>Snap29</i> mRNA is ubiquitously expressed during mouse embryogenesis....	95
3.1.3. Aim 1. Summary.....	98
3.2. Aim 2. Generation and characterization of the <i>Snap29</i> mutant mouse line on a mixed genetic background.....	100
3.2.1. Homozygous deletion of exon 2 results in a protein null mutation in <i>Snap29</i> embryos and mice.....	100
3.2.2. Homozygous <i>Snap29</i> knockout mice on a mixed genetic background (CD1/FvB) survive to adulthood.....	102
3.2.3. <i>Snap29</i> homozygous mutants are morphologically distinguishable from their normal littermates.....	104
3.2.4. Epidermal defects are present before the onset of skin abnormalities in <i>Snap29</i> homozygous mutant mice.....	110
3.2.5. Skeletal abnormalities in <i>Snap29</i> knockout mice.....	113
3.2.6. Assessment of craniofacial abnormalities in <i>Snap29</i> mutant mice.....	114
3.2.7. Psychomotor retardation in <i>Snap29</i> heterozygous and homozygous mutant mice.....	115
3.2.7.1. Rotarod and grip strength and assessment.....	117
3.2.7.2. Gait abnormalities in <i>Snap29</i> mutant mice.....	120
3.2.8. Brain malformations in <i>Snap29</i> <sup>lam1/lam1</sup> homozygous mutant mice.....	122
3.2.9. <i>Snap29</i> homozygous mutant male mice are infertile.....	129
3.2.10. Clinical seizures.....	133
3.2.11. Aim 2. Summary.....	133

<b>CHAPTER 4: DISCUSSION .....</b>	<b>151</b>
4.1. General overview.....	134
4.1.1. The possible role of <i>SCARF2</i> in 22q11.2DS.....	135
4.1.2. The possible role of <i>SNAP29</i> in 22q11.2DS.....	137
4.1.3. 22q11.2DS unmasks rare variants in <i>SCARF2</i> and <i>SNAP29</i> .....	143
4.1.4. Haploinsufficiency of <i>TBX1</i> explains some of the major phenotypes found in 22q11.2DS.....	143
4.1.5. Haploinsufficiency for <i>TBX1</i> and one or both of <i>SNAP29</i> and <i>SCARF2</i> might explain phenotypic variability found in 22q11.2DS.....	144
4.2. Contiguous gene syndromes .....	147
4.3. Mouse models in human disease.....	149
<b>CHAPTER 5. CONCLUSIONS AND FUTURE DIRECTIONS.....</b>	<b>151</b>
5.1. Conclusions .....	151
5.2. Future Directions.....	152
5.2.1. Determine whether the <i>Snap29</i> knockout line models brain abnormalities seen in the patients.....	152
5.2.2. Investigating possible causes of motor defect in mutant mice.....	153
5.2.3. Evaluation of possible behavioral abnormalities in <i>Snap29</i> <sup>lam1/lam1</sup> mice.....	153
5.2.4. Examine possible ophthalmological problems in <i>Snap29</i> <sup>lam1/lam1</sup> mice....	154
<b>CHAPTER 6. REFERENCES .....</b>	<b>156</b>
<b>COPYRIGHT PERMISSIONS .....</b>	<b>182</b>



## **LIST OF ABBREVIATIONS**

### **GENES**

<i>CHD7</i>	Chromodomain helicase DNA-binding protein 7
<i>COMT</i>	Catechol-O-methyltransferase
<i>CRKL</i>	V-crk avian sarcoma virus CT10 oncogene homolog-like
<i>CTIP2</i>	Coup-TFI interacting protein 2
<i>DGCR8</i>	DiGeorge Syndrome Critical Region Gene 8
<i>HIRA</i>	Histone cell cycle regulator
<i>PRODH</i>	Proline dehydrogenase (oxidase) 1
<i>RANBP1</i>	RAN binding protein 1
<i>SATB2</i>	Special AT-rich sequence binding protein 2
<i>SCARF2</i>	Scavenger receptor class F, member 2
<i>SMARCB1</i>	SWI/SNF related, matrix associated, actin dependent regulator of chromatin, subfamily b, member 1
<i>SNAP29</i>	Synaptosomal associated protein 29
<i>SRY</i>	Sex-determining Region of the Y chromosome
<i>STX17</i>	Syntaxin 17
<i>TBR1</i>	T-box, brain 1
<i>TBX1</i>	T-box1
<i>TXNRD2</i>	Thioredoxin reductase 2
<i>VAMP8</i>	Vesicle associated membrane protein 8
<i>ZDHHC8</i>	Zinc finger DHHC-type containing 8

## **OTHER ABBREVIATIONS**

22q11.2DS	22q11.2 deletion syndrome
BLAST	basic local alignment search tool
BrdU	bromodeoxyuridine
CAFS	conotruncal anomaly face syndromes
cDNA	complementary DNA
CEDNIK	cerebral dysgenesis, neuropathy, ichthyosis, and keratoderma
CES	cat eye syndrome
CGS	contiguous gene syndrome
CHD	congenital heart defects
CNS	central nervous system
CP	cortical plate
CR	Cajal-Retzius
CSF	sulcal cerebrospinal fluid
CT	corticothalamic
DGS	DiGeorge syndrome
DNA	deoxyribonucleic acid
E	embryonic day
EdU	5-ethynyl-2'-deoxyuridine
EGF	epidermal growth factor
ER	endoplasmic reticulum
ERGIC	ER-Golgi intermediate compartment
FNP	frontonasal prominence

GnRH	gonadotropin-releasing hormone
GW	gestational week
hCG	human chorionic gonadotropin
H&E	hematoxylin and eosin stain
hmz	homozygous
htz	heterozygous
IKMC	International Knockout Mouse Consortium
IZ	intermediate zone
LB	lamellar body
LCR	low copy repeats
LH	luteinizing hormone
miRNA	microRNA
MLPA	multiplex ligation-dependent probe amplification
mm	millimeter
MMS	microdeletion or microduplication syndrome
MZ	marginal zone
NCBI	National Center for Biotechnology Information
NCC	neural crest cells
NPC	neural progenitor cell
NT	not typed
OE	olfactory epithelium
OV	otic vesicle
P	postnatal day
PBST	phosphate-buffered saline with 0.1% Tween 20
PCR	polymerase chain reaction

PP	preplate
PVDF	polyvinylidene fluoride
Q	glutamine
R	arginine
RI-MUHC	Research Institute of McGill University Health Center
RNA	ribonucleic acid
S	second
SC	stratum corneum
SDS-PAGE	sodium dodecyl sulfate polyacrylamide gel electrophoresis
sgRNA	single guide RNA
SMA	supplementary motor area
SNAP	soluble NSF attachment protein
SNARE	Soluble N-ethylmaleimide-sensitive factor Attachment Protein Receptor
SNP	single-nucleotide polymorphism
SP	subplate
SR	scavenger receptors
SV	synaptic vesicles
TC	thalamocortical
TDR	typically deleted region
TGN	trans-Golgi network
t-SNAREs	target SNARE
VCFS	velocardiofacial syndrome
VDEGS	Van den Ende-Gupta syndrome
v-SNARE	vesicle SNARE
VZ	ventricular zone

WB	western blot
WM	white matter layer
WMISH	whole mount <i>in situ</i> hybridization
wt	wild type

## **LIST OF FIGURES**

### **CHAPTER 1**

Figure 1. Genes deleted in the 22q11.2 syndrome.....	29
Figure 2. Models to explain the various rearrangements of 22q11DS.....	30
Figure 3. Typical representation of a patient with VDEGS syndrome.....	46
Figure 4. Congenital malformations associated with CEDNIK syndrome.....	49
Figure 5. Deletion of the 22q11.2DS syntenic region in mouse chromosome 16 only models a subset of abnormalities.....	52
Figure 6. Neuronal birth and cortical layer formation.....	61
Figure 7. Progression from A <sub>s</sub> spermatogonia to spermatids.....	68
Figure 8. Overview of the intercellular trafficking pathway.....	70
Figure 9. Vesicle budding and fusion.....	71
Figure 10. Formation and disassociation of SNARE complex.....	73

### **CHAPTER 3**

Figure 11. WMISH results at E7.5 and E8.5 for <i>Scarf2</i> .....	90
Figure 12. E9.5-E11.5 WMISH results for <i>Scarf2</i> .....	91
Figure 13. Expression of <i>Scarf2</i> mRNA in E10.5 and E12.5.....	92
Figure 14. E13.5 <i>in situ</i> results for <i>Scarf2</i> .....	93
Figure 15. E14.5 WMISH results for <i>Scarf2</i> .....	94
Figure 16. E7.5-E8.5 WMISH results for <i>Snap29</i> .....	96
Figure 17. E9.5 and E10.5 WMISH results for <i>Snap29</i> .....	97
Figure 18. Section <i>in situ</i> results for <i>Snap29</i> .....	98
Figure 19. Alignment of the deletions with the original <i>Snap29</i> cDNA sequence.....	101

Figure 20. Deletion of exon2 results in a protein null mutation in <i>Snap29</i> homozygous embryos and mice.....	102
Figure 21. Average weight by genotype of <i>Snap29</i> knockout mice.....	105
Figure 22. P1 and P3 body measurement analysis.....	106
Figure 23. Homozygous <i>Snap29</i> mice are morphologically differ from their littermates and have thicker epidermis.....	109
Figure 24. Skin malformations in hmz mutant <i>Snap29</i> knockout mouse on a mixed genetic background(CD1/FvB).....	110
Figure 25. H & E staining and TEM in dorsal skin of P1 pups.....	112
Figure 26. Skeletal deformity in hmz mutant <i>Snap29</i> mice.....	114
Figure 27. E17.5 body weight and measurement analysis.....	115
Figure 28. Measurement of psychomotor retardation in <i>Snap29</i> P3 pups.....	116
Figure 29. Assessment of neuromuscular coordination in 5 weeks old mice by Rotarod.....	117
Figure 30. Assessment of muscle strength by Grip strength meter in 7 and 14 weeks old mice.....	119
Figure 31. Gait analysis of <i>Snap29</i> knockout mice.....	121
Figure 32. Representative images of brains from E17.5.....	123
Figure 33. Hematoxylin and Eosin staining of E17.5 brains.....	123
Figure 34. Nissl staining in E17.5 brains.....	124
Figure 35. Analysis of brain size in E17.5, P1 and P3 stages.....	125
Figure 36. MRI of 11 weeks old <i>Snap29</i> mutant mice.....	126
Figure 37. Expression of cortical layer markers in E17.5 brains.....	127
Figure 38. Counting of cortical layer organization markers.....	128
Figure 39. Analysis of BrdU and EdU labeled E17.5 brains.....	129
Figure 40. Histological analysis of <i>Snap29</i> <sup>-/-</sup> testis.....	132

## CHAPTER 4

Figure 41. 22q11.2DS unmask rare variants in <i>SCARF2</i> and <i>SNAP29</i> .....	143
Figure 42. Different size of deletions encompassing <i>TBX1</i> , <i>SCARF2</i> , and <i>SNAP29</i> genes within the 3 Mb region of 22q11.2.....	145
Figure 43. Three possible different mechanisms leading to 22q11.2DS phenotype.....	147



## **LIST OF TABLES**

### **CHAPTER 1**

Table 1. The list of common and rare features associated with 22q11.2DS.....	33
Table 2. Subset of clinical manifestations found in 22q11.2DS patients.....	34
Table 3. Phenotypic abnormalities shared between patients with 22q11.2DS, and patients with mutation in <i>SNAP29</i> and <i>SCARF2</i> .....	41
Table 4. Overlap and differences in subset of malformations found in 22q11.2DS and CEDNIK patients.....	48
Table 5. The list of candidate genes for the neuropsychiatric conditions.....	50

### **CHAPTER 3**

Table 6. Mendelian segregation of the mutant allele; genotype distribution of embryos and offspring.....	103
Table 7. Genotype distribution of embryos and offspring in pre and postnatal periods.....	104
Table 8. Onset of skin abnormalities in <i>Snap29</i> mice and their survival.....	108
Table 9. Fertility assessment for <i>Snap29</i> knockout male mice.....	130
Table 10. Measurement of male reproductive organs.....	131
Table 11. Phenotypic abnormalities shared between patients with a single mutation in <i>TBX1</i> , <i>SNAP29</i> or <i>SCARF2</i> .....	146

## **ACKNOWLEDGMENTS**

First and foremost, I would like to thank the Almighty God who was always with me and has provided me with all the strength I needed to move forward in life.

I offer my sincerest gratitude to my supervisor, Dr. Loydie Jerome-Majewska, for her day to day supervision, advice, and guidance on this research project. Dr. Jerome-Majewska has supported me with her patience and knowledge throughout my PhD studies and has helped me at every step. The experience and independence that I have learned during my PhD in her laboratory is invaluable for my future career and for my personal development.

I would like to express my deepest gratitude for my country, Azerbaijan, for their financial support during my studies.

Additionally, I would like to offer my gratitude to the members of my supervisory committee, Dr. Daniel Duffort and Dr. Nancy Braverman, for their comments, suggestions and understanding. I feel so lucky to have such special supervisors in my PhD and thank them all for giving me only good memories of my overseas education.

In all these years, I feel so lucky to be blessed with only friendly and cheerful people, not only at the university but also in laboratory environment. I would like to give special thank to current and past members of the Majewska laboratory: Dominic Hou, Marie-Claude Beauchamp, Maira Moreno Garcia, Timothée Revil, Samuel Bader and Alessia Field, Sabrina Alam, Apinder Kaur, Wesley Chan, Merve Younussi and Swati Gupta for their helpful suggestions and friendship.

I also would like to give my special acknowledgment to Dr. Aimee Ryan for the academic support, for the analytical and extremely facilitative approach during all of our

interactions, her feedback on my presentations during and outside of lab meetings, and finally for her kindness and support during my education at McGill University.

I would like to give my special gratitude to Mr. Ross Mackay for being so helpful throughout my PhD, without his experience, kindness, and help I would not be able to escape from many troubles.

In addition, I would like to thank everyone in the Department of Human Genetics at McGill University for their kindness and for their friendly attributes

I am also grateful to Emma Brasell for her sincere support and advice during my thesis writing period and Alina Mehdi for supporting my overseas education.

Words fail me when trying to show my greatest appreciation for my husband Sadullah Keser, the love of my life. He deserves special mention for his unconditional patience, support, prayers, love, persistence, and encouragement to achieve my best.

I also owe special thanks to my dearest friend Abeer Al Tuwaijri for being there whenever I needed her, for supporting me in every step during my Master and PhD degrees, for her everlasting love and kindness.

Last but not least, I would like to take this opportunity to express my love and profound gratitude to my beloved mother for giving me life, for educating and providing me with unconditional support to follow my dreams, and to my children, Elina, Emil, and Selina Keser for their ever-lasting smiles, which relieved me whenever I was frustrated. and my sister Aynura for taking care of my kids during my difficult periods.

Lastly, I would like to mention the name of my unforgettable, dearest grandmother

Mahiye Salimova, who encouraged me to be a scientist from my childhood, who presented me to everyone as a scientist from very early childhood. I believe that she is following my achievements and is proud of me in, somewhere around and also in my heart. Thank you so much for being my mother and for the everlasting love you seeded into my heart. This PhD is dedicated to your memory.

## **THESIS FORMAT**

This thesis is in the traditional monograph style, which follows the “Guidelines for Thesis Preparation” of the Faculty of Graduate Studies and Research at McGill University. The thesis consists of four chapters. Chapter one is an introduction and literature review that presents the background material for this thesis and states the hypothesis and aims of my research. Chapter two delineates the materials and methods that were used in my project.

The data in Chapter 3 (results) contains 2 parts: 1) mRNA expression data for 2 genes, *Scarf2* and *Snap29*; and 2) characterization of a novel mouse model harbouring the *lam1* mutation in the *Snap29* gene. Manuscripts for both sections are in preparation. Chapter four comprises a detailed discussion of my findings. Chapter five provides conclusions and possible future directions for the project. References for all chapters are provided in chapter five of the thesis.

## **CONTRIBUTION OF AUTHORS**

### **CHAPTER 3. RESULTS**

**Section 3.1. Aim 1. Characterize mRNA expression of *Scarf2* and *Snap29* during mouse organogenesis.** Vafa Keser performed and analyzed cloning reactions, analyzed and interpreted Sanger sequencing results and designed and generated the mRNA probes. All animal work, dissections, embryo collection, embedding, sectioning and *in situ* experiments were performed by Vafa Keser. Dr. Loydie A. Jerome-Majweska coordinated all aspects of the project.

**3.2. Aim 2. Generation and characterization of the *Snap29* mutant mouse line on a mixed genetic background.** sgRNAs design and synthesis, genotyping, Sanger sequence analysis, colony maintenance, matings, dissections, embryo body, brain, weight measurements, phenotype characterization and fertility assessment were done by Vafa Keser. Microinjections were performed by Dr. Mitra Cohan (McGill University). All skin experiments (collection, H&E, western blot, TEM analysis) were completed by Sabrina Alarm. BrdU and EdU were injected by Dominic Hou. Cortical sections, immunohistochemistry and analyses were done by Dr. Lim Youngshinin in Dr. Jeffrey Alan Golden's laboratory (Harvard Medical School), spermatogenesis was evaluated by Dr. Christian O'Flaherty and Dr. Maria Fernandez (McGill University), Nissl staining was performed by the histopathology core of the MUHC, and MRI was performed at the small animal imaging core of the MUHC. Jeannie Mui aided in TEM experiments (Facility for Electron Microscopy Research (FEMR) - McGill University). Dr. Loydie A. Jerome-Majweska designed the project and oversaw all aspects of the project.

## **ORIGINALITY AND SIGNIFICANCE**

This thesis reports the first comprehensive expression patterns of two developmentally important genes, *Scarf2* and *Snap29*, before and during the onset of mouse organogenesis. The study also describes a novel constitutive knockout mouse line for the *Snap29* gene and the pre- and postnatal phenotypes of homozygous knockout *Snap29* mice (*Snap29<sup>lam1/lam1</sup>*) for the first time (except skin conditions). *Snap29<sup>lam1/lam1</sup>* homozygous mutant mice survived to adulthood, unlike homozygous mutants carrying a similar deletion of exon 2 on the inbred C57BL/6 genetic background (Schiller *et al.*, 2016 and Williams *et al.*, 2016) showing the power of genetic modifiers on the mixed genetic background. Furthermore, this work provides evidence for the possible contribution of *Snap29* mutations to the phenotypic spectrum of abnormalities found in a subset of 22q11.2DS patients. The study also reveals a novel role of *Snap29* in male fertility, which might be associated with the fertility problems seen in 22q11.2DS patients. Additionally, though the skin phenotype described in homozygous mutant *Snap29* mice differs from those of CEDNIK patients, motor dysfunctions present at birth in homozygous *Snap29* mutant mice, may account for motor problems seen in CEDNIK patients. Finally, homozygous mutant *Snap29<sup>lam1/lam1</sup>* mice display craniofacial dysmorphism, which is also found in CEDNIK and 22q11.2 deletion syndrome patients.

## CHAPTER 1. INTRODUCTION AND LITERATURE REVIEW

**1.1. 22q11.2 deletion syndrome.** 22q11.2 deletion syndrome (22q11.2DS) is a contiguous gene syndrome that is characterized by a 1.5 – 3 Mb deletion of the chromosome 22q11.2 region. It is the most common chromosomal microdeletion syndrome, with a prevalence of nearly 1 in 4000 live births (McDonald-McGinn *et al.*, 2015). The inheritance mode appears to be autosomal dominant and 93% of patients carry a *de novo* deletion (McDonald-McGinn *et al.*, 1999). Several genomic conditions that have overlapping phenotypic characteristics have been collected under the term 22q11.2DS, which encompasses DiGeorge, velocardiofacial, and conotruncal anomaly face syndromes (DGS/VCFS/CAFS), and subsets of patients with Opitz G/BBB and Cayler cardiofacial syndromes (Driscoll *et al.*, 1993, Burn *et al.*, 1993, Matsuoka *et al.*, 1994, McDonald-McGinn *et al.*, 1995, Giannotti *et al.*, 1994, McDonald-McGinn *et al.*, 1997).

**1.1.1. Mechanisms/pathophysiology.** Abnormalities of the 22q11.2 region arise as a result of genomic rearrangements which include deletions, duplications, and translocations (Shaikh *et al.*, 2001). These rearrangements are thought to result from the structure of the region, namely, chromosome 22-specific duplications or low copy repeats (LCRs) that are considered to be the highly unstable (Shaikh *et al.*, 2001, Shaikh *et al.*, 2000, Stankiewicz and Lupski, 2002). Indeed, Shaikh *et al.* (2000) discovered 4 LCRs in typically deleted region (TDR) carrying duplicated modules that have 97–98% nucleotide sequence identity with one another. The TDR is approximately 3 Mb long and occurs in 85-90 % of patients (Shaikh *et al.*, 2000, Hacıhamdioğlu *et al.*, 2015). The 4 LCRs are identified using the letters A-D (Figure 1).

Deletions in the TDR result from non-allelic homologous recombination (McDonald-McGinn *et al.*, 2015). Within the 3 Mb region, smaller, proximal, nested deletions occur between



either A–B (approximately 1.5 Mb) or A–C regions (approximately 2 Mb). Deletions between B–D and C–D regions occur rarely (Oskarsdottir *et al.*, 2004) and are less penetrant compared to the typical deletion (McDonald-McGinn *et al.*, 2015).

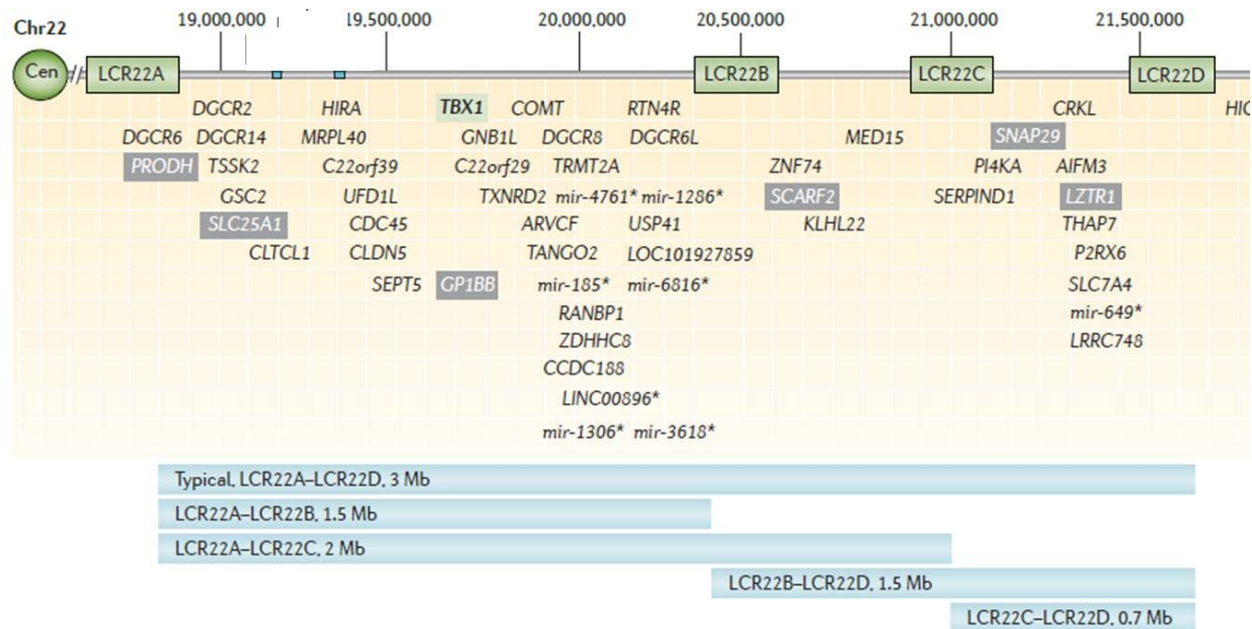


**Figure 1. Genes deleted in the 22q11.2 syndrome.** About 90% of patients have the common 3 Mb deletion that comprises 4-low copy number repeats (LCRs): LCR A, LCR B, LCR C and LCR D in the region. The 3 Mb region includes approximately 45 functional genes including *SNAP29* and *SCARF2*, which have been shown to contribute to developmental syndromes. 8% of patients carry the 1.5 Mb nested deletion. Atypical deletions within B and D or C and D occur rarely (McDonald-McGinn *et al.*, 2015).

Two possible mechanisms have been proposed by Shaikh *et al.* (2000) to explain genomic rearrangements leading to 22q11.2DS: interchromosomal or intrachromosomal misalignments during meiosis or mitosis. In interchromosomal recombination, reciprocal deletion and duplication events may result from crossover between the modules within separated LCRs that occur in the same orientation in the homologous chromosomes. In intrachromosomal recombination, inversely located modules may generate a stem-loop and crossover between LCRs, resulting in deletion of the DNA sequences within the loop (Figure 2; Shaikh *et al.*, 2000).

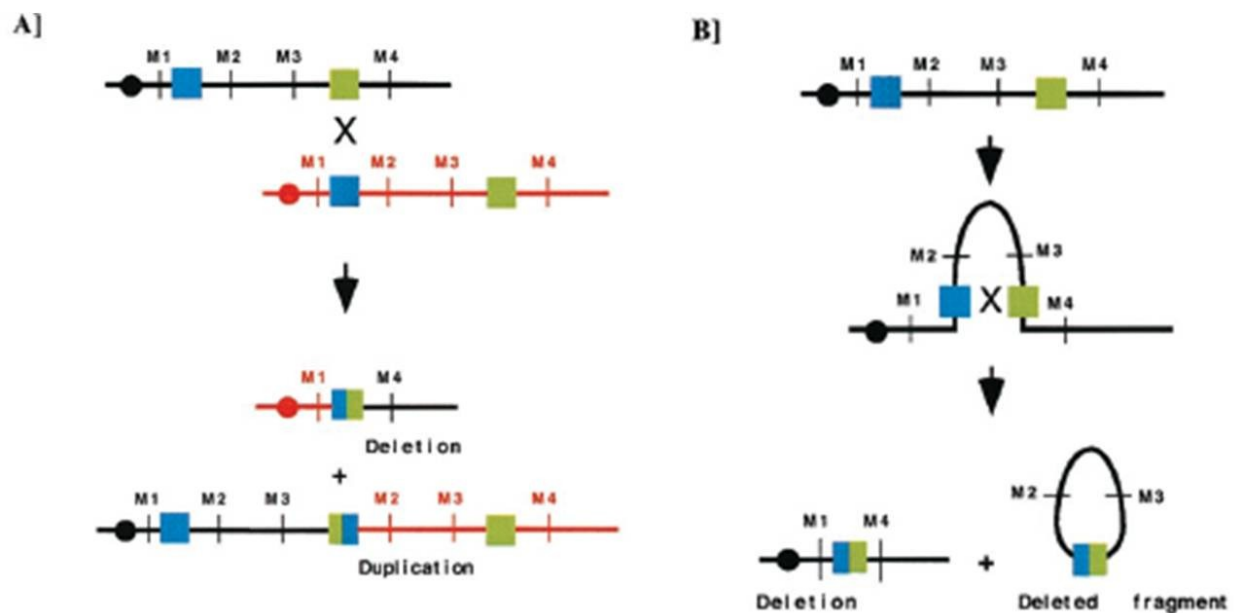


**Figure 2. Models to explain inter- and intra- chromosomal rearrangements of 22q11DS.** A. An interchromosomal misalignment during meiosis I between the two homologs of chromosome 22 leads to reciprocal deletion and duplication. B. An intrachromosomal recombination between LCRs located in the same chromosome form a “stem-loop”, which leads to the deletion of intervening DNA within the loop during mitosis or meiosis. Homologous chromosomes are shown in black and red lines, and LCRs in green and blue boxes. Centromeres are depicted as black and red circles (Shaikh *et al.*, 2001).

Phenotypes of patients carrying the deletion are highly variable suggesting that the deletion is not completely penetrant. Although haplosufficiency for two genes (*TBX1* and *CRKL*) located in the deleted region has been shown to contribute to some developmental malformations, such as cardiac defect, craniofacial, thymus and parathyroid glands malformations (Jerome *et al.*, 2001, Zweier *et al.*, 2007, Racedo *et al.*, 2015), the reasons for variability between phenotypes are not understood. However, the highly variable phenotypes of patients suggest that the combined effect of this multi-gene deletion, gene dosage, recessive variants located in the intact allele, and modifying effects of other genes located elsewhere in the genome might have roles in the mechanism of the syndrome (McDonald-McGinn *et al.*, 2015). It is also known that patients with mutations in *CHD7* (chromodomain helicase DNA-binding protein 7), which causes CHARGE syndrome (Jyonouchi *et al.*, 2009), or in *TBX1* (T-box 1) (Yagi *et al.*, 2003, Zweier *et al.*, 2007) and deletions in genomic regions 10p13–14 (Daw *et al.*, 1996) and 11q23-ter11 phenocopy abnormalities seen in patients with 22q.11.2DS (Grossfeld *et al.*, 2004).

**1.1.2. Developmental aspects of 22q11.2DS.** Most of the common congenital malformations and defects seen in 22q11.2DS patients are related to aberrant development and subsequent abnormal function of the derivatives of the pharyngeal arches and pouches, which include craniofacial structures, thymus, parathyroid glands, aortic arch, and the conotruncal region of the heart. Abnormal migration of neural crest cells has also been shown to contribute to abnormalities (McDonald-McGinn *et al.*, 2015, Scambler, 2000). All three germ layers, together with neural crest cells, play a role in the development of these structures.

Some of the phenotypes seen in patients are secondary effects of major dysfunctions (secondary phenotypes), such as hypocalcaemia due to hypoplasia or aplasia of parathyroid

gland, or immune deficiencies due to thymus defects. Congenital cardiac defects seen in patients are due to abnormal development of the arteries from the mesoderm-derived endothelium as well as defects in the cardiac outflow tract that receive contributions from neural crest cells (McDonald-McGinn *et al.*, 2015, Scambler, 2000).

**1.1.3. Clinical manifestations.** More than 80 congenital defects and malformations in different combinations, and more than 180 clinical manifestations have been shown to be associated with 22q11.2DS (Scambler, 2000, Monteiro *et al.*, 2013, McDonald-McGinn *et al.*, 1997, Swillen *et al.*, 2000, Tobias *et al.*, 1999). 22q11.2DS is the most common cause of syndromic palatal anomalies, and the second-most common cause of congenital heart disease (CHD) and developmental delays in children (McDonald-McGinn *et al.*, 2015). There is no record of any patients without any clinical observations (Baldini *et al.*, 2006). While some of these phenotypes can be lethal, patients might have only mild features (McDonald-McGinn *et al.*, 2011). Comparisons between patients carrying the 3Mb and those with smaller deletions in the region did not show consistent phenotypic differences (Bassett *et al.*, 2011, McDonald-McGinn *et al.*, 2015). However, inherited deletions seem to cause more severe cognitive phenotypes (Swillen *et al.*, 1999). Frequencies of some common characteristics are shown on Table 1 (Bassett *et al.*, 2011).

**Table 1. List of common and rare features associated with 22q11.2DS.**

<b>COMMON FEATURES</b>	<b>LESS COMMON FEATURES</b>
dysmorphic facial features (>90% of cases)	dermatitis (35%)
hypernasal speech (crying) and/or nasal regurgitation (>90%)	obesity (35%, adults)
learning disability/mental retardation/developmental delay (90%)	structural urinary tract anomaly (31%)
motor and/or speech delays (>90%)	hypothyroidism (20%)
palatal and related (75%)	short stature (20%)
hypocalcemia and/or hypoparathyroidism (>60%)	hyperthyroidism (5%)
cardiovascular (50%-75%)	ophthalmology (15%)
psychiatric disorders (60%)	multicystic dysplastic kidneys (10%)
hearing loss (30%-50%)	dental problems
scoliosis (45%)	failure to thrive
recurrent infections (35%-40%)	cervical spine anomalies/thoracic butterfly vertebrae
Skeletal (36%)	

(Basset *et al.*, 2011, Ming *et al.*, 1997).

**1.1.3.1. Craniofacial findings associated with 22q11.2 deletion syndrome.** Many individuals with 22q11.2DS share characteristic dysmorphic facial features, such as a long face, malar flattening, hypertelorism, short palpebral fissures, hooded/swollen eyelids, nasal abnormalities, micrognathia, a small mouth, asymmetric crying faces, and auricular abnormalities. However, diagnosis of the syndrome is challenging in some patients based on facial appearance alone (McDonald-McGinn *et al.*, 1996, McDonald-McGinn *et al.*, 2005). Other craniofacial abnormalities include velopharyngeal insufficiency, dental anomalies, cleft lip and palate, craniosynostosis, and microcephaly (Gripp *et al.*, 1997, McDonald-McGinn *et al.*, 2001). A list of common craniofacial findings is shown in Table 2.

**Table 2. Overlap and differences in subset of malformations found in 22q11.2DS and CEDNIK patients.**

<b>22q11.2DS patients</b>	<b>CEDNIK patients</b>
<b>CRANIOFACIAL CHARACTERISTICS</b>	
microcephaly	microcephaly
facial dysmorphism	facial dysmorphism
elongated and asymmetric face	elongated face
micrognathia	micrognathia
retruded chin	small chin
-	small anterior fontanelle
<b>External oral anomalies</b>	
-	high palate with thick alveolar margin
-	Small mouth
bifid uvula	bifid uvula
submucous, overt cleft palate	-
cleft lip	-
short philtrum	-
malar flatness	-
<b>Nasal features</b>	
bulbous nasal tip	pointed, prominent nasal tip
broad and prominent nasal root	flat broad nasal root
hypoplastic alae nasi	-
nasal dimple	-
wide nasal bridge	-
narrow alar base	-
<b>External eye and ophtalmologic findings</b>	
upslanting palpebral fissures	down slanting palpebral fissures
hypertelorism	hypertelorism
strabismus	strabismus
-	antimongolian eye slant
-	macular atrophy
-	hypoplastic optic disk
-	roving eye movements
-	reduced conductance from peripheral retina
-	retinal prolems
-	lacked visual fixation
-	squint
-	astigmatism
hooded eyelids	-

ptosis	-
refractory errors	-
posterior embryotoxon	-
tortuous retinal vessels	-
sclerocornea	-
coloboma	-
amblyopia	-
tortuous retinal vessels	-
sclerocornea	-
anophthalmia	-
cataract	-
<b>Ear anomalies</b>	
-	abnormal ear
-	large ear
thick overfolded, squared-off and crumpled helices	-
microstomia	-
microtic, cupped or posteriorly rotated ears attached lobes	-
preauricular pits or tags	-
small, low-set ears	-
sensorineural and conductive deafness	sensorineural deafness
<b>Skin conditions</b>	
seborrhea or dermatitis	eczematous dermatitis
-	collodion phenotype
-	palmoplantar keratoderma
-	lamellar ichthyosis
-	xerosis
severe acne	
<b>Skeletal problems</b>	
scoliosis	kyphoscoliosis
clinodactyly	clinodactyly
-	long toes
-	club feet
-	contracture of joints
	coxa valga
	broad first toes
servical spine anomalies	-
idiopathic leg pains in childhood	-
sacral sinus	-

cervical cord compression	-
craniosynostosis	-
upper/lower extremity pre and post axial polydactyly	-
horacic butterfly vertebrae	-
<b>CNS abnormalities</b>	
polymicrogyria	polymicrogyria
recurrent (often hypocalcemic) seizures	seizures
-	spastic quadriplegia
-	perisylvian polymicrogyria
-	absent or small corpus callosum
-	dysgenesis of the corpus callosum
-	cortical dysplasia
-	severe neurological impairment
-	ventricular asymmetry
dysfunction of white matter microstructure	diffuse white matter
unprovoked epilepsy	-
cerebellar abnormalities	-
neural tube defects	-
enlarged sylvian fissures	-
tethered cord	-
abdominal migraines	-
decrease in total brain volume	-
increased CSF in temporal and posterior brain regions	-
reduced temporal gray matter	-
hemiparesis	-
<b>Growth and developmental features</b>	
mental retardation	peripheral nerve low-amplitude response
failure to thrive	failure to thrive
speech delay	lacked speech
	severe global developmental delay
motor delay	-
learning disabilities	-
short stature	short stature
<b>Neuropsychiatric disorders</b>	
psychiatric disorders	-
childhood disorders (eg, attention-deficit, autism )	-
anxiety and depressive disorders	-



schizophrenia and other psychotic disorders	-
<b>Motor defects</b>	
general neuromotor deficits	psychomotor retardation
delayed walking	delayed sitting and walking
hypotonia	trunk hypotonia, poor head and trunk control
	reduced tone at birth
	increased tone with marked head lag
tendon reflexes	tendon reflexes
-	thin knees in fixed flexion
-	reduced muscle bulk
gross and fine motor deficits	deficits in gross and fine motor skills
balance and coordination defect	-
hemiplegia	-
coordination/balance deficits	-
problems with motor speed	-
motor deficits in axial stability and graphomotor skills	-
asymmetric crying facies	-
Gait disorder	-
<b>Additional features</b>	
hypoglycaemia	hypoglycaemia
feeding problems	feeding problems
-	dislocated hips
-	high-pitched cry
-	pneumonia
-	inverted nipples
-	unable to smile, fix or follow
-	dysphagia and aspiration
-	hirsutism

**1.1.3.2. Brain abnormalities.** Children with 22q11.2DS have reduced white and grey (frontal cortices, the cingulate gyrus, and the cerebellum) matters, as well as low thalamus volume, which is correlated with poor attention and executive functioning, visuo-spatial deficit, and susceptibility to schizophrenia (Shashi *et al.*, 2010, Bearden *et al.*, 2004, Bish *et al.*, 2004). Global brain volumetric reduction, including cerebellum and hippocampus, was also noted (Tan *et al.*, 2009). Increase in cortical thickness in multiple frontal regions, and insula and sulcal cerebrospinal fluid (CSF) in temporal and posterior brain regions was reported also (Bearden *et al.*, 2004, Jalbrzikowski *et al.*, 2013). While microcephaly is fairly common in 22q11.2DS, polymicrogyria is seen only in subset of patients (McDonald-McGinn *et al.*, 2011, Ghariani *et al.*, 2002).

**1.1.3.3. Cardiovascular abnormalities.** Cardiac defects are the most common abnormality that leads to diagnosis of the syndrome, especially during prenatal sonographical screening (Hacıhamdioğlu *et al.*, 2015). Conotruncal heart defects (tetralogy of fallot, truncus arteriosus, interrupted aortic arch type B, and ventricular septal defect) are the most common cardiac findings. Generally, congenital heart diseases are considered the main cause of death (approximately 87%) among children diagnosed with 22q11.2DS (McDonald-McGinn *et al.*, 2001 and McDonald-McGinn *et al.*, 2015).

**1.1.3.4. Immunodeficiency.** 75% of pediatric patients with 22q11.2DS have immunodeficiency due to thymic hypoplasia, which leads to impaired thymocyte development (McDonald-McGinn *et al.*, 2011, Gennery *et al.*, 2012). The range of immunodeficiencies is highly variable in patients, however, most of the patients present with only a mild form of immunodeficiency.

Clinical manifestations include recurrent and chronic infections, impaired humoral activity, and abnormal T cell number and function (Gennery *et al.*, 2012).

**1.1.3.5. Endocrine abnormalities.** Hypocalcaemia due to hypoparathyroidism is highly prevalent and results in tetany, seizures, feeding difficulty, stridor and fatigue. Additionally, hypo- and hyper- thyroidism, growth hormone deficiency, intrauterine growth retardation, and short stature may also present in 22q11.2DS patients as abnormal endocrine manifestations (McDonald-McGinn *et al.*, 2015).

**1.1.3.6. Gastrointestinal abnormalities.** 22q11.2DS patients present with a number of gastrointestinal abnormalities including intestinal malrotation, nonrotation, Hirschsprung disease, imperforate anus, esophageal atresia, and tracheoesophageal fistula. Some of these abnormalities in turn cause feeding and swallowing problems as a secondary phenotype (McDonald-McGinn *et al.*, 2015). Gastro-oesophageal reflux disease, oesophageal dysmotility, nasopharyngeal reflux, vomiting, and constipation are common in children with 22q deletions (Eicher *et al.*, 2000).

**1.1.3.7. Risk of malignancy in 22q11.2DS.** Patients with 22q11.2DS are considered to be at high risk for malignancies. A recent study by Lambert *et al.* (2017) reported the overall prevalence of malignancies in 22q11.2DS patients to be approximately 5.7 per 1,000 individuals. A few genes in the deleted region have been associated with malignancies in patients: *COMT* (McDonald-McGinn *et al.*, 2006), *SMARCB1* (Bosse *et al.*, 2014) and *DGCR8* (Gregory and Shiekhhattar, 2005). However, it is not yet clear if it is due to the deletion of a specific gene in the region (Lambert *et al.*, 2017, Stevens *et al.*, 2017). Thymic hypoplasia has been also proposed to

be partially responsible for the development of malignancies as immunodeficiency increases the risk of infections by carcinogenic viruses (Stevens *et al.*, 2017). Summary of some other associated clinical observations are shown in Table 3.

**Table 3. Subset of clinical manifestations found in 22q11.2DS patients.**

<b>Abnormality</b>	<b>Associated features, details</b>	<b>References</b>
Genitourinary	bilateral or unilateral renal agenesis, dysplastic or cystic kidneys, duplicated collecting system, hydronephrosis, cryptorchidism, hypospadias, absent uterus or inguinal hernia	Wu <i>et al.</i> 2002
Developmental delays	gross and fine motor difficulties, language delay and speech deficits, learning difficulties and variable cognitive development	Sobin <i>et al.</i> 2006
Psychiatric disorders	anxiety, attention-deficit, autism, schizophrenia, mood disorders, cognitive deficits, visual spatial abnormalities, impaired executive function, depression	Tang <i>et al.</i> 2014
Skeletal abnormalities	both upper and lower limbs deformity, including polydactyly, clubfoot, severely over folded toes, syndactyly, supernumerary ribs (17%), “butterfly” vertebral body, hypoplastic vertebrae, hemivertebrae, vertebral coronal clefts	Ming <i>et al.</i> 1997
Skin	dermatitis, severe acne	Basset <i>et al.</i> 2011
Ocular	strabismus, amblyopia, structural ocular abnormalities, posterior embryotoxon, tortuous retinal vessels, sclerocornea, Peter anomaly, coloboma	Hacıhamdioğlu <i>et al.</i> 2015, McDonald-McGinn <i>et al.</i> 2011
Hearing	posteriorly rotated ears or simple helices (as external ear phenotypes), permanent hearing loss (both conductive and sensorineural hearing loss)	McDonald-McGinn <i>et al.</i> 2011
Motor and movement	hypotonia, poor muscle strength and motor coordination, gross (crawling and walking independently) and fine motor delays, low facial tone, motor speech disorder, poor fine motor coordination, posture, oral motor coordination and tongue retraction, problems with tempo/speed, coordination, motor deficits in axial stability and graphomotor skills	Gerdes <i>et al.</i> 1999, Swillen <i>et al.</i> 1999 and 2005, Roizen <i>et al.</i> 2010
Reproduction	normal for women, reduced in men	Costain 2011
Other	malignancies like hepatoblastoma, renal cell carcinoma, and Wilms tumor, neural tube defects, congenital diaphragmatic hernia, seizures, early-onset Parkinson disease	McDonald-McGinn <i>et al.</i> 2015, Basset <i>et al.</i> 2011

**1.1.4. Diagnosis.** Diagnosis of the syndrome is challenging due to the highly variable clinical manifestations that can affect almost any organ or system (Monteiro *et al.*, 2013). However, there are common phenotypes, such as typical facial dysmorphism, cardiac defects, palatal and immunologic alterations, learning difficulties, and behavioral problems that could indicate the presence of the syndrome but require confirmatory testing. In many cases, prenatal ultrasound is useful to identify the syndrome through detection of cardiac defects (Chen *et al.*, 2008). 22q11.2 deletion is usually identified by multiplex ligation-dependent probe amplification (MLPA), analysis of polymorphic DNA markers, real-time PCR, or SNP (single-nucleotide polymorphism) microarrays (Sgardioli *et al.*, 2017, Hacıhamdioğlu *et al.*, 2011, McDonald-McGinn *et al.*, 2015). These techniques, particularly clinical microarray, detect all different 22q11.2 deletions.

**1.1.5. Genes within the TDR.** The TDR of 22q11.2DS harbours 90 genes (46 protein coding) and the small, proximal 1.5 Mb deletion encompasses 55 of these genes (30 protein coding). Of the 90 genes, seven encode microRNAs (miRNAs), ten are non-coding RNAs (including one read-through transcript), and 27 are pseudogenes. In the mouse, 40 of the 46 protein-coding genes of the 3 Mb human TDR are conserved on chromosome 16. For the 1.5 Mb proximal deletion region, 27 of the 30 protein-coding genes are conserved. 31 of the 40 conserved genes have knockout models in different organisms, 13 being in mouse (Guna *et al.*, 2015). Some of the genes located in the region have been investigated as potential candidates for the associated phenotypes of the syndrome. The genes that had been linked to major associated characteristics seen in the patents (including genes examined in this study) are briefly presented below.

**T-box transcription factor (*TBX1*).** The most studied gene in the TDR is *TBX1* (mapped to the LCR22A–B region). This is the only gene mutated in some patients with no deletion but with 22q11.2DS characteristic features (described in section 1.1.6).

**Crk-like protein (*CRKL*).** The cytoplasmic adaptor *CRKL* (v-crk avian sarcoma virus CT10 oncogene homolog-like), mapped to the LCR22C–D region, has also been strongly associated with the etiology of cardiac phenotypes in patients with distal LCR22B–D and nested LCR22C–D deletions that do not include *TBX1* (Racedo *et al.*, 2015). It has been shown that loss of function of *CRKL* causes embryonic lethality due to cardiac malformation (Park *et al.*, 2006). Additionally, *CRKL* knockout mice have exhibited craniofacial malformations (Park *et al.*, 2006) as well as heart defects similar to 22q11.2DS patients. Guris *et al.* (2006) identified a genetic interaction between *Crkl* and *Tbx1* in cardiovascular development. The authors showed that compound heterozygosity of *Tbx1* and *Crkl* caused increased incidence and expressivity of aortic arch defects. Furthermore, evaluation of a *Crkl* allelic series in mice revealed a dose sensitive effect of *Crkl* on the development of the cardiac outflow tract, indicating it might be a modifier of cardiac malformations in patients with a nested distal deletion and no apparent *TBX1* deletion (Rasedo *et al.*, 2015).

**DiGeorge Syndrome Critical Region Gene 8 (*DGCR8*).** Another gene in the region, *DGCR8*, encodes a double-stranded RNA-binding protein that mediates the biogenesis of miRNAs. *DGCR8* might be interesting due to possible implications in miRNA-related etiology of behavioural and neuronal deficits associated with the 22q11.2DS (Stark *et al.*, 2008). Details of the knockout mouse phenotype for this gene are described in Table 5.

**Scavenger receptor class F, member 2 (*SCARF2*).** *SCARF2* (also known as *SREC-II*) is a member of the scavenger receptor family class F. Scavenger receptors (SRs) belong to the cell surface pattern recognition receptor family, which plays an important role in diverse biological processes, including endocytosis, adhesion, antigen presentation, pathogen clearance, lipid transport, and even function as taste receptors. This diversity is due to the large number of family members, as well as their capacity to bind to heterogeneous ligands (Canton *et al.*, 2013). SRs are grouped into 10 classes, named A-J, based on their structure and function (Zani *et al.*, 2015, Yu *et al.*, 2015). SRs are predominantly expressed on myeloid cells (Yu *et al.*, 2015) and are known to be involved in the pathophysiological state of a number of disorders, such as atherosclerosis, pathogen infections, immune surveillance, neurodegeneration, metabolic disorders, and cancer (PrabhuDas *et al.*, 2014, Zani *et al.*, 2015, Yu *et al.*, 2015).

*SCARF2* belongs to class F, which contains only two members: *SCARF1* (*SREC1*) and *SCARF2*. Class F SRs carry an extracellular domain containing multiple putative epidermal growth factors (EGF)-like repeats, a single transmembrane region, and an intracellular-cytoplasmic domain that contains a number of positively charged residues, suggesting its involvement in intracellular signalling. The function of the gene is not well studied and its only known protein interaction is with *SCARF1*. Unlike *SCARF1*, *SCARF2* has poor scavenger receptor activity. Both *SCARF1* and *SCARF2* are predominantly expressed in the human heart, lung, ovary, placenta, and the endothelial cells of the umbilical vein (Ishii *et al.*, 2002). A recent study also indicated that *SCARF2* might regulate the host immune response of innate immune cells during bacterial infection (He *et al.*, 2015).

Homozygous mutations in *SCARF2* are associated with a congenital, autosomal recessive syndrome named VDEGS. VDEGS is characterized by craniofacial and skeletal abnormalities,



such as blepharophimosis, a flat and wide nasal bridge, malar and/or maxillary hypoplasia, prominent ears, a narrow and beaked nose, everted lower lip, palatal abnormalities, down-slanting eyes, slender ribs, hooked clavicles, bowed long bones, and respiratory problems (Figure 3). Some of these features have also been shown in 22q11.2DS patients (Table 3; Anastasio *et al.*, 2010, Bedeschi *et al.*, 2010). Homozygous *Scarf2* null mice are viable, they display increased tibia length, decreased erythrocyte cell number, and decreased hemoglobin content (<https://www.mousephenotype.org/data/genes/MGI:1858430>). Expression data was not reported for most tissues affected in VDEGS.

Mutations in *SCARF2* are associated with 22q11.2DS (Bedeschi *et al.*, 2010). It has been shown that recessive *SCARF2* mutations located on the intact chromosome of 22q11.2DS patients can be unmasked due to the deletion. This results in compound heterozygosity and leads to the atypical VDEGS-related phenotypes observed in patients (Bedeschi *et al.*, 2010).



**Figure 3. Typical representation of a patient with VDEGS syndrome.** Patients with *SCARF2* mutations develop VDEGS syndrome with distinct craniofacial dysmorphism and skeletal malformations that are also seen in 22q11.2DS patients. (A), bilateral sclerocornea, short palpebral fissures, underdeveloped ala nasi, low hanging columella, everted lower lip; (B), brachycephaly, low-set ears and increased posterior angulation, rethronathia; (C), dolichostenomelia, genu varus; (D), slender fingers, camptodactyly; (E), bilateral adducted thumbs; (F), scoliosis, slender ribs; (G), slender long bones, short ulnas bilaterally not articulated with the radii; (H), long metacarpus and phalanges (Migliavacca *et al.*, 2014).

**Synaptosomal associated protein 29 (SNAP29).** *SNAP29* is a ubiquitously expressed SNARE protein that plays a crucial role in SNARE complex assembly in a variety of intracellular membrane fusion events and is implicated in synaptic transmission (Qingning *et al.*, 2001, Ping-Yue *et al.*, 2005, Rapaport *et al.*, 2010, Guo *et al.*, 2014). It has been suggested that *SNAP29* mediates neurotransmitter release and inhibits disassembly of SNARE complex, which drives the fusion of membranes during vesicular trafficking (Sprecher *et al.*, 2005, Qingning *et al.*, 2001, Ping-Yue *et al.*, 2005). Details of membrane fusion during vesicular trafficking are discussed in section 1.3 of this thesis. More recently, *SNAP29* has also been implicated in kinetochore formation (Morelli *et al.*, 2016) and a novel heterozygous variant in *SNAP29* was shown to be associated with nocturnal frontal lobe epilepsy in a patient (Lichao *et al.*, 2017).

Mutations in *SNAP29* have been associated with 22q.11.2DS and CEDNIK, a syndrome that presents with a number of clinical manifestations that include mild skin defects at birth or in the first few months of life (5 and 11 months of age), failure to thrive, cerebral malformations, developmental delays, severe mental retardation, roving eye movements during infancy, trunk hypotonia, poor head control, craniofacial dimorphisms, and mild deafness (Figure 4; Sprecher *et al.*, 2005 and Fuchs-Telem *et al.*, 2011). *SNAP29* gene is considered one of the top candidate genes that may play an important role in the pathogenesis of schizophrenia (Saito *et al.*, 2001, Luo *et al.*, 2014). Importantly, a subset of phenotypes found in CEDNIK patients have also been described in 22q11.2DS patients (Table 3; McDonald-McGinn *et al.*, 2013). Similarities and differences in craniofacial, central nervous system (CNS), and motor defect phenotypes between CEDNIK and 22q11.2DS are shown in Table 4.

**Table 4. Phenotypic abnormalities shared between patients with 22q11.2DS and patients with mutations in *SCARF2* and *SNAP29*.**

22q11.2DS	<i>SCARF2</i> <sup>-/-</sup>	<i>SNAP29</i> <sup>-/-</sup>
CNS	YES	YES
craniofacial	YES	YES
hearing loss	NR	<b>YES</b>
ophthalmological	YES	YES
parathyroid	NR	NR
thymus	NR	NR
ophthalmological	YES	YES
cardiac	NR	NR
motor	YES	YES
developmental delay	NR	<b>YES</b>
feeding	NR	<b>YES</b>
skeletal	YES	YES
dental	<b>YES</b>	NR
renal	<b>YES</b>	NR
respiratory	YES	YES
skin	NR	YES

Comparison of phenotypes between 22q11.2DS patients and the patients carrying mutations in *SNAP29* and *SCARF2* with no deletion, suggests possible contribution of these two genes to the syndrome. Phenotypes shown in red are shared either with 22q11.2DS and *SCARF2* patients or 22q11.2DS and *SNAP29* patients.

Two mouse models with mutations in *Snap29* have been reported to display similar skin phenotypes as patients, these include condensed stratum corneum (SC) with a number of lipid droplets, abnormal epidermal barrier formation, disrupted lamellar body (LB) function, irregular lipid profiles, and aberrant vesicular trafficking (Schiller *et al.*, 2016). However, all homozygous *Snap29* null mice on the inbred genetic background (C57BL/6) are reported to die within a few hours of birth with severe skin abnormalities. Thus, existing models are not helpful for investigating postnatal phenotypes found in 22q11.2DS and CEDNIK patients.

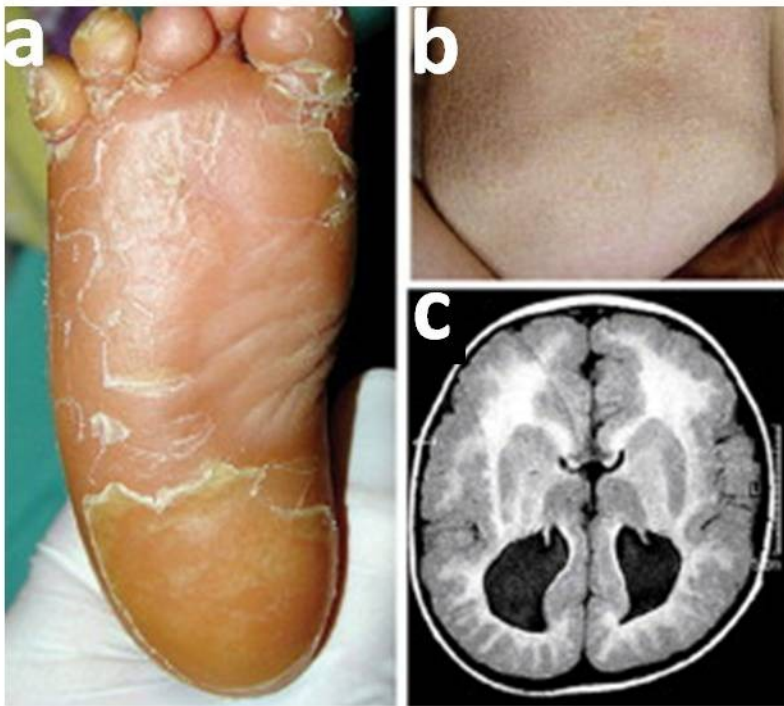


**Figure 4. Congenital malformations associated with CEDNIK syndrome.** CEDNIK patients present with number of birth defects including A) palmoplantar keratoderma, B) lamellar ichthyosis, and C) brain abnormalities, such as cortical dysplasia, pachygyria with polymicrogyria, and absence of corpus callosum (Sprecher *et al.*, 2005).

**Candidate genes for neuropsychiatric conditions.** Since neuropsychiatric disorders encompass the major group of late onset conditions in 22q11.2DS (Philip and Bassett , 2011, Bassett *et al.*, 2005, Fung *et al.*, 2015, McDonald-McGinn *et al.*, 2015), it is of great importance to find genes and pathways responsible for these disorders. In fact, 22q11.2 deletion is considered the most common cause of intellectual disability after Down syndrome (McDonald-McGinn *et al.*, 2015). There are a number of candidate genes for the neuropsychiatric conditions seen in 22q11.2DS patients, as 41 of 46 protein-coding genes in the TDR are expressed in the human brain (Guna *et al.*, 2015). Phenotypes of knockout mouse models generated for subset of these candidate genes recapitulate human neuropsychiatric conditions. The list of genes and phenotypes of the knockout mouse models are shown in Table 5.

**Table 5. The list of candidate genes for the neuropsychiatric conditions**

Gene name	Short description	22q11.2DS association	Knockout mouse phenotypes associated with 22q11.2DS	References
<i>COMT</i>	encodes for catechol- <i>O</i> -methyltransferase	impaired cognition and susceptibility to schizophrenia	impairment in emotional and social behavior	Bassett <i>et al.</i> , 2007, Gogos <i>et al.</i> , 1998
<i>PRODH</i>	encodes for enzyme proline dehydrogenase	type I hyperprolinaemia, seizures and intellectual disability, psychiatric and behavioral phenotypes, motor dysfunction	decreased sensorimotor gating, prepulse inhibition, impaired fear conditioning	Goodman <i>et al.</i> , 2000, Raux <i>et al.</i> , 2007, Guna <i>et al.</i> , 2015, Gogos <i>et al.</i> , 1999
<i>ZDHHC8</i>	encodes a palmitoyltransferase	susceptibility to schizophrenia	abnormal axonal growth and terminal arborization, implications in	Liu <i>et al.</i> , 2002, Chen <i>et al.</i> , 2004, Mukai <i>et</i>

			synaptic connections and working memory	<i>al.</i> , 2015
<i>RANBP1</i>	encodes for a binding protein for the small GTPase Ran	microcephaly, altered cortical precursor proliferation and neurogenesis	microcephalic embryos and altered proliferation of cortical progenitors	Paronett <i>et al.</i> , 2015
HIRA	encodes a histone chaperone	cardiovascular phenotype	abnormal cardiac development, abnormal embryonic tissue and neural plate morphology, defective placenta, craniofacial abnormalities, failure of brain to fuse	Farrell <i>et al.</i> , 1999, Roberts <i>et al.</i> , 2002
TXNRD2	encodes a mitochondrial form important for scavenging reactive oxygen species in mitochondria	cardiac phenotype	severe anemia and growth retardation due to perturbed cardiac development and augmented apoptosis of hematopoietic cells	Prasad <i>et al.</i> , 2014, Conrad <i>et al.</i> , 2006
DGCR8	encodes a subunit of the microprocessor complex which mediates the biogenesis of microRNAs from the primary microRNA transcript	metabolite imbalances, cognitive, neurocognitive, psychiatric disorders and cardiac disease	reduced dendritic spine number, reduced dendritic complexity, decreased prepulse inhibition and abnormal spatial working memory (het-KO)	Sellier <i>et al.</i> , 2014, Strak <i>et al.</i> , 2008, Fenelon <i>et al.</i> , 2011, Napoli <i>et al.</i> , 2015

**1.1.6. Mouse models for 22q11.2DS.** In order to understand the molecular basis of the syndrome, several mouse models have been generated either carrying deletions in syntenic regions of mouse chromosome 16, which is homologous to the TDR of human chromosome 22 (Botta *et al.*, 1997, Lund *et al.*, 2000), or point mutations in the genes located in the TDR. Although a few of these models recapitulated some of the phenotypes, none of them were able to phenocopy the full spectrum of features seen in patients (Figure 5).

**Figure 5. Deletion of the 22q11.2DS syntenic region in mouse chromosome 16 models a subset of abnormalities.** Genes located in the TDR of human chromosome 22 are conserved in mouse chromosome 16. However, their positions are changed in clusters (shown in different colors) along the chromosome or they can have a different order within conserved clusters (the human and mouse chromosomal regions are not to scale). A number of mouse models have been generated to model the syndrome and are displayed as lines corresponding to the approximate



deletion size (labeled Df1, Df2, Df3, Df4, Lgdel, Kimber *et al.* and Puech *et al.*) along with the phenotypes observed. Location of the *SNAP29* and *SCARF2* genes is indicated by red arrows. TDR, typically deleted region (Modified from Botta *et al.* 2001).

The first mouse model of DGS (Df1) was engineered using Cre-loxP. It carried about a 1 Mb heterozygous deletion that encompassed 18 orthologues of genes located in the TDR (Lindsay *et al.*, 1999). Df1 mice developed cardiovascular abnormalities similar to 22q11.2DS patients due to the abnormal development of the fourth pharyngeal arch arteries, as well as thymic and parathyroid hypoplasia, and learning and behavioural abnormalities (Taddei *et al.*, 2001). No other abnormalities were seen in this model.

A second model was generated by Kimber *et al.* (1999) using conventional gene targeting that allowed them to delete 7 genes encompassing about 150 kb of the proximal region of the TDR. Heterozygous mice for this deletion did not recapitulate any characteristics of 22q11.2DS patients.

Puech *et al.* (2000) were able to generate a 550 kb deletion by Cre-mediated recombination of LoxP sites that partially overlapped with the Df1 model. The model covered the deletion of 16 genes from the TDR. Although the heterozygous mice did not show any features of 22q11.2DS patients, it helped to narrow down the list of candidate genes responsible for common phenotypes seen in patients and suggested that the causal gene is not among these 16 genes.

Studies by 3 different groups in 2001 (described below) showed that cardiovascular defects observed in Df1 mice were due to *Tbx1* haploinsufficiency in the deleted LCR22A–LCR22B region (Lindsay *et al.*, 2001, Merscher *et al.*, 2001, Jerome *et al.*, 2001). *Tbx1* is a member of T-box family of transcription factors and is involved in specification of mesoderm, heart and limb (Bollag *et al.*, 1994, Dastjerdi *et al.*, 2007, Xu *et al.*, 2014). Lindsay *et al.* (2001) generated 3 nested deletions (Df2, Df3 and Df4) within the previously established Df1 model to identify the gene causing heart defects in the Df1 model and were able to narrow down the candidate genes to *Tbx1*. A hemizygous 1.5 Mb deletion that corresponds to the deletion of 24 genes located in the TDR of 22q11.2DS was created by Merscher *et al.*, (2001) using a cre-loxP method (Lgdel). Heterozygous mice for this deletion showed conotruncal and parathyroid abnormalities that were rescued by a BAC (bacterial artificial chromosome) containing the *TBX1* gene, indicating *TBX1* involvement in the etiology of cardiac and parathyroid abnormalities seen in 22q11.2DS.

Finally, heterozygous mutations in *Tbx1* showed a high incidence of reduced or absent fourth aortic arches, similar to the heterozygous Df1 phenotype (Jerome *et al.*, 2001). Homozygous mutations resulted in death at birth and a number of the same developmental anomalies that are observed in 22q11.2DS patients including absence of the thymus and parathyroid glands, abnormal facial structure, abnormal vertebrae, cleft palate, and cardiac defects. In contrast, only a few patients with the 22q11.2DS phenotype and no obvious deletion were found to carry a *TBX1* mutation, despite screening of more than 200 patients, suggesting involvement of other genes (Jaouadi *et al.*, 2018, Sgardioli *et al.*, 2015, Xu *et al.*, 2014, Yagi *et al.*, 2003, Lindsay *et al.*, 2001).

**1.1.7. Screening.** It is important to diagnose the syndrome as early as possible in order to prevent complications such as neonatal seizures due to hypocalcaemia (Cheung *et al.*, 2014). Families in which one of the parents carries the deletion are recommended to screen their babies for the 22q11.2 deletion, as there is a 50% risk of transmission. Chorionic villus sampling, amniocentesis, and genetic diagnosis would be choices for those families to identify the syndrome during pregnancy. Fetal ultrasonography might identify some anatomic abnormalities seen in 22q11.2DS, such as congenital heart defects (CHD), cleft palate, renal anomalies, polyhydramnios, polydactyly, diaphragmatic hernia, club feet, tracheo-oesophageal fistula, and neural tube defects. Parents of children carrying 22q11.2DS should also be tested, as they might have the deletion but be mildly affected or they may have somatic mosaicism (McDonald-McGinn *et al.*, 2015).

**1.1.8. Management.** Due to highly variable phenotypes and multisystem involvement, management of 22q11.2DS patients should be individualized. The International 22q11.2DS consortium under the 22q11.2 society generated management parameters for 22q11.2DS patients as reviewed by McDonald-McGinn *et al.* (2015). Primarily, it recommends to identify the syndrome as early as possible, take into consideration the multisystem nature of the syndrome and patients' cognitive ability when they are treated, and to promote involvement of family members to improve outcome of the treatment (McDonald-McGinn *et al.*, 2015). Learning difficulties, psychiatric disorders, CHD, immunodeficiency, and other consequences of 22q11.2DS that demand patient care drastically affect the daily life of patients and their families. To increase the quality of life and decrease the stress of both patients and families, it is important that families and caregivers work together and support each other (Karas *et al.*, 2014). Recognition and treatment of psychiatric disorders and integrated treatment methods will

optimize the quality of life for both patients and their families (reviewed by McDonald-McGinn *et al.*, 2015).

### **1.1.9. Normal development of structures affected in 22q11.2DS patients; facial structures, brain, reproductive and motor system**

**1.1.9.1. Face development.** The face starts to develop during the 4<sup>th</sup> week of embryonic life and is complete by week 12. Cells of different origins contribute to the development of the face; the head ectoderm forms the face, oral cavity, and neural crest mesenchyme to the first branchial arch and its derivatives. Facial prominences (swellings) that are generated by proliferation of mesenchyme lift the surface ectoderm and give rise to different structures of the face. A frontonasal prominence (FNP) that is predominantly of neural crest origin forms paired medial nasal processes and a pair of lateral nasal processes. These processes will form the forehead, nose dorsum, and nose apex (Som P.M. and T.P. Naidich, 2013).

The nasal (olfactory) placodes that develop bilaterally in the lower part of the FNP by ectodermal thickening are the precursors of future olfactory epithelium (OE), the structure that controls the sense of smell (Som P.M. and T.P. Naidich, 2013).

The first pharyngeal arch originates from the mesoderm and neural crest. It forms a pair of mandibular processes that will give rise to lower cheek, chin, lower lip, and a pair of maxillary processes. The maxillary processes will fuse with the medial nasal processes to give rise to the upper cheek, upper lip, and upper jaw. Fusion of the lower extension of the medial nasal processes (named intermaxillary process) will then form the philtrum (Som and Naidich, 2013). A mesenchymal mass extends posteriorly from the intermaxillary process to form the primary

palate. Maxillary processes give rise to a pair of medial mesenchymal extensions that fuse with each other and with the primary palate to form the secondary palate and the definitive palate, respectively (Som and Naidich, 2013).

**1.1.9.2. Eyelid development.** The eyelids originate from the neural crest mesenchyme and from 2 cutaneous folds of ectoderm in the sixth week, which then fuse to each other in the 10<sup>th</sup> week (Som P.M. and T.P. Naidich, 2014).

**1.1.9.3. Ear development.** The mammalian ear originates from all three germ layers and the neural crest cells (NCC) (Anthwal N and Thompson H, 2016). Tissues from the first and second pharyngeal arches that are filled by NCCs contribute to the middle and outer ear (Sandell, 2014), while the inner ear arises from the otic vesicle. The outer ear pinna and ear canal form during the sixth gestational week (GW) in humans (reviewed by Carlson *et al.*, 2014) and the pinna reaches its adult morphology at GW22. The neural crest of the first and second arches forms the middle ear ossicles. The otic vesicle (OV), an epithelial sac that gives rise to the structures of the inner ear, the vestibular system for sensing motion and gravity, and the cochlea for sensing sound, are all derived from the otic placode (Sandell, 2014). Developmental defects of the outer and middle ear result in conductive hearing loss, whereas inner ear abnormalities lead to sensorineural hearing loss.

**1.1.9.4. Brain development.** The brain and central nervous system originate from neuroectodermal stem cells, which are neural progenitor cells (NPCs). Brain development starts with the differentiation of epiblast cells into NPCs at the beginning of gastrulation. Molecular signalling coming from the primitive node, the migrating cells, and the cells that will become the neural progenitors contributes to this differentiation. The primitive node also generates different

signals to establish the basic rostral-caudal organization of the forebrain, hindbrain, and spinal cord structures of the embryonic nervous system (Stiles and Jernigan., 2010).

The first formed brain structure is the neural tube, which develops during E20-27. NPCs positioned along the rostral-caudal midline of the upper layer of the three-layered embryo are called the neural plate. Two ridges of the neural plate elevate, fold inward, and fuse to form the lumen of the tube (Copp *et al.*, 2003). The single layer of NPCs in the central cavity of the lumen will give rise to the ventricular system, named the ventricular zone (VZ). The brain is generated by NPCs located in the most rostral region of the neural tube, while the hindbrain and spinal column originate from NPCs located more caudally. Precursors of forebrain (prosencephalon, which will later differentiate into the telencephalon and diencephalon), midbrain (mesencephalon) and hindbrain (rhombencephalon, which will later differentiate into the metencephalon and myelencephalon) are formed shortly before neural tube closure in the anterior end of the tube (Stiles, 2008).

The neocortex is the surface layer of the brain and provides the network for information processing. The basic patterning of sensorimotor regions within this layer is established by the end of GW8. Various molecular signals play a role in differentiation of the neocortex into cortical areas. The interaction of two signalling molecules, Emx2 and Pax6, is essential for this patterning. In the presence of a high concentration of Pax6 and a low concentration of Emx2, NPCs give rise to neurons for the motor cortex region, whereas the inverse situation contributes to the generation of neurons for the visual cortex. Equal levels of Emx2 and Pax6 induce production of neurons for somatosensory areas (Stiles and Jernigan., 2010).

The first fissure of the cortex, the longitudinal fissure, is positioned between two cerebral

hemispheres and appears in GW8 in the rostral part of the brain then develops caudally till GW22 (Chi *et al.*, 1977). Primary sulci develop between GW14-26. Secondary and tertiary sulci form between GW30-35, and GW36 until the postnatal period, respectively, by branching off from the primary sulci.

Brain development in the fetal period (from GW9 through the end of gestation) consists mostly of neuron production, migration, and differentiation. Neuron production starts with symmetrical cell division in order to increase the size of the NPCs from GW25 to GW42 in the VZ. Starting from E42, the division mode changes to asymmetrical, which gives rise to one neural progenitor and one neuron per division (Wodarz and Huttner, 2003). Asymmetrical division is predominant by the end of cortical neurogenesis, which is approximately day 108 (Stiles *et al.*, 2010). The cell bodies of these neurons form the grey matter of the brain. Generated neurons migrate radially from the VZ out to the developing neocortex. The first neurons produced migrate by somal translocation in which neurons use their own cytoplasmic process to move out from the VZ (Nadarajah and Parnavelas, 2002). The neurons produced later use instead the basal processes of radial glial cells as a scaffold to migrate out of the VZ into the developing cortical plate, this is called radial glial guides (Nadarajah and Parnavelas, 2002).

The first sets of neurons that migrate from the VZ form the preplate (PP), whereas the next batch of migrating neurons divides the preplate into the transient brain layers: the marginal zone (MZ) and the subplate (SP). The MZ is considered to be crucial for neuronal migration, as it contains special neurons called the Cajal-Retzius (CR) cells. The CR cells control the positioning and migration of the neurons via the secreted extracellular matrix protein, Reelin (Valiente and Marin, 2010).

The cortical plate (CP) is generated between the MZ and SP regions. After generation of

the CP, the migration of neurons continues in an inside-out manner to form the 6-layered cortex (Cooper, 2008). The earliest neurons that migrated to the CP produce the deepest (6<sup>th</sup>) layer, and the latest migrating neurons produce the more superficial layers (Figure 6).

After the neurons reach their destination in the cortex, the next step in the development of the cortex is differentiation of the neurons. In this step, neurons form neuronal processes, axons, and dendrites, enabling them to communicate with other neurons. Axons develop synapses at connection points with their target cells, helping them to transmit electrochemical information and communicate with the target cells.



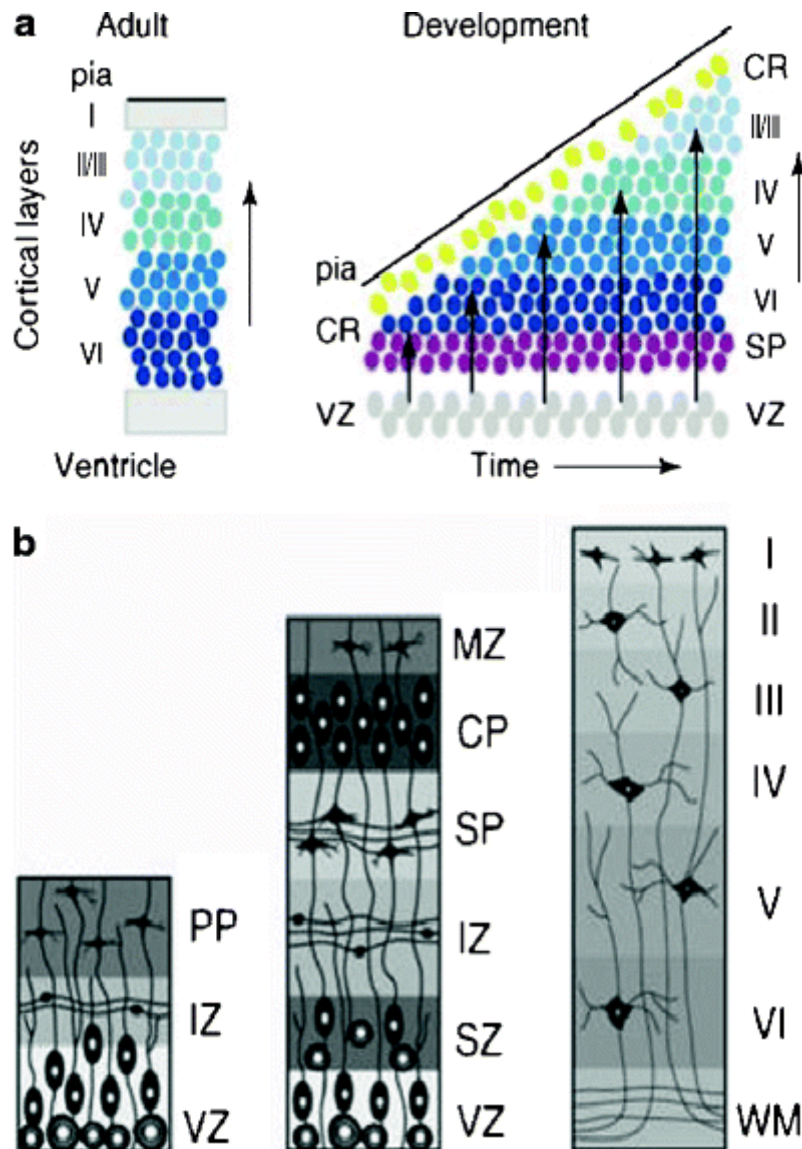


**Figure 6. Neuronal birth and cortical layer formation.** a. Neurons migrate in an inside-out manner; the earliest born neurons form the deepest layer and latest born migrate to the most superficial layer. b. Formation of cortical layers; the preplate (PP) layer forms first and then splits into the marginal zone (MZ) and the subplate (SP). The third panel demonstrates the six mature cortical layers (I-VI). Intermediate zone (IZ), white matter layer (WM) (Joan Stiles and Terry L. Jernigan, 2010).

**1.1.9.5. Sensorimotor development.** The thalamocortical circuit consists of two pathways: the thalamocortical (TC) and the corticothalamic (CT). Formation of the circuit starts late in the second trimester of pregnancy and is completed by GW26 (Kostovic and Jovanov-Milosevic, 2006). The two pathways provide reciprocal connections between the thalamus and the cortex, which is the main route of transmission of sensorimotor information to the cerebral cortex and to send feedback from the cortex back to the thalamus. The formation of this circuit relies on the subplate layer of the developing brain; axons from TC and CT pathways establish their first connections with the neurons of the subplate layer before they link to the cortical and the thalamic neurons. The subplate neurons are believed to guide these axons to their destination (Stiles and Jernigan, 2010).

**1.1.9.6. Pre and postnatal motor development and regulation.** Motor development is a continuous process that depends on the interaction of various elements, such as the continuous changes in neuromuscular maturation, the physical growth and behavioral characteristics of the child, the tempo of physical growth, biological maturation and behavioral development, the residual effects of prior movement experiences, and the new movement experiences (Malina, 2004).

Fetal movements play an important role in proper physical development. The first prenatal movements are generally observed at GW5-6 (de Vries, 1982). These movements are the result of functional synapses forming between nerves of the spinal cord and muscle fibers. A diverse type of generalized, spontaneous movements and postures are seen in fetuses in the first trimester. Body and limb movements increase later on in pregnancy until space becomes limited in the womb (de Vries and Hopkins, 2005). Spontaneous movements generated by the central nervous system (CNS) form sensory experiences in fetuses. Sensory experiences, in turn, initiate

neural activity that assists in shaping neural development (Hepper, 2003).

Spontaneous movements are also characteristic of infants. 67 different forms of movement have been recorded in the first year of life. These repetitive movements contribute to the development of the child by giving them experience and the movements become intentional over time. Gross motor play, which is a modified form of spontaneous large movement involving repeated actions with various forms, contributes to the development of bones and muscles (Pellegrini & Smith, 1998). Aimed actions are first seen at 11–24 weeks of age when the range of mobility decreases and control of the movements increases (Berthier and Keen, 2006, Konczak and Dichgans, 1997).

Posture is crucial for motor activity as most other actions develop based on proper posture. Development and control of proper posture depends on perception and how the body will deal with the physical environment, such as the force of gravity (Adolph and John Franchak, 2017). Motor skills turn into the consistent and precise adult-like movements with age and experience (Adolph and Berger, 2006).

**1.1.9.6.1. Motor regulation.** One of the main regions that controls motor function in the brain is the primary motor cortex, or M1, which is located in the frontal lobe of the brain. M1 produces neural impulses that are transmitted through spinal cord circuits to activate skeletal muscles that will control the execution of movement. The primary motor cortex has specialized areas for every part of the body located on opposite sides (the left hemisphere controls the right part of the body) and these areas are arranged somatotopically. The size of the area depends on how sophisticated a task that area is responsible (Schwerin *et al.*, 2013).

The posterior parietal cortex, the premotor cortex, and the supplementary motor area (SMA) are considered the secondary motor cortices. The posterior parietal cortex regulates motor function from visual perception. The premotor cortex manipulates the more proximal muscles and trunk muscles, while the supplementary motor area is involved in the planning of complex movements and in coordinating two-handed movements. Information acquired by the supplementary motor area and the premotor regions is sent to the primary motor cortex, as well as to brainstem motor regions (Schwerin *et al.*, 2013).

Neurons from M1, SMA, and the premotor cortex generate the fibers of the corticospinal tract, the main pathway for control of voluntary movements in humans. Posture and balance, coarse movements of the proximal muscles, head coordination, and neck and eye movements in response to visual targets are controlled by motor pathways derived from motor neurons of the subcortex. Signals from the primary motor cortex radiate through the corticospinal route to the interneurons and the motor neurons of the ventral horn of the spinal cord. Axons of the ventral horn deliver the signals to the ventral roots to innervate individual muscle fibers. The alpha motor neurons of the spine innervate muscle fibers that assist force generation, while the gamma motor neurons innervate fibers within the muscle spindle to measure the length or stretch of the muscle. The Golgi tendon organ connecting the muscle to the skeleton relays the signals about the force of the muscle contraction to the motor centers. Signals received from muscle spindles, Golgi tendon organs, and other sensory organs are conducted to the cerebellum, which controls the timing and coordination of the motor behaviour. Complex motor movements are regulated by specialized subcortical regions named the basal ganglia, which relay the motor action accomplishment to other subcortical brain regions and the cortex (Schwerin *et al.*, 2013).

**1.1.9.7. Reproductive system development.** The sexual differentiation and determination of the reproductive system is guided by the presence of the *SRY* gene (Sex-determining Region of the *Y* chromosome). If *SRY* is absent in the genome, then the embryo is destined to be a female and will form female reproductive structures and external genitalia.

The development of the reproductive system starts during GW5 with the development of primordial gonads, which are located medially to two parallel internal ductal systems: the mesonephric (Wolffian) duct and the paramesonephric (Mullerian) duct. These ducts later contribute to the development of the reproductive system; wolffian ducts generate the tube of the epididymus, ductus deferens, ejaculatory duct, and seminal vesicle in males, whereas Müllerian ducts forms the Fallopian tubes, uterus, cervix, and the upper two-thirds of the vagina, in the females. The cells of the fertilized embryos are sexually bipotential until GW7 (Rao *et al.*, 2013). From GW7-GW8, the gonads start to differentiate. However, the maturation of the system only begins in puberty (Carrol *et al.*, 2007).

**1.1.9.7.1. Development of female reproductive system.** The gonads of females differentiate into the ovaries in GW8 and will produce germ cells and secrete the female sex hormones, estrogen and progesterone. The production of the hormones is induced by gonadotropin-releasing hormone (GnRH), which is released by placental human chorionic gonadotropin (hCG). The ovarian surface epithelial cells contribute to the development of the follicles, which contain the oocytes. The mullerian ducts give rise to the fallopian tubes, uterus, and upper vagina. Formation of female external genitalia is completed by GW11 (Carrol *et al.*, 2007).

After birth, sexual development is arrested until restoration of GnRH production in adolescence. During puberty, ovaries start to produce estrogen and progesterone under the control of the hypothalamic GnRH. Anterior pituitary follicle stimulating hormone (FSH) and

luteinizing hormone (LH) lead to the follicular development, ovulation, corpus luteum formation, and menstruation (Carrol *et al.*, 2007).

**Oogenesis** is the process of differentiation of the ovum into the ova from primordial germ cells (PGCs) in the female gonads (the ovaries). Female gametes have all the necessary materials for the development of the ova. The first part of meiosis begins during the embryonic stage. The germ cells, oogonia, divide throughout GW2 to GW7 by mitosis to increase the number and enter the first meiotic division (Pinkerton *et al.*, 1961). The oogonia that undergo the first meiotic division are called primary oocytes and are arrested in the diplotene stage of the first meiotic prophase until puberty. During puberty, these primary oocytes will finish this division to generate secondary oocytes, which will complete meiosis if they are fertilized (Gilbert *et al.*, 2000).

**1.1.9.7.2. Development of male reproductive system.** SRY protein expressed by somatic mesenchymal cells of the developing gonads initiates differentiation of the male reproductive system. The gonads of the males differentiate into the testes at GW7. Sertoli cells originate from the mesenchymal cells producing SRY and play an important role in supporting spermatogenesis. The Sertoli and Leydig cells contribute to the differentiation of the male genital ducts. Production of hCG and LH triggers the Leydig cells to secrete male sex hormones, including testosterone. The production of testosterone stimulates the differentiation of the wolffian duct and the mesonephric tubules. The development of the vas deferens occurs from the wolffian duct, while the müllerian duct degenerates under the effect of anti-müllerian hormone secreted by the Sertoli cells of the testes. The wolffian duct also gives rise to the epididymis, the seminal vesicles, and the ejaculatory duct. The male external genitalia begins to develop under the influence of dihydrotestosterone, which is made through conversion of the testosterone. The

male reproductive system is completely formed at birth, however it is not mature. As in females, LH and FSH secretion is halted at birth and further maturation of the reproductive systems, recommences in adolescence (Kavoussi and Burnett, 2013).

**Spermatogenesis** is the differentiation of the mature sperm cells from PGCs occurs in the seminiferous tubules. The Sertoli cells differentiated from the tubules are very important for nourishing and protecting the developing sperm cells. The process of the spermatogenesis occurs between the Sertoli cells (Gilbert *et al.*, 2000).

The PGCs first divide to form the A<sub>1</sub> type of spermatogonia, the stem cells that can regenerate themselves and also produce the A<sub>2</sub> type of spermatogonia. The A<sub>2</sub> spermatogonia then divide to generate the A<sub>3</sub> type of spermatogonia, which in turn give rise to the A<sub>4</sub> spermatogonia.

The A<sub>4</sub> spermatogonium is capable of both self-renewal and differentiation into the intermediate spermatogonium. Intermediate spermatogonia are the first committed stem cell type that produce spermatozoa, which divide mitotically to give rise to the type B spermatogonia, the precursors of the primary spermatocytes. The primary spermatocytes form a pair of secondary spermatocytes by meiotic division. The secondary spermatocytes then undergo the second step of meiotic division to yield haploid spermatid cells. Subsequently, the differentiation of spermatids results in the formation of sperm (Figure 7). After maturation, the sperm cells undergo spermiogenesis, a process that prepares the sperm for fertilization (Gilbert *et al.*, 2000).

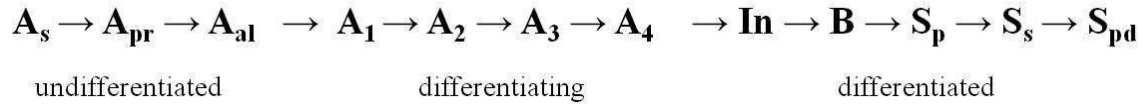


**Figure 7. Progression from  $A_s$  spermatogonia to spermatids.** Two daughter cells derived from one  $A_s$  spermatogonium form a pair of spermatogonia ( $A_{pr}$ ).  $A_{pr}$  spermatogonia produces a chain of four  $A_{al}$  spermatogonia by mitotic division, which in turn divide to the chains of 8, 16 or 32  $A_{al}$  spermatogonia. The  $A_{al}$  spermatogonia differentiate into type  $A_1$  spermatogonia. The  $A_1$  cells divide to  $A_2$  spermatogonia, and  $A_2$  in turn, divide to  $A_3$  spermatogonia, a division of which generates  $A_4$  spermatogonia.  $In$  and  $B$  spermatogonia are generated by next two mitotic divisions. Then  $B$  spermatogonia form primary spermatocytes, which give rise to secondary spermatocytes. Secondary spermatocytes form spermatids. A single ( $A_s$ ); A paired ( $A_{pr}$ ) and A aligned ( $A_{al}$ ); differentiating cells:  $A_1$ - $A_4$ , intermediate ( $In$ ) and  $B$  spermatogonia.

**1.2. Overview of intracellular trafficking pathways.** In this section, I will discuss the intercellular trafficking pathways as *Snap29*, the central focus of my thesis, is implicated in this process.

Eukaryotic cells transport materials between cell compartments and connect with their environment by vesicular trafficking. Trafficking of membranes is essential to maintain cellular homeostasis and for signalling (Tokarev *et al.*, 2000-2013). There are two main pathways, exocytotic and endocytotic, through which proteins and lipids are transported to various final intra- or extra-cellular destinations within vesicles. Cargo molecules synthesized in the



cytoplasm and endoplasmic reticulum (ER) are transported through the Golgi apparatus, to the plasma membrane by the exocytotic pathway. In this pathway, secreted proteins synthesized in the ER that have undergone correct post-translational modification and folding, are packed into ER-derived vesicles that form with the help of special coat (COPII) and adaptor proteins, and exit the ER at ER exit sites. Proteins pass quality control in the ER–Golgi intermediate compartment (ERGIC) and misfolded proteins are returned to the ER via COPI-coated vesicles. Correctly folded proteins pass through cis and trans Golgi stacks to the trans-Golgi network (TGN), where they are sorted into specific vesicles to go to the plasma membrane (Figure 8). Finally, the vesicles are docked to the acceptor membrane with the help of tethers and fuse to target membranes with the help of SNARE proteins (Figure 9; Yap *et al.*, 2009).

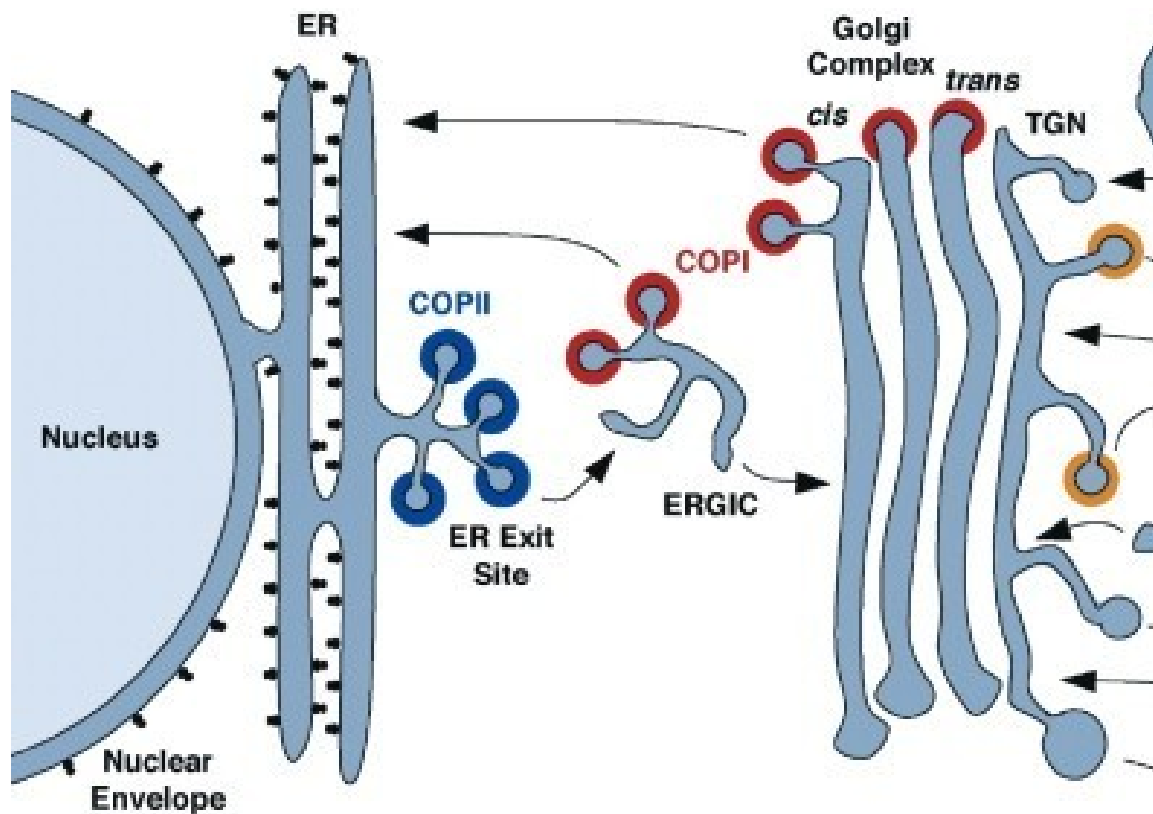


**Figure 8. Overview of the intercellular trafficking pathway.** Cargo molecules synthesized in ER are trafficked through the Golgi apparatus, to the plasma membrane. Secreted proteins that have undergone correct post-translational modification and folding, are transported via ER-derived COPII vesicles to the ERGIC and then, to the Golgi complex and exit the ER. The misfolded proteins are trafficked back to the ER via COPI-coated vesicles. Correctly folded proteins pass through Golgi complex to go to the plasma membrane where they fuse to the target membranes with the help of SNARE proteins (this figure was modified from Bonifacino and Glick, 2004).

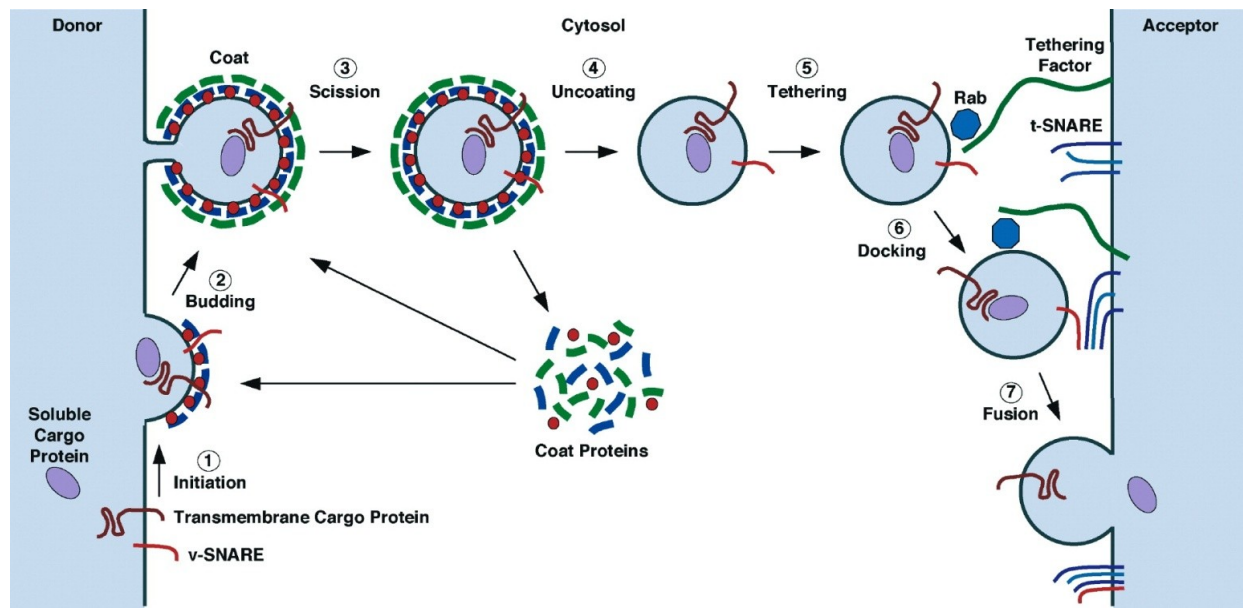


**Figure 9. Vesicle Budding and Fusion.** Vesicle trafficking involves several steps; it starts with initiation of coat assembly in the donor compartment followed by budding, scission and uncoating of the vesicle. Uncoated vesicles tethered to the acceptor compartment by the help of Rabs and tethering factors and Docks via SNARE complex (Bonifacino and Glick, 2004).

In the endocytotic pathway, materials are carried from the plasma membrane to the lysosome. The materials are delivered to tubular and vacuolar organelles from either the cell surface through endocytosis or from the TGN. Proteins internalized by endocytosis may be trafficked via late endosomes and degraded in the lysosome or returned back to the surface by recycling endosomes. (Yap *et al.*, 2009).

### 1.3. SNARE proteins and their role in membrane fusion during vesicular trafficking.

*SNAP29*, the gene that I studied during my PhD, plays a crucial role in SNARE complex

assembly during intracellular membrane fusion events; it is because of that SNARE proteins will briefly be discussed in this section.

SNARE proteins are key regulators of membrane fusion events in all trafficking steps of the secretory pathway, with the exception of extracellular membrane fusion, mitochondrial, and peroxisomal fusions (Jahn R, Scheller RH., 2006). SNAREs (Soluble N-ethylmaleimide-sensitive factor Attachment Protein REceptor) are a superfamily of small proteins that share an evolutionarily conserved stretch of 60–70 amino acids named the SNARE motif and are characterized by the ability to form a coiled-coil structure (Jahn, Scheller , 2006). SNAREs were originally classified as v-SNAREs (vesicle SNAREs) and t-SNAREs (target SNAREs) based on their location (Söllner *et al.*, 1993). However, they were reclassified later as Q-SNAREs and R-SNAREs based on which highly conserved residue, glutamine (Q) or Arginine (R), contributes to the four  $\alpha$ -helix bundle during fusion (Fasshauer *et al.*, 1998). Fusion is mediated by the formation of the trans-SNARE complex (the four  $\alpha$ -helix bundle) between SNAREs located on opposing membranes (Jahn R, Scheller RH., 2006) and is generally composed of three Q-SNAREs and one R-SNARE. It is postulated that assembly of SNAREs provides the driving force behind fusion and SNARE motifs "zip" opposing membranes from their N-terminal ends towards their C-terminal, which in turn initiates the fusion (Lin *et al.*, 1997). After the completion of fusion, all SNAREs participating in the complex are located in the fused membrane and adopt the *cis*-configuration, which is biologically inactive (Jahn R, Scheller RH., 2006). The SNARE complex is disassembled by the ATPase NSF (Söllner *et al.*, 1993) with the help of soluble NSF attachment protein (SNAP) cofactors (Figure 10; Jahn R, , 2006).

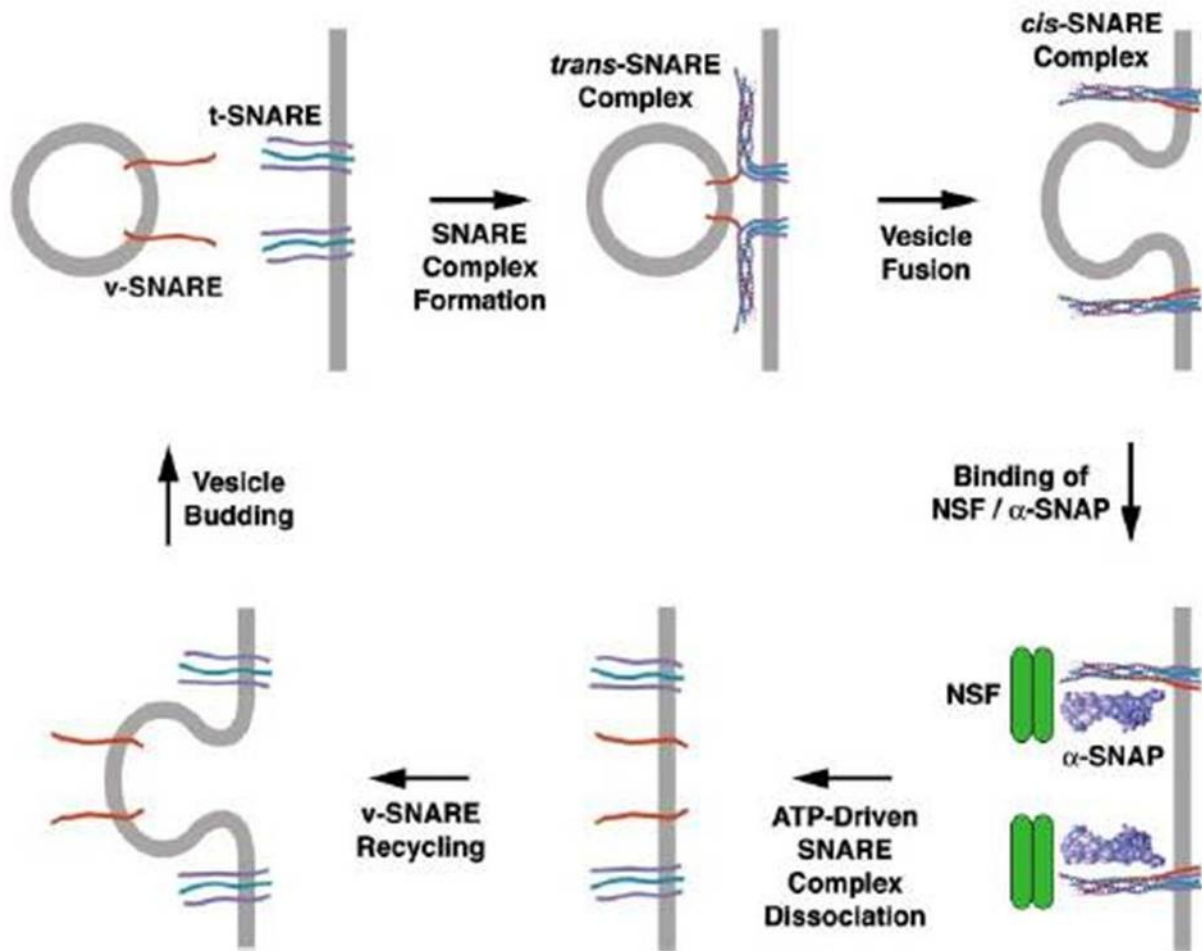


**Figure 10. Formation and disassembly of the SNARE complex.** v-SNAREs located on vesicles bind to a t-SNARE on the target membrane to form a stable four-helix bundle named a trans-SNARE complex, which drives fusion of membranes. After fusion is complete, the trans-SNARE complex becomes a cis- complex. NSF is recruited by the  $\alpha$ -SNAP that binds to the complex. NSF hydrolyzes ATP and dissociates the complex. (This figure was modified from Bonifacino and Glick, 2004).

**1.3.1. SNARE proteins mediate synaptic vesicle fusion.** Synaptic vesicles (SVs) are small vesicles located at presynaptic terminals and are filled with neurotransmitters essential for communication both between neurons and from neurons to their target tissues. Neurotransmitters are synthesized in the cytoplasm of the presynaptic terminals and are transported into SVs where they are released by calcium-triggered exocytosis. Upon receiving an electrical stimulus, voltage-dependant calcium channels open, which in turn results in an increase in the concentration of intracellular calcium. The high calcium level triggers the fusion of SVs with the presynaptic plasma membrane and subsequent release of neurotransmitters by SV exocytosis (Neher & Sakaba, 2008; Südhof, 2004). After fusion, the SVs are recycled by endocytosis, re-filled with neurotransmitters, and are used in the next cycle (Südhof, 2004, Takamori *et al.*, 2009). The fusion of SVs with the presynaptic plasma membrane during exocytosis is mediated by SNARE proteins (Südhof, 2013). SNARE complexes in SVs consist of a v-SNARE, synaptobrevin 2 (syb2), located in the vesicles and two t-SNARES, syntaxin-1 and SNAP-25, located in the target presynaptic plasma membrane (Südhof, 2004). The mechanism driving the fusion is summarized in section 1.3.

Recent studies showed that SNAP29 functions as a negative regulator of SNARE complex disassembly after fusion; the binding of SNAP29 to the assembled SNARE complex prevents the binding of  $\alpha$ -SNAP, thus preventing the disassembly of the complex and slow down the synaptic vesicle recycling (Su *et al.*, 2001).

**1.3.2. SNARE-mediated membrane fusion in autophagy.** Autophagy is the cellular pathway in which cytoplasmic materials, proteins, and organelles are enclosed in double-membraned vesicles called autophagosomes and are fused to lysosomes for degradation. During this

process, membrane fusion is a crucial step for autophagosome formation, maturation, and lysosomal degradation (Wang *et al.*, 2016). Formation of the pre-autophagosomal structure called a phagophore occurs *de novo* by nucleation of pre-existing membranes (reviewed by Rubinsztein *et al.*, 2012). These membranes, or precursor vesicles, fuse to form the phagophore via the SNARE-mediated membrane fusion mechanism that was discussed above (See section 1.3). SNARE proteins, including SNAP29, are crucial for autophagosome maturation (fusion with lysosomes). The Q-SNARE protein STX17, which is located in the external membrane of autophagosomes, interacts with SNAP29 and VAMP8 to mediate fusion between autophagosomes and lysosomes (Itakura *et al.*, 2012). It has been shown that the formation of a SNAP29-containing SNARE complex is boosted if O-GlcNAc sites of SNAP29 are disrupted, which in turn leads to increased fusion between autophagosomes and both endosomes and lysosomes, and a subsequent increase in autophagic flux (Guo *et al.*, 2014).

**1.3.3. SNAREs in development.** SNARE proteins play an important role in development as part of vesicular trafficking. Many essential developmental processes rely on proper membrane fusion, such as fertilization, cell division, and neurotransmitter release (Hepp *et al.*, 2001). SNARE proteins are found to be expressed in early developmental stages. They are produced in mammalian sperm and ovaries, where they play a role in exocytosis during fertilization (Ikebuchi *et al.*, 1998, Grosse *et al.*, 2000, Ramalho-Santos *et al.*, 2000, Hepp *et al.*, 2001).

SNAREs have also been observed in retina, lungs, brain (including the cerebellum) and in the developing neurons (Hepp *et al.*, 2001 and Osen-Sand *et al.*, 1993). Involvement of SNAREs in vesicle fusion for membrane expansion in axonal growth in the central and

peripheral nervous systems (Osen-Sand *et al.*, 1993), as well as in neurotransmission in differentiated neurons has been shown also (Osen-Sand *et al.*, 1996).

**1.3.4. Diseases associated with SNARE proteins.** As a key regulator of membrane fusion machinery and neurotransmission, SNAREs have been proposed to stand at the base of many neurodegenerative disorders, such as Alzheimer's, Parkinson's, and Huntington's diseases (Morton *et al.*, 2001, Yang *et al.*, 2015, Sharma *et al.*, 2012). Some mental disturbance-related abnormalities were also associated with SNAREs, such as bipolar disorder and schizophrenia (Honer *et al.*, 2002). SNAP25 deficiency was observed in the brain of Down syndrome patients (Greber *et al.*, 1999) and in several neuropsychiatric disturbances, epilepsy, and attention-deficit/hyperactivity disorder (Corradini *et al.*, 2009). SNAREs also have been implicated in impaired insulin secretion in type 2 diabetes (Nagamatsu *et al.*, 1999).



#### 1.4. RATIONALE, OBJECTIVES AND HYPOTHESIS

About 90% of 22q11.2DS patients have a 3 Mb deletion comprising the region that includes *SCARF2* and *SNAP29* yet existing mouse models for 22q11.2DS do not include either of these genes. It has been shown in a subset of 22q11.2DS patients that hemizygous deletion of the chromosome can uncover recessive, deleterious variants in the intact *SCARF2* or *SNAP29* alleles, resulting in craniofacial, skeletal, and neurological manifestations (Bedeschi *et al.*, 2010 and McDonald-McGinn *et al.*, 2013). Two patients with mutations in *SNAP29* and hemizygous for 22q11.2 were atypical and did not have any skin abnormalities, a hallmark of CEDNIK, while only one patient had neurological abnormalities (McDonald-McGinn *et al.*, 2013), suggesting that mutations in *SNAP29* may show variable penetrance and/or expressivity. Thus, we hypothesized that, when hemizygosity for *SCARF2* and/or *SNAP29* is present in combination or alone, it may be responsible for a subset of abnormalities found in 22q11.2DS patients, such as facial dysmorphism, skeletal and cortical malformations, and neurological defects.

Taking into consideration that the deletion found in 90% of patients comprises the region that includes *SCARF2* and *SNAP29*, that existing mouse models of 22q11.2DS do not include *Scarf2* and/or *Snap29* (Figure 5), and the fact that there are phenotypic abnormalities shared between patients with 22q11.2DS and patients with VDEGS or CEDNIK syndrome who do not carry a deletion in chromosome 22 (Table 3), we postulate that ***SCARF2* and *SNAP29* will be expressed in the precursors of tissues affected in patients with 22q11.2DS, VDEGS, and CEDNIK syndrome, and that mice with mutations in *Snap29* can be used to uncover the etiology of congenital malformations found in patients with CEDNIK syndrome and the contribution of *SNAP29* to 22q11.2DS.** To address this hypothesis, My aims were to: first analyze the expression of *Scarf2* and *Snap29* genes during organogenesis. Secondly, in order to

determine whether the loss of *Snap29* function models the abnormalities found in CEDNIK and 22q11.2DS patients, we generated and characterized abnormalities in a novel *Snap29* knockout mutant mouse line on a mixed genetic background using CRISPR/Cas9.

## CHAPTER 2. MATERIALS AND METHODS

### 2.1. Animals

All procedures and experiments were performed according to the guidelines of the Canadian Council on Animal Care and approved by the Animal Care Committee of the RI-MUHC. CD1 mice were purchased from Charles River laboratories. The *Snap29* mutant mouse line (*Snap29<sup>lam/lam</sup>*) was generated on a mixed genetic background (CD1 and FvB) and maintained on the mixed genetic background.

### 2.2. Embryo collection

CD1 mice were used for all experiments listed in the Aim 1 results section. For all other results sections, embryos were collected from the *Snap29* line, which is the mixed genetic background of CD1/FvB. The day of plug was used to indicate pregnancy and to designate embryonic day (E) 0.5. Homozygous (hmg) mutant pups and embryos were generated from mating of *Snap29* heterozygous (htz) mice. Embryonic samples from mice at developmental stages E7.5-E17.5 were collected. Briefly, deciduas or embryos were removed from the uterus of pregnant females after mating to males at the appropriate stage, the yolk sac was used for genotyping, embryos or deciduas were fixed in 4% PFA overnight and were stored in PBS.

### 2.3. Cloning and probe generation

*In situ* probe for *Scarf2* and *Snap29* were generated from E10.5 CD1 embryos, RNA was extracted from the embryos using TriZOL (Invitrogen) according to the manufacturer's instructions. SuperScript® II Reverse Transcriptase (Thermo Fisher Scientific) Kit was used to synthesize a complementary DNA (cDNA). Primers were designed and used to amplify exons 1-

4 of *Scarf2* and exons 2-5, including 207 bp of the 3' UTR of *Snap29*. Primers used: *Scarf2*fwd: GACTGCTGCTGCTGCTCTG and *Scarf2*rev: GATCGCACCGGGAAGTAG, *Snap29*fwd: AGCCCAACAGCAGATTGAAA and *Snap29*rev: AAAACTCAGCAGAACAGCTCAA. The cDNA fragment was cloned into TOPO using a TA Cloning Kit (Invitrogen). The cloned cDNAs were verified by Sanger sequencing. DIG RNA Labeling Mix (Roche) was used to produce digoxigenin labeled probes, according to the manufacturer's instructions. Sense and antisense probes were linearized using KpnI-HF and XbaI enzymes, respectively (BioLabs). SP6 and T7 polymerases (Roche) were used to produce sense and antisense probes, respectively.

## **2.4. *In situ* hybridization**

E7.5-E14.5 embryos were collected from pregnant CD1 females, fixed in 4% paraformaldehyde overnight at 4°C and dehydrated in methanol (for whole mount) or ethanol (for *in situ* sections). For *in situ* hybridization on sections, deciduas and embryos were serially sectioned at 5 µM. Antisense probes were used to detect the expression of *Scarf2* and *Snap29*, and sense probes were used as a control. Protocols used for whole mount or sectioning *in situ* hybridization were previously described (Revil *et al.*, 2013).

## **2.5. Generation of *Snap29* knockout mice line using CRISPR/Cas9**

The *Snap29* knockout mouse line (*Snap29<sup>lam1</sup>*) was generated on a mixed genetic background (CD1 and FvB) using CRISPR/Cas9 methodology (Henao-Mejia *et al.* 2016). Briefly, four guide RNA (gRNA) sequences flanking exon 2 of the mouse *Snap29* gene (gRNA1 and gRNA2 located in intron 2 and gRNA3 and gRNA4 located in intron 3) were designed using the online services of Massachusetts Institute of Technology (<http://crispr.mit.edu>). The gRNAs

were synthesized using GeneArt Precision gRNA Synthesis Kit (Thermo Fisher Scientific). 50ng/ul Cas9 mRNA (Sigma) together with the 4 gRNAs (6.25ng/μl) were microinjected into the pronucleus of fertilized eggs collected from the mating of wild type (WT) CD1 and FvB mice. Injected embryos were transferred into uteri of pseudopregnant foster mothers (CD1, Charles River laboratories).

## **2.6. Genotyping**

Standard polymerase chain reaction (PCR) was used for genotyping. Three primer PCR (Right primer: GACTGAGTCTCACCTGGTCC, Left primer1: TGGCTTTTGGGAATGACTTG, Left primer3: CCATTCTGCTCAGGTGGAG) enabled detection of embryos and pups carrying the wild type (750 and/or 435 bp amplicons) or mutant allele (240 and 300 bp amplicons).

## **2.7. Western Blot (WB)**

Western blot was performed as previously described (Jerome-Majewska *et al.*, 2010, Gupta *et al.*, 2016). Briefly, lysates from postnatal day 1 (P1) dorsal skin were collected in 1× RIPA lysis buffer. Sodium dodecyl sulfate polyacrylamide gel electrophoresis (SDS-PAGE) was used to resolve the equal amounts of protein, which was then transferred to a polyvinylidene fluoride (PVDF) membrane, Bio-Rad). 5% non-fat dry milk in PBST (Phosphate-buffered saline with Tween 20) was used to block membranes followed by incubation with primary and secondary antibodies. The ECL plus Western Blotting Detection System (GE Healthcare) was utilized to detect the immunoreactive bands and images were taken with Bio-Rad's ChemiDoc MP System (catalog # 1708280). The obtained bands were digitally analyzed using ImageJ software (Image lab Version: 5.2.1 12 7847). The following antibodies were used: SNAP29

rabbit monoclonal antibody (1:5000, AbCam), and beta-actin (1: 5000, Cell Signalling), anti-rabbit secondary antibody (1:5000, Cell Signalling) was used as a loading control.

## **2.8. Hematoxylin and Eosin (H&E) Staining**

Whole brains isolated from E12.5 and E17.5 embryos, whole embryos collected from E12.5 and E14.5 litters, and dorsal skin from E16.5 and P1 stages were fixed in 4% paraformaldehyde overnight at 4°C. Samples were then dehydrated in ethanol, embedded in paraffin, and serially sectioned at 5µm thicknesses on a microtome (Leica RM2155). Subsequently, the sections were stained with H&E according to the previously published protocol (Cardiff *et al.*, 2014).

## **2.9. Skeletal preparations**

Alcian blue/Alizarin red skeletal and cartilage preparations were used to stain skeleton and cartilages of E14.5, E16.5, P1 and P3 pups (Hogan *et al.* 1994, Mallo *et al.* 1997 and protocol from Steve Rodda of McMahon Lab (available online)). Briefly, whole mount E14.5 and E16.5 embryos and P3 pups were treated with ethanol and acetone for 24 hours after eviscerating and removal of skin (for E16.5 and P3 animals) and stained with Alcian Blue/Alizarin Red stain (Sigma) for 3-4 days at 37°C on a rocker. Stained embryos and pups were incubated in 1% KOH for 72-96 hours and washed with 1% KOH/glycerol mixture.

## **2.10. Body and brain measurements**

Length of body, head and brain measurements were done either by standard ruler or using the Infinity Analyze program (release 5.0.2. Luminera Corporation, Figure 22 C). Pictures

obtained from the dorsal view of brains were used to measure length, diameter and perimeters of regions of the brains, as shown in Figure 33. The ratio of brain weight to body weight was calculated to normalize the measurements.

### **2.11. Nissl Staining**

Coronal sections (5  $\mu$ m) of E17.5 wild type and homozygous *Snap29* mouse embryonic brains were used. These sections were stained with cresyl violet by the histopathology core of the MUHC (McGill University Health Center).

### **2.12. Immunohistochemistry and histological staining for cortex**

Paraffin sections (E17.5, coronal, 6 mm) were used for immunohistochemistry as previously described with slight modification (Lim *et al.*, Exp Neurology, 2010, 221 (1):86-97). Briefly, after deparaffinization and rehydration, the sections were incubated with 1% H<sub>2</sub>O<sub>2</sub>/methanol for 10 min. Antigen retrieval was performed by incubating sections at 100°C in 0.01M citric acid for 10 min. Sections were blocked with 10% goat serum for 1 hr, incubated with primary antibodies at 4°C overnight, and then incubated with the appropriate secondary antibody conjugated with biotin (1:1000, Vector Lab) at RT for 1 hr. Finally, the antibodies were detected using the ABC kit (1:1000, Vector Laboratories, PK-6100) at RT for 1 hr. For antigens of nuclear proteins, sections were treated with 0.5% triton X-100 for 10 min before the blocking step. The signal was detected with immPACT DAB (Vector Laboratories, SK-4105) and each section was counterstained with diluted Hematoxylin (1:30, Leica Biosystems, 3801570). The primary antibodies used in this study are TBR1 (rabbit, 1:1000, Abcam, ab31940), CTIP2 (rat,

1:200, Abcam, ab18465), Reelin (mouse, 1:200, Milipore, MAB5364), and SATB2 (mouse, 1:200, Bio Matrix Research, BMR00263).

### **2.13. BrdU and EdU injection**

Pregnant mice were injected with BrdU (50 mg/kg, i.p.) at E12.5 and E13.5, and with EdU injection (50 mg/kg, i.p.) at E14.5 and E15.5, respectively. Embryos were collected at E17.5 and fixed in 4% PFA for 48 hours.

### **2.14. BrdU and EdU staining**

Paraffin sections (E17.5, coronal, 6 mm) were used for BrdU and EdU double staining. After deparaffinization and rehydration, antigen retrieval was performed as described above (section 2.12). The sections were treated with 2N HCl for 30 min at RT, 0.1M sodium tetraborate for 10 min, and finally with 0.5% Triton X-100 for 10 min. After blocking with 10% goat serum for 1 hr, the primary anti-BrdU antibody (Abcam, ab6326, 1:100 in 1% goat serum/PBS) was incubated for 4°C overnight. Goat anti-rat IgG-Alexa Fluoro 594 (1:200, Invitrogen) was applied as a secondary antibody for 1 hr, followed by Click-iT reaction cocktail (Alexa Fluoro 488, Invitrogen, C10337) for 30 min according to the manufacturer's recommendation. Hoechst 33342 was used for nuclear staining.

### **2.15. Cell counting**

Two serial sections from 3 WT or 4 mutant (Mut) E17.5 embryos were used for quantification of each cortical layer marker (total 6 sections for WT and 8 sections for Mut). 10x images were taken from the cortical sections (at the level of internal capsule) and the boxed area



shown in Figure 38 A was selected (200 mm wide) and divided into 8 different layers (with an equal distance between layers) spanning from the pial surface to the intermediate zone (Grids 1-8; 1 being closest to pial surface). The ventricular and subventricular zones were excluded. TBR1, CTIP2, SATB2 positive cells were counted using Automatic Threshold (Yen) in Image J and Reelin positive cells were counted using Manual Threshold (Yen). Total cells (Hematoxylin positive) were counted using Automatic Local Threshold (Otsu). The percentage of TBR1+/total, CTIP2+/total, SATB2+/total cells was plotted for each of the 8 layers. Error bars are Mean +/- SEM. The percentage of Reelin/total cells was plotted for Grid 1 (Error bars are Mean +/- SD). Multiple t-tests were performed in Prism 8. The differences between WT and Mut are not statistically significant for all the layer markers tested here.

## **2.16. Magnetic resonance imaging (MRI)**

The MRI studies were performed using Bruker Biospec 70/30 preclinical MRI scanner with a mouse head surface coil. The 3D anatomical images were obtained using a steady-state free precession (SSFP) balanced sequence [repetition time (TR)/echo time (TE) = 5.9 millisecond /3.0 millisecond, flip angle = 30 degree, resolution = 0.110 x 0.110 x 0.110 mm, field of view = 18 x 18 x 9 mm].

## **2.18. Grip strength measurement**

Mice were held by the base of their tail and lowered toward the mesh of the grip strength meter (Bioseb Model GS3). After they grasped it with their forepaws, the body of the mouse was lowered to be at a 45 degree position with the mesh. The mouse was then pulled by the tail away

from the mesh until the grip was broken. Nine trials were performed for each mouse and the average was used as the grip strength score for that mouse (Tanaka *et al.*, 2017).

### **2.19. Rotarod**

Rotarod (47600, KYS Technology, UGO Basile S.R.L, Italy) testing was performed as previously described (Dorninger *et al.*, 2017). Briefly, mice were tested on an accelerating rotarod mode (4-40 rpm in 300 sec) for 500 sec. The latency to fall (in seconds) was recorded. Two rotations in the cylinder were considered as a fall. Each mouse had 3 days training with 3 trials per day and the fourth day was the experimental day. The mean value of the three trials on the experimental day was used for statistical analysis.

### **2.20. CatWalk Automated Quantitative Gait Analysis**

The CatWalk program (CatWalk XT 10.6, Noldus, Leesburg, VA. USA) was used to analyze the gait of the mice according to the manufacturer's instructions and published procedures (Hamers *et al.*, 2006). Animals were trained for 3 days before the final measurements were collected. A minimum of 3 compliant runs were acquired with the following run criteria: Min. Duration: 0.5 sec, Max. Duration: 8 sec, Max. Variation: 60%, Min. Number of Compliant Runs: 3. Parameters of acquisition are as follows: Camera Gain: 15 db, Green Intensity Threshold: 0.3, Red Ceiling Light: 17.4 V, Green Walkway Light: 16 V, Camera Position: 24 cm from the glass. The mean of all compliant runs per mouse was used to calculate the gait of mice within different groups, according to sex and genotype. Comparisons were made for each training day (day 1-3), for the actual experimental day (day 4) and for the total of all 4 days. All three categories of gait parameters as classified in Hamers *et al.*, (2006) (parameters related to

individual paws, the position of footprints, and the time-dependent relationship between footprints) were assessed.

### **2.21. Testis collection and histology**

WT or *Snap29<sup>lam/lam</sup>* male mice were euthanized and testes were dissected, weighed and fixed immediately with Bouin fixative for 24 hours. The tissue was processed using routine paraffin embedding methods. Paraffinized tissue blocks were sectioned at 5µm thickness and stained with haematoxylin and eosin (H&E).

### **2.22. Perfusion**

2.5% glutaraldehyde in sodium cacodylate buffer was used to perfuse the P1 mice. The collected tissues were kept in the cacodylate buffer at 4°C before proceeding to Transmission Electron Microscopy.

### **2.23. Transmission Electron Microscopy (TEM)**

TEM was performed as previously described (Khatchadourian *et al.*, 2007) using FEI Tecnai 12 BioTwin 120 kV TEM imaged with an AMT XR80C CCD Camera System.

### **2.24. Statistical analysis**

Analyses were performed with Prism 8. Before applying ANOVA analysis, we determined whether the data fit a Gaussian distribution using A D'Agostino-Pearson normality test. A pairwise post-hoc Tukey HSD followed to assess which genotype statistically differ from the others. When data did not fit a Gaussian distribution, a Kruskal-Wallis test was performed,

followed by a Dunn's test post-hoc test to determine statistical difference. The  $\alpha$  level for all tests was 0.05.

## **CHAPTER 3. RESULTS**

### **3.1. Aim 1. Characterize mRNA expression of *Scarf2* and *Snap29* during mouse organogenesis**

We hypothesized that *SCARF2* and *SNAP29* genes will be expressed in precursors of tissues affected in their associated syndromes; 22q11.2DS, VDEGS and CEDNIK syndrome. Since mouse and human development are similar, we expected that the two genes will be expressed in the structures affected in human. In order to test this hypothesis, the mRNA expression of *Scarf2* and *Snap29* genes were examined in developing mouse embryos between E7.5-E14.5. Probes containing cDNA fragments of *Scarf2* and *Snap29* were used in order to detect the expression of the genes during mouse embryonic stages. Whole mount (WMISH) and section *in situ* hybridization techniques were utilized according to standard protocols (Section 2.4).

#### **3.1.1. *Scarf2* is broadly expressed during mouse organogenesis with stronger expression in primordium of cartilages**

WMISH revealed mRNA expression of *Scarf2* in the head fold and mesoderm of the embryo, as well as in extraembryonic tissues; the amnion, allantois and chorionic plate at E7.5 (Figure 11A). However, no expression was detected at stage E8.5 (Figure 11 B) using this technique.

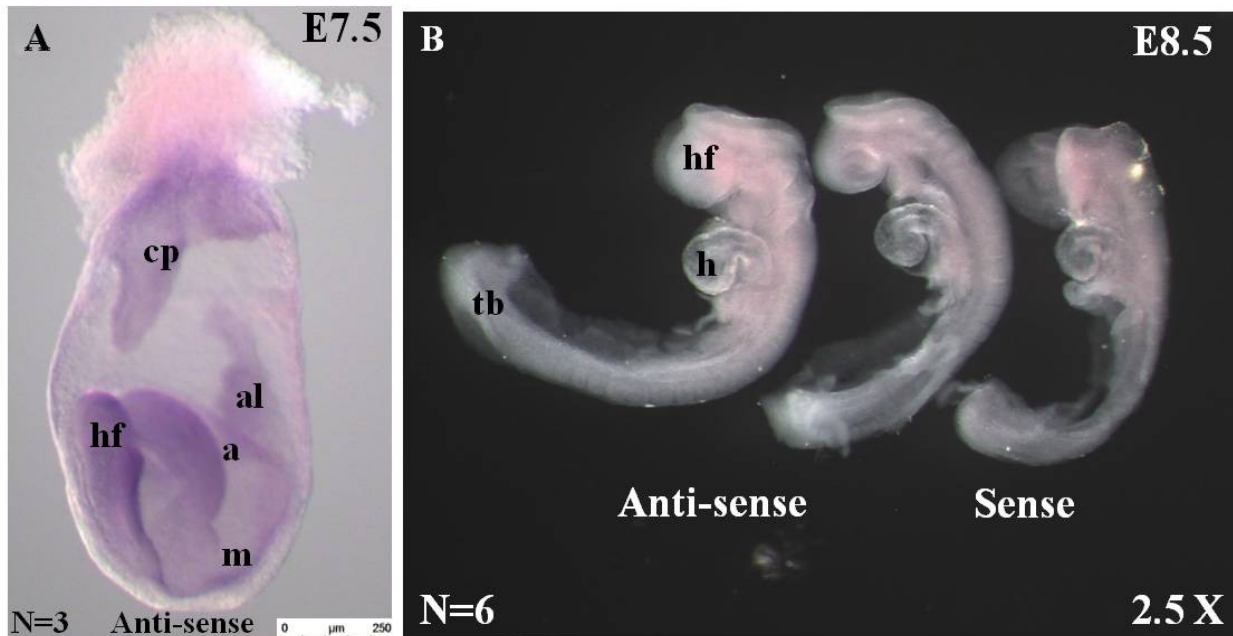


**Figure 11. WMISH results at E7.5 and E8.5 for *Scarf2*.** A. *Scarf2* mRNA was detected in embryonic and extraembryonic tissues at E7.5 by WMISH. B. No *Scarf2* expression was detected at stage E8.5. hf, headfold; m, mesoderm; a, amnion; al, allantois; cp, chorionic plate; h, heart; tb, tail bud (figures are not to scale).

At E9.5, expression was present in the developing brain, branchial arches, olfactory placode, optic and otic vesicles, heart, neural tube, somites and in the forelimb bud (Figure 12 A). *Scarf2* was broadly expressed at E10.5 with higher expression in the craniofacial region, including the olfactory placode, optic and otic vesicles, maxillary component of the first branchial arch, and branchial arches. Expression has also been observed in the mesencephalic floor plate region, the boundary of the mid and hindbrain, heart, somites, both limb buds, and cranial ganglia (Figure 12B). At E11.5, similar to E10.5, high expression was recorded in the

mesencephalic floor plate region, the boundary of the mid and hindbrain, olfactory placode, optic and otic vesicles, both fore and hind limbs, maxillary component of the first branchial arch, branchial arches, heart, somites, and cranial ganglia (Figure 12C).

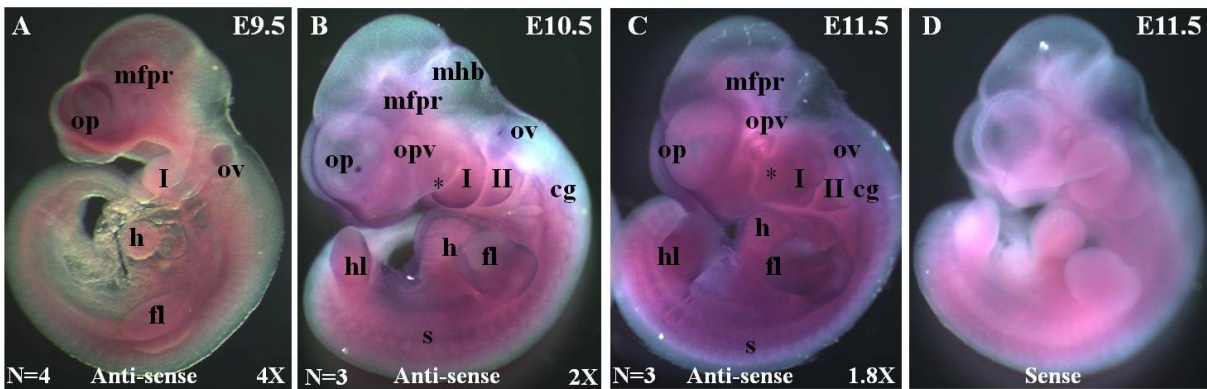


**Figure 12. E9.5-E11.5 WMISH results for *Scarf2*.** A-D *In situ* hybridization reveals broad expression of *Scarf2* at E9.5 to E11.5 with higher expression in the craniofacial region, pharyngeal arches, olfactory placode, optic vesicle, limb buds, and cranial ganglia. op, olfactory placode; opv, optic vesicle; mfpr, mesencephalic floor plate region; mhb, boundary of mid and hindbrain; ov, otic vesicle; fl, fore limb; hl, hind limb; \*, maxillary component of the first branchial arch; I, II, branchial arches; h, heart; s, somites; cg, cranial ganglia (figures are not to scale).

Section *in situ* at E10.5 confirmed presence of *Scarf2* in many tissues including foregut, neural tube; heart, aorta, and midgut (Figure 13A). At E12.5, expression was observed in certain regions by WMISH, such as the craniofacial region, including tongue and palate (Figure 13B).

*Scarf2* also was expressed in limbs, pinnae, neural tube and cartilage primordium of ribs and vertebrae in the body (Figure 13C).

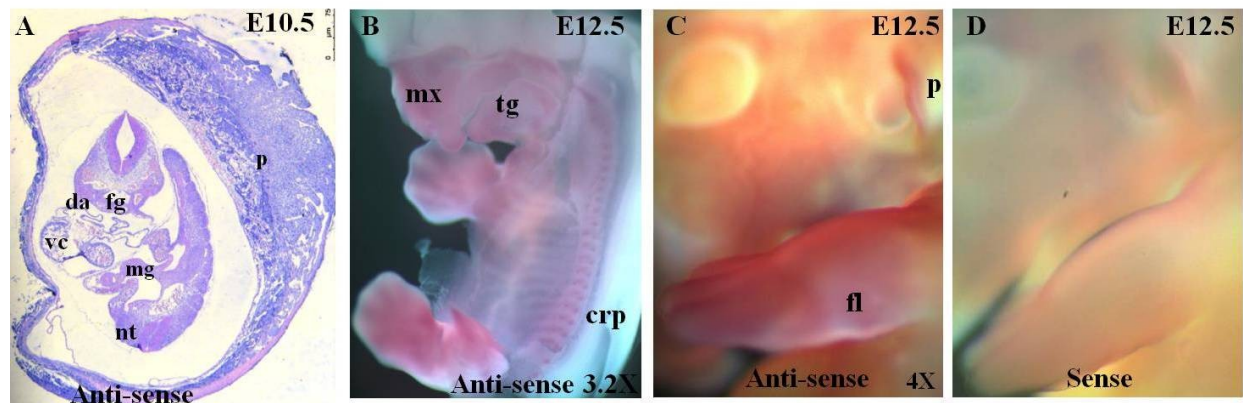


**Figure 13. Expression of *Scarf2* mRNA in E10.5 and E12.5.** A. Section *in situ* at E10.5 detected *Scarf2* in many tissues including foregut, neural tube; heart, aorta, midgut, and placenta. At E12.5 WMISH showed expression in the craniofacial region, including tongue and palate, limbs, pinna, neural tube and cartilage primordium of ribs and vertebrae. fg, pharyngeal region of foregut; nt, neural tube; vc, common ventricular chamber; da, right dorsal aorta; mg, midgut; p, placenta; mx, maxilla; tg, tongue; cpr, cartilage primordium of ribs; mhb, boundary of mid and hindbrain; p, pinna; fl, fore limb.

At E13.5, *Scarf2* showed expression in many tissues in the different parts of the body, as shown in Figures 14, including the craniofacial region, fore, mid and hind brains, tongue, palate, maxilla and mandible, lower incisor tooth bud, thyroid gland, heart, liver, lungs, kidneys, upper cervical dorsal root ganglion, limbs, pinnae, neural tube, tibia, fibula, cartilage primordia of ribs



and vertebrae, and the placenta. Strong cartilage-specific expression was noted in cartilage primordia of certain facial bones, such as the hyoid, temporal, basisphenoid, and turbinate bones, as well as the shaft of the upper ribs and first costal cartilage (Figure 14A and B).

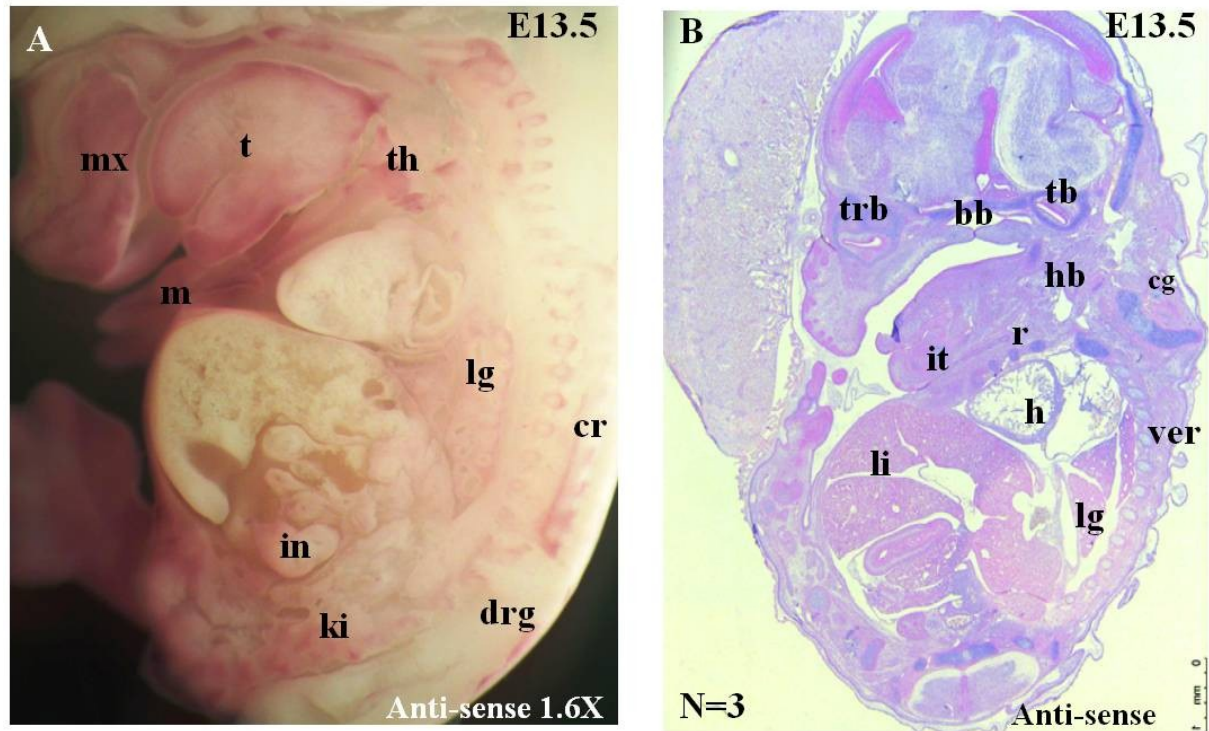


**Figure 14. E13.5 *in situ* results for *Scarf2*.** A. WMISH and B. *in situ* hybridization of whole embryo sections detected a broad expression pattern of *Scarf2* at E13.5. *In situ* sections revealed that *Scarf2* is expressed in the cartilage primordia of different bones in various parts of the E13.5 embryo (including primordia of craniofacial bones, vertebra, and ribs) consistent with bone malformation found in VDGEs patients (dark purple regions in B). mx, maxilla; m, mandible; tg, tongue; th, thymus; lg, lung; ki, kidney; cr, cartilage primordium of ribs; drg, dorsal root ganglia; in, intestine; hb, hyoid bone; ver, vertebra; tb, temporal bone; r, ventral part of shaft of ribs; it, lower incisor tooth; h, heart; trb, turbinate bones; cg, upper cervical dorsal root ganglion; tb, ossification within cartilage primordium of mid shaft region of tibia; fb, ossification

within cartilage primordium of mid shaft region of fibula; bb, basisphenoid bone; lg, lung; li, liver.

At E14.5 expression is detected only in extremities of digits and pinna using WMISH (Figure 15).

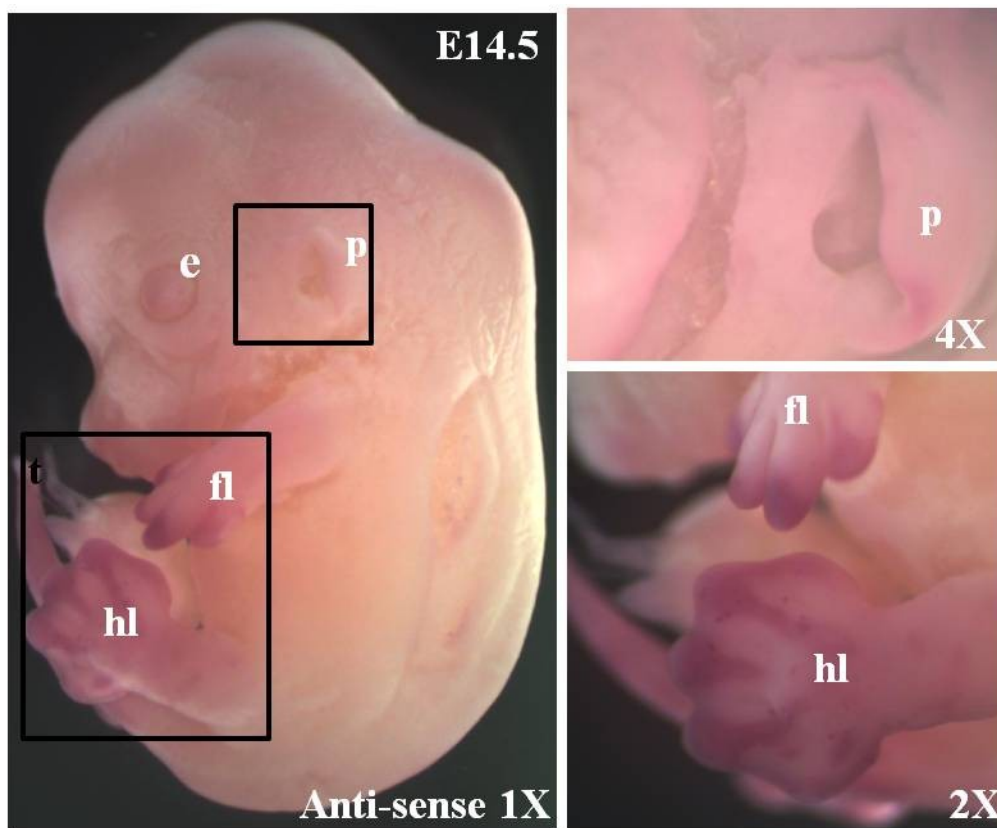


**Figure 15. E14.5 WMISH results for *Scarf2*.** At E14.5, digits and pinna specific. expression is revealed by WMISH. e, eye (e); p, pinna; fl, proximal region of fore and hl, hind limbs

In a summary, *Scarf2* is a broadly expressed gene during development; it is expressed in precursors of tissues affected in VDEGS patients, including branchial arches that will give rise to the craniofacial structures and the somites that will form the cartilage of the vertebrae and ribs, as well as the muscles of the rib cage, limbs, and back. Expression of this gene is higher in cartilage primordia of different bones in various parts of developing mouse embryo, including primordia of craniofacial bones, vertebra and ribs at E13.5, structures that are severely malformed in VDEGS patients. However, the expression of the gene is detected in tissues not known to be affected in the patients, such as liver and lungs.

### **3.1.2. *Snap29* mRNA is ubiquitously expressed during mouse embryogenesis**

WMISH showed expression of the gene in the head fold and mesoderm of the developing embryo, as well as in extraembryonic tissues: the amnion, allantois, and chorion at E7.5 (Figure 16A and B). High expression of *Snap29* was detected in the developing craniofacial region, secondary heart field and tail bud of E8.5 embryos (Figure 16 C).

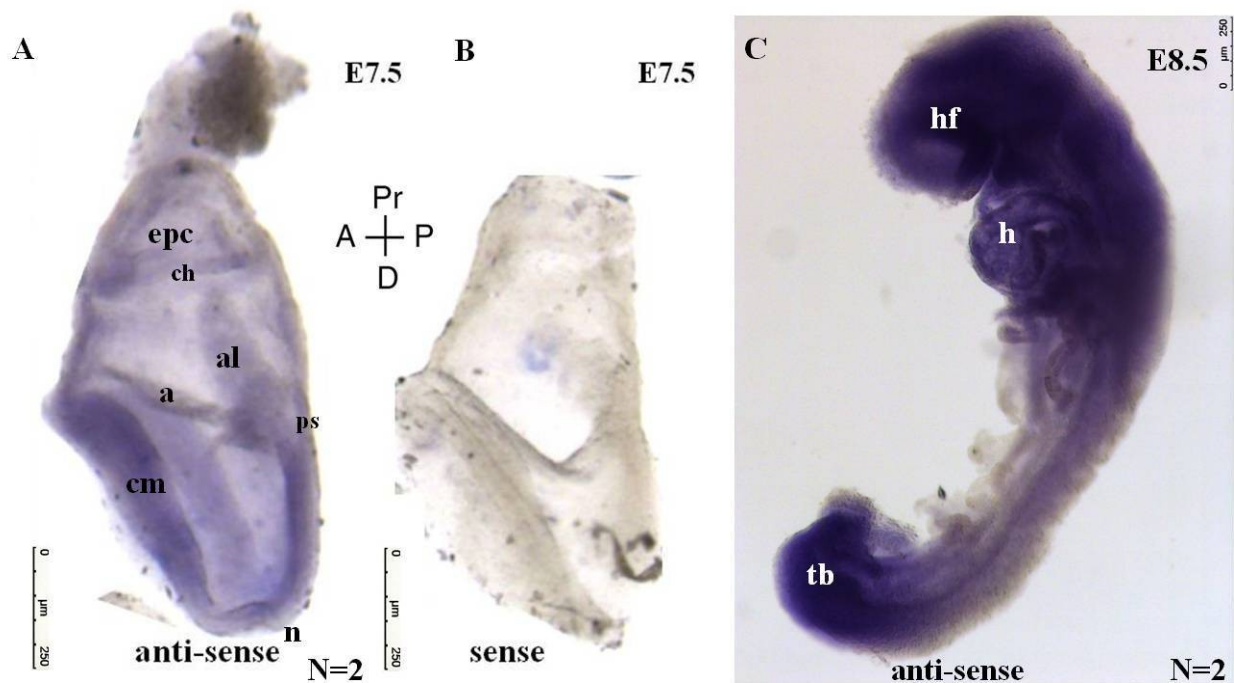


**Figure 16. E7.5-E8.5 WMISH results for *Snap29*.** A. *In situ* hybridization reveals expression of *Snap29* in embryonic and extraembryonic regions at E7.5, B. The sense control does not show any staining. C. At E8.5 strong expression is observed in head folds, heart and tail bud region. epc, ectoplacental cone; ch, chorion; al, allantois; a, amnion; cm, cranial mesenchyme; n, node; ps, primitive streak.

At E9.5 expression is visible in the developing craniofacial region, olfactory placode, optic and otic vesicles, somites, neural tube, and fore limb bud (Figure 17A). Ubiquitous expression of the gene was detected at E10.5 by WMISH (Figure 17B).

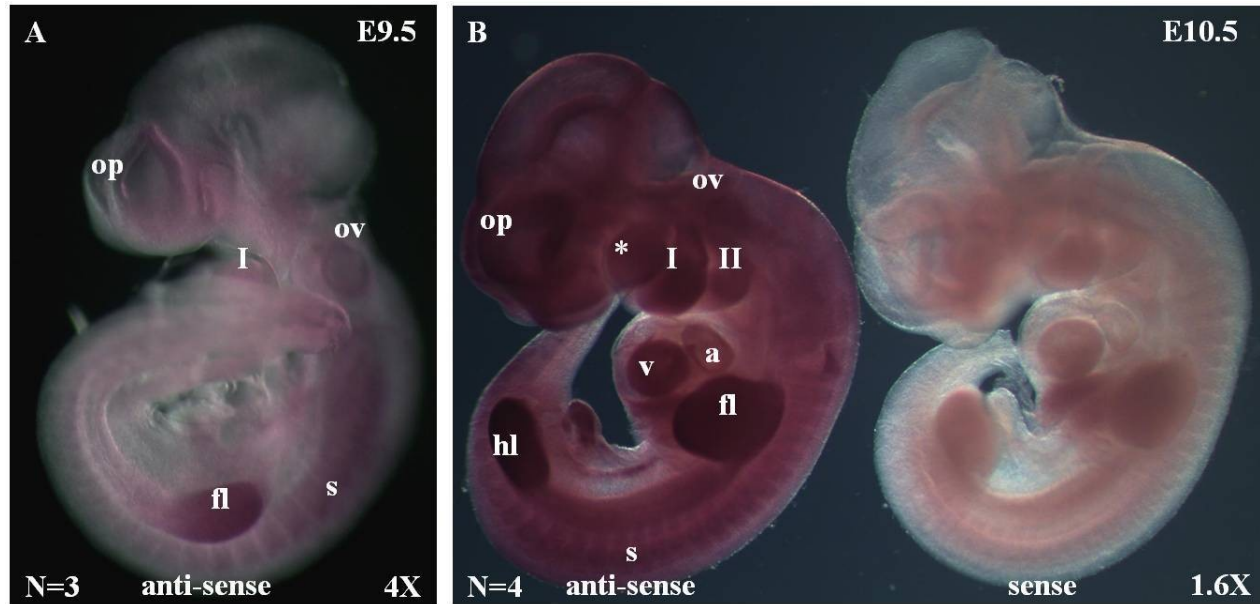


**Figure 17. E9.5 and E10.5 WMISH results for *Snap29*.** A. WMISH shows expression of *Snap29* in the olactory placode, 1<sup>st</sup> brancial arch, otic vesicle and somites at E9.5. B. Ubiquitous expression at E10.5. op, olfactory placode; ov, otic vesicle; I, II, branchial arches; v, ventricle; a, atrium; \* maxillary component of the first branchial arch; fl forelimb; hl, hindlimbs; s, somites.

*In situ* hybridization on sections of E10.5 embryos confirmed that *Snap29* was expressed in all structures (Figure 18A). *Snap29* expression was found to be ubiquitous in E12.5 sections (Figure 18 B and C) as well. However, the signal was less in the mid lens and midline neural retina of the eyes, the central neural tube, and the mid dorsal root ganglia compared to other tissues (Figure 18 B and C).



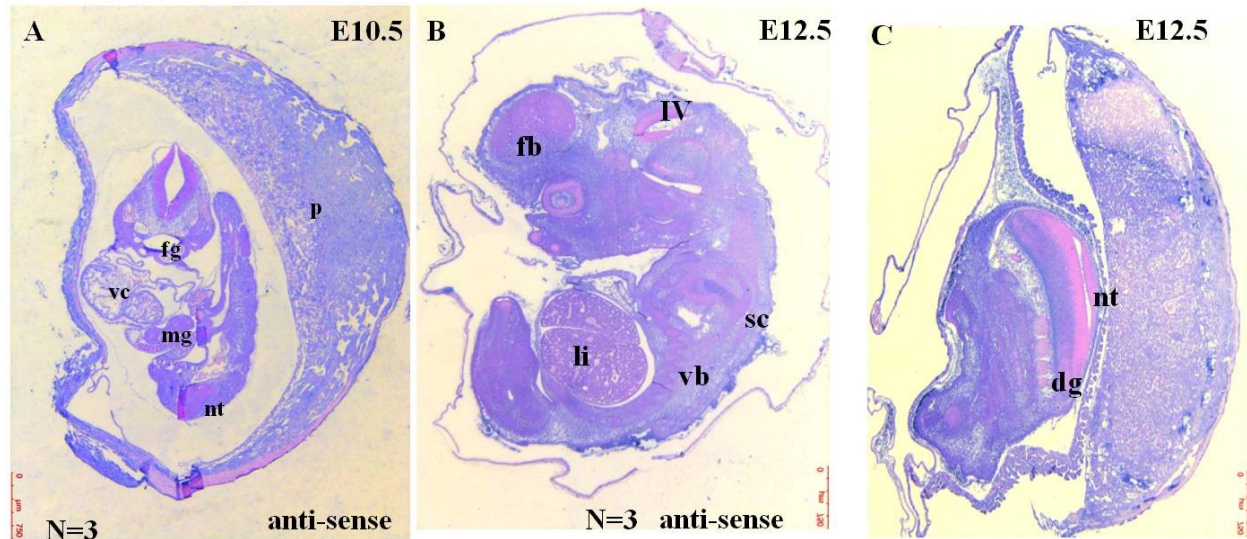


**Figure 18. Section *in situ* results for *Snap29*.** A. Section *in situ* hybridization on whole embryo sections confirms ubiquitous expression of *Snap29* mRNA in E10.5. B. Ubiquitous expression is also observed at E12.5. fg, pharyngeal region of foregut; nt, neural tube; vc, common ventricular chamber; da, right dorsal aorta; mg, midgut; p, placenta; fb, fore brain, iv, 4<sup>th</sup> ventricle; li, liver; vb, vertebra body; dg, mid dorsal root ganglia; nt, central neural tube.

To summarize, *Snap29* mRNA was found to be expressed in precursors of tissues malformed in patients, including the branchial arches, the developing brain, otic and optic vesicles that will contribute to the development of the middle ear and eye, palate, and overlying ectoderm that will form the skin, as well as in many other tissues.

**3.1.3. Aim 1. Summary:** Expression of the *Scarf2* and *Snap29* genes was analysed before and during organogenesis, E7.5-E14.5. We found that both genes are expressed in the embryonic precursors of organs that are affected in human patients with mutations in these genes. In

addition, expression was observed in a number of additional sites not known to be affected in patients.

## **3.2. Aim 2. Generation and characterization of the *Snap29* mutant mouse line on a mixed genetic background**

**3.2.1. Homozygous deletion of exon 2 results in a protein null mutation in *Snap29* embryos and mice.** *Snap29* gene was chosen to be investigated further because patients with mutations in *Snap29* gene have severe congenital malformations in multiple tissues showing the importance of the gene in many developmental pathways.

Mouse models with a mutation in *Snap29* on the inbred C57 genetic background were previously reported to die a few hours after birth with severe skin abnormalities (Schiller *et al.*, 2016). However, no additional systems or organs were examined. In addition, since *Snap29* was not included in 22q11.2DS mouse models, we generated a novel mutant mouse line for *Snap29*, on a mixed genetic background. To do so we used the CRISPR/Cas-mediated genome engineering technique. Two pairs of single guide RNAs (sgRNAs) flanking exon 2 of *Snap29* were chosen according to their highest score (scored by the online services of Massachusetts Institute of Technology according to the possible offtargets and specificity) and nucleotide preference (Figure 20A; Xu *et al.*, 2015). To test sgRNAs they were microinjected into blastocysts. PCR based genotyping (with primers designed outside of the deleted region) showed successful exon 2 deletion in lysates of 4/8 blastocysts. To generate the mouse line, Cas9 mRNA and two pairs of the tested sgRNAs were injected into mouse zygotes on a mixed genetic background (CD1/FvB). Of the 14 mice born from microinjections, four carried the desired exon 2 deletion in heterozygosity (*Snap29*<sup>lam1/+</sup>). 3 females carrying the deletion were mated to wild type CD1 males to establish a colony. Sanger sequencing was used to confirm that mice used to



establish the *Snap29* mutant colony carried the deletion. The deletions covered 459 bp and 539 bp, indicating that all 4 sgRNAs cut (Figure 19).

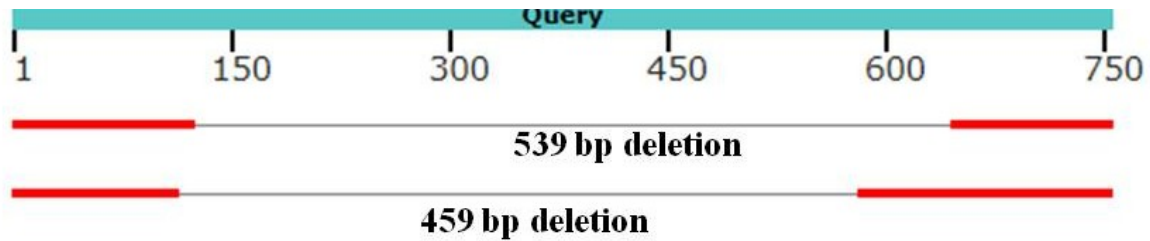


**Figure 19. Alignment of the deletions with the original *Snap29* genomic DNA sequence.** Using 4 sgRNAs two different mouse lines with deletion of *Snap29* exon 2 were obtained. Alignment was performed by Basic Local Alignment Search Tool (BLAST) in National Center for Biotechnology Information (NCBI) center.

Analysis of *Snap29* mutant embryos and pups with deletions generated using the two different sgRNAs revealed a similar penetrance and expressivity after 7 generations of backcrossing to the outbred CD1 genetic background, therefore, these numbers have been combined.

To determine the level of SNAP29 protein expression after the deletion, western blot analysis was performed. Western immunoblotting showed that SNAP29 was reduced in protein lysates obtained from the skin of P1 heterozygous pups and absent in homozygous pups (Figure 20 B and C).

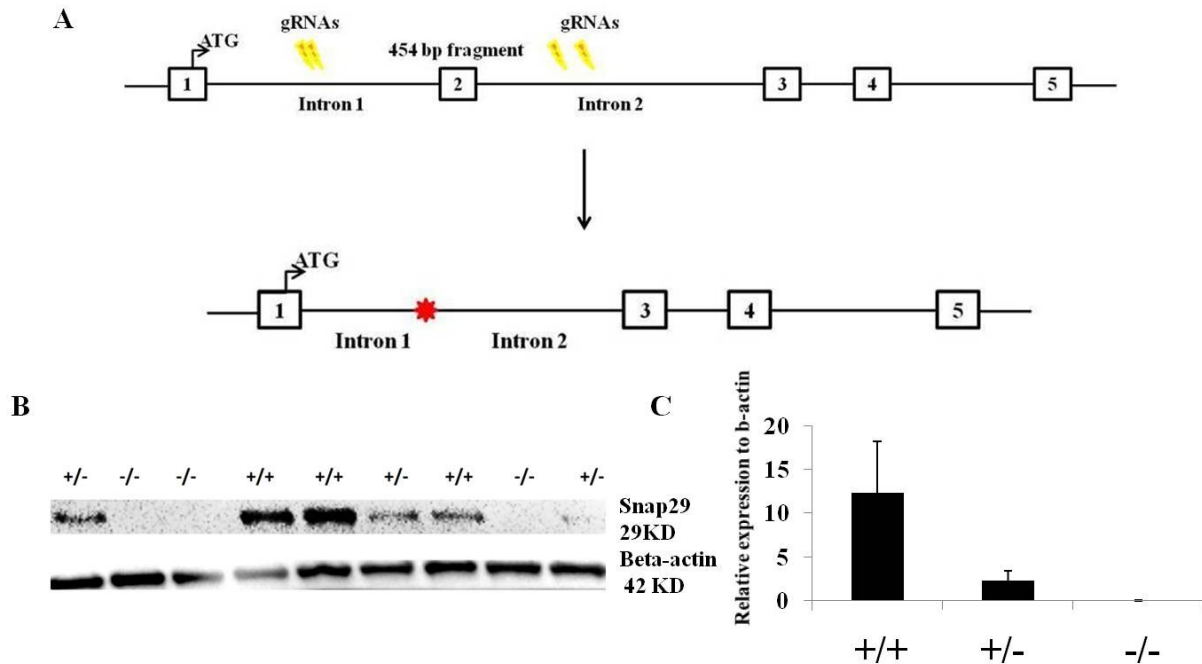


**Figure 20. Deletion of exon2 results in a protein null mutation in *Snap29* homozygous mutant embryos and pups.** A. Location of 4 different sgRNAs flanking exon 2 (indicated in yellow) used to generate a deletion (red star) in *Snap29*. B. A representative western blot shows SNAP29 protein is reduced in skin lysates from P1 heterozygous pups and absent in homozygotes. C. Levels of SNAP29 relative to beta-actin wt, wild type; htz, heterozygous; hmz, homozygous mutant.

**3.2.2. Homozygous *Snap29* knockout mice on a mixed genetic background (CD1/FvB) survive to adulthood.** We evaluated Mendelian segregation at different stages since previous knockout models with exon 2 deletion were reported to die a few hours after birth (Schilleret *al.* 2016). At birth, normal Mendelian segregation of the mutant allele was found after mating of heterozygous males to wild type CD1 females or their heterozygous littermates (Table 6).

**Table 6. Mendelian segregation of the mutant *Snap29* allele**

<b>matings</b>	<b>wt</b>	<b>htz</b>	<b>hmz</b>	<b>total # of embryos and pups</b>	<b>NT (resorptions)</b>	<b>#litter</b>	<b>chi square</b>	<b>P- value</b>
<b>htz x htz</b>	<b>339</b>	<b>617</b>	<b>349</b>	<b>1484</b>	<b>173 (27)</b>	<b>118</b>	<b>4.016</b>	<b>0.1343</b>
<b>htz x CD1</b>	<b>210</b>	<b>238</b>		<b>455</b>	<b>7</b>	<b>36</b>	<b>1.750</b>	<b>0.1859</b>

The *Snap29* allele segregates at the expected Mendelian frequency after mating of heterozygous brothers and sisters (htz x htz) and mating of heterozygous male mice to wild type CD1 females (htz x wt). wt, wild type; htz, heterozygous; hmz, homozygous mutant; NT, not typed.

*Snap29*<sup>lam1/+</sup> heterozygous mice showed no apparent morphological abnormalities, survived to adulthood, and were fertile. 67.5% of *Snap29*<sup>lam1/lam1</sup> homozygous mutant mice survived to weaning and adulthood (Table 7 and 8), unlike homozygous mutants carrying a deletion of exon 2 on the inbred C57BL/6 genetic background (Schiller *et al.*, 2016). Thus, presumably genetic modifiers on the mixed genetic background allowed mice with a loss-of-function mutation in *Snap29* to survive to adulthood, thus facilitating studies aimed at determining if phenotypic abnormalities found in human patients with mutations in *SNAP29* are modeled in *Snap29* mutant mice.

**Table 7. *Snap29* genotype distribution of embryos and offspring in pre and postnatal periods**

stage	wt	htz	hmz (dead)	not typed	# embryo/pup	#litter	chi square	p value
E11.5	28	45	29	25	127	9	1.431	0.4889
E16.5	36	51	33	15	135	10	2.85	0.2405
P1	37	52	39	4	132	12	4.563	0.1022
P20	33	84	27	16	176	17	4.500	0.1054
P20	33	84	40 (13)	16	176	17	1.395	0.4979

Analysis of number of embryos and pups from htz x htz mating in different stages showed the expected ratio of genotype distribution. Although 32.5% of hmz mutant pups died in the early postnatal period (P0-P7), 67.5% of *Snap29* homozygous mutant mice on a mixed CD1 genetic background survived to adulthood.

**3.2.3. *Snap29* homozygous mutants were morphologically distinguishable from their normal littermates.** In majority of the cases *Snap29*<sup>lam1/lam1</sup> homozygous mutant pups can be distinguished from their littermates because of their low body weight (Figure 21A and B) and reduced size at birth (Figure 22 A and B) (the date of birth is P0). Although this trend can be seen in the graph bars below (Figure 21), this difference was not statistically significant by one-way ANOVA.

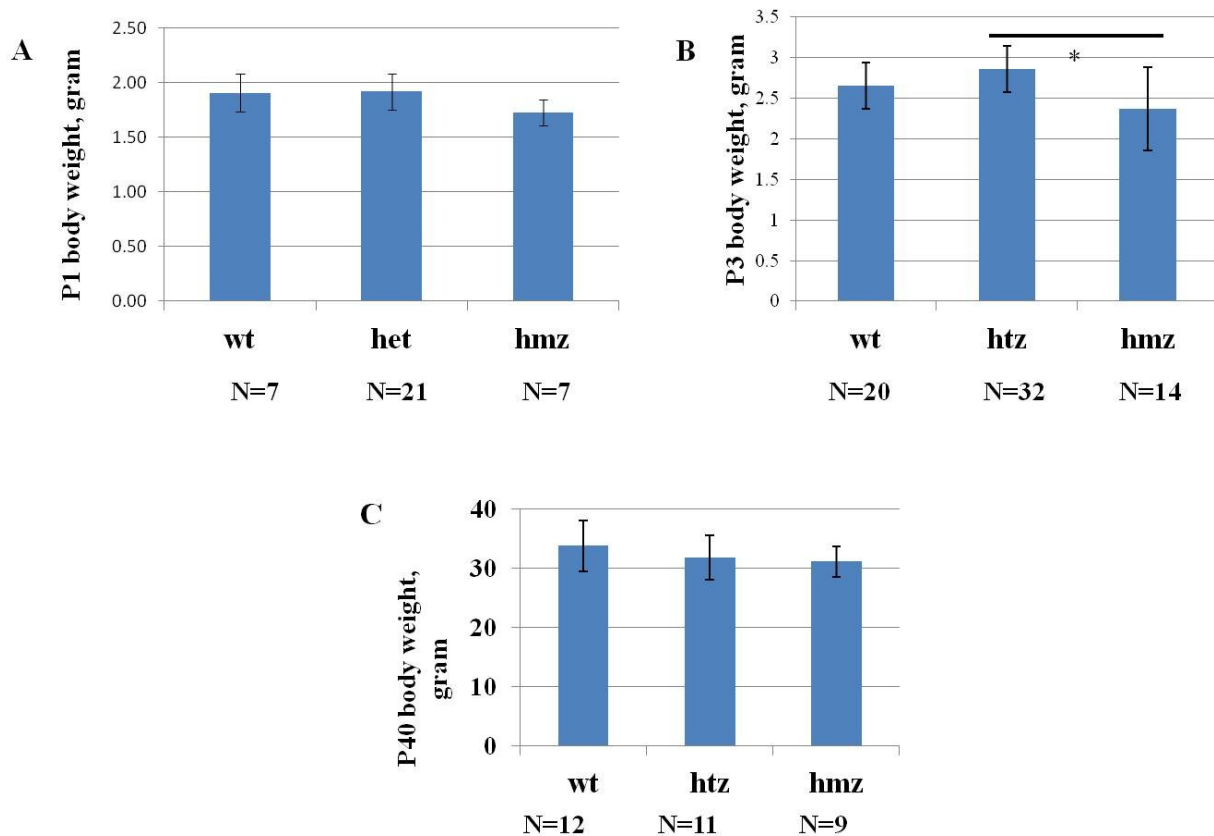


**Figure 21. Average weight by genotype of *Snap29* knockout mice.** A. Body weight of homozygous null, heterozygous mutant and wild type *Snap29* mice at P1; B. at P3; and C. at 6 weeks of age.

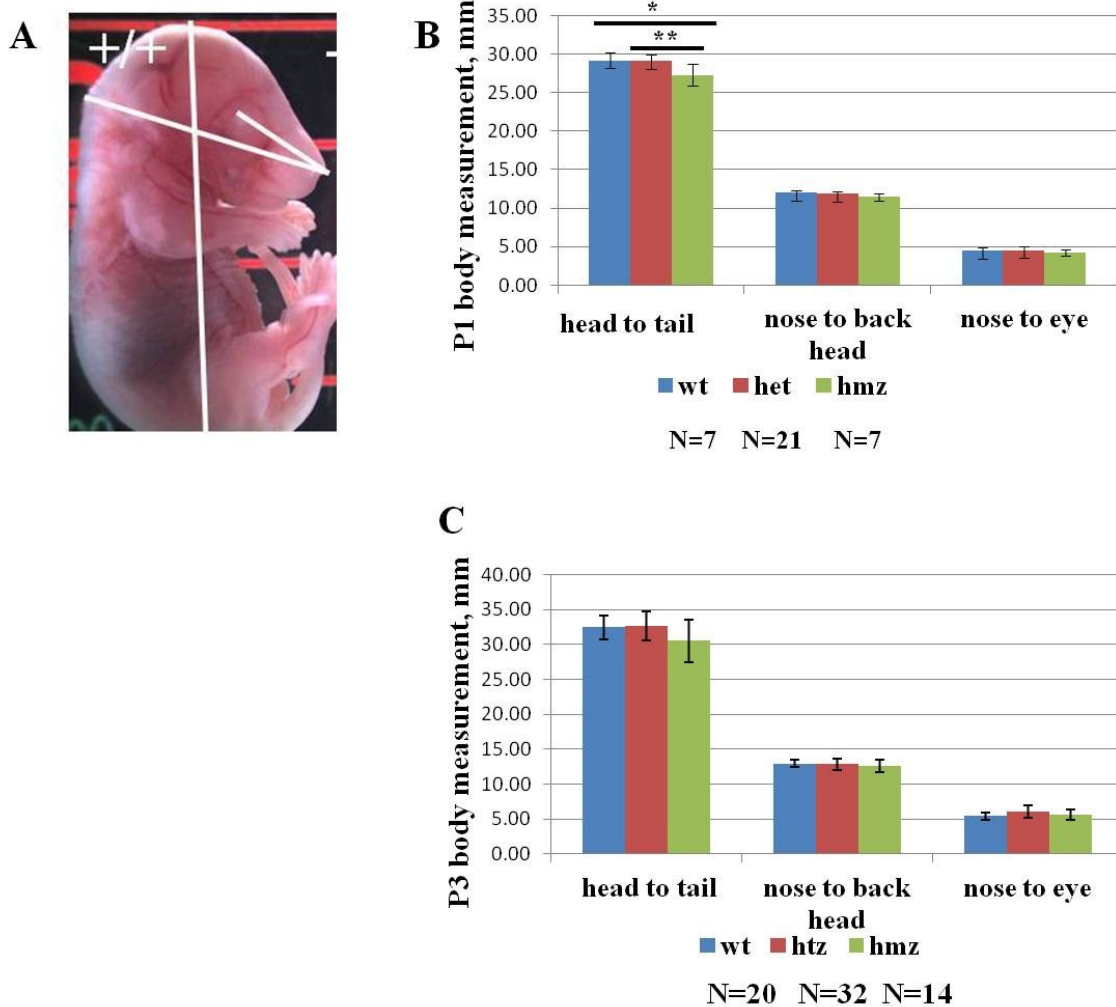


**Figure 22. P1 and P3 body measurement analysis.** A. Example of body measurements. B. At the P1 stage *Snap29* hmz mutant mice are smaller when compared to htz mutants and wild type littermates, Measurements of the distance between different parts of the facial structures did not show significant differences between genotypes. C. At the P3 stage, homozygous animals are still smaller than their littermates, with no statistical significance and like P1 there is no statistically significant difference between the length of facial structures among the different genotypes. wt, wild type, htz, heterozygous, hmz, homozygous null.

Up to now we could genotype 47 hmx mutant mice from 18 litters (in some cases we could not obtain DNA as mothers cannibalized their sick pups). Some litters have been assessed every single day for different parameters. Skin abnormalities were first apparent in *Snap29* homozygous mutants at P2 (n=16/40 of followed pups, Table 8). Skin abnormalities were classified as severe or moderate, depending on the extent of scaling or peeling observed (Table 8). Most mice with moderate scaling (n=12/40 pups which were followed for skin conditions), dry skin (n=7/40 pups which were followed for skin conditions), or no obvious skin problems (n=4/40 pups which were followed for skin conditions) survived to adulthood. Two homozygous mutant pups died within a few days of birth with abnormal motor problems (but no apparent skin problems) that were not observed in littermates. Nonetheless, all *Snap29<sup>lam1/lam1</sup>* homozygous mutant mice that survived to P7 also lived to adulthood and recovered from the skin defects (n=27). 100% of surviving *Snap29<sup>lam1/lam1</sup>* homozygous mutant mice had scaling on the ears and paws (n=25/25), including those with no obvious skin defects in the early perinatal period (n=4). These surviving homozygous mutant mice recovered their body size before weaning (Figure 21C), but are distinguishable from their wild type and heterozygous littermates because of their thickened and reddish ears, and their swollen genitalia in both sex groups (Figure 23). In addition, a few homozygous mutant mice showed severe ichthyosis on their nose later in life (n=3/25).

**Table 8. Onset of skin abnormalities in *Snap29* hmz mutant mice and their survival**

Mouse No	Genotype	Stage when skin problem appeared	Phenotype	Existence of motor problem	Dead or saced
43hmz		P1	severe skin shedding	NA	dead
44hmz		P2	severe skin shedding	NA	saced
254hmz		NO SKIN PHENOTYPE	no obvious phenotype	NA	no
257hmz		P2	skin shedding	NA	dead
259hmz		p3	cannot move	yes	saced
294hmz		NA	NA	NA	no
451hmz		P2	mild skin shedding, dry skin, small	yes	saced
452hmz		P2	mild skin shedding, dry skin, small	yes	saced
453hmz		P2	mild skin shedding, dry skin, seizure	yes	no
454hmz		p5	mild skin shedding, dry skin, seizure	yes	no
506hmz		P3	skin shedding	NA	saced
507hmz		P2	skin shedding	yes	saced
565hmz		p2	skin shedding, small, developmental delay	no	dead
566hmz		NO SKIN PHENOTYPE	no obvious phenotype at the time of death (p1)	NA	dead
610hmz		P4	dry skin	no	no
611hmz		P4	dry skin, slightly small	no	no
613hmz		P4	dry skin, slightly small	no	no
653hmz		P6	skin shedding	no	no
675hmz		p6	severe skin shedding, small	yes	no
680hmz		p6	mild skin shedding, small	no	no
691hmz		NO SKIN PHENOTYPE	no obvious phenotype	NA	no
699hmz		p4	dry skin, skin shedding, small	yes	no
700hmz		NO SKIN PHENOTYPE	no obvious skin problem	no	no
701hmz		P2	severe skin shedding	no	dead
723hmz		p2	skin shedding	NA	dead
724hmz		NO SKIN PHENOTYPE	no obvious phenotype at the time of death (p3)	yes	dead
725hmz		p3	skin shedding	yes	dead
932hmz		NA	NA	NA	no
936hmz		NA	NA	NA	no
937hmz		NA	NA	NA	no
943hmz		NA	NA	NA	no
945hmz		NA	NA	NA	no
946hmz		NA	NA	NA	no
1012hmz		p4	skin shedding	yes	dead
1013hmz		p2	mild skin shedding	no	dead
1096hmz		p2	severe skin shedding, small	yes	dead
1097hmz		p3	skin shedding	yes	dead
1098hmz		p3	very dry skin	yes	dead
1099hmz		p4	very dry skin	yes	saced
1100hmz		p2	dry skin, later shedding	yes	saced
1121hmz		p2	mild skin shedding	yes	no
1126hmz		p5	mild dry skin	no	no
1135hmz		NO SKIN PHENOTYPE	no obvious phenotype	NA	no
1186hmz		p2	dry skin	no	no
1187hmz		p2	dry skin, later mild shedding	no	no
1189hmz		p2	dry skin, later mild shedding	no	no
1372hmz		p0	dry skin, later shedding, small	yes	dead

Approximately, 67% of *Snap29<sup>lam1/lam1</sup>* homozygous mutant mice survived to adulthood. Based on the extent of scaling or peeling observed skin abnormalities were classified as severe, or moderate. Most mice with only moderate scaling and dry skin or with no obvious skin problems survived to adulthood (n=16/25). wt, wild type, htz, heterozygous, hmz, homozygous null, saced, sacrificed.



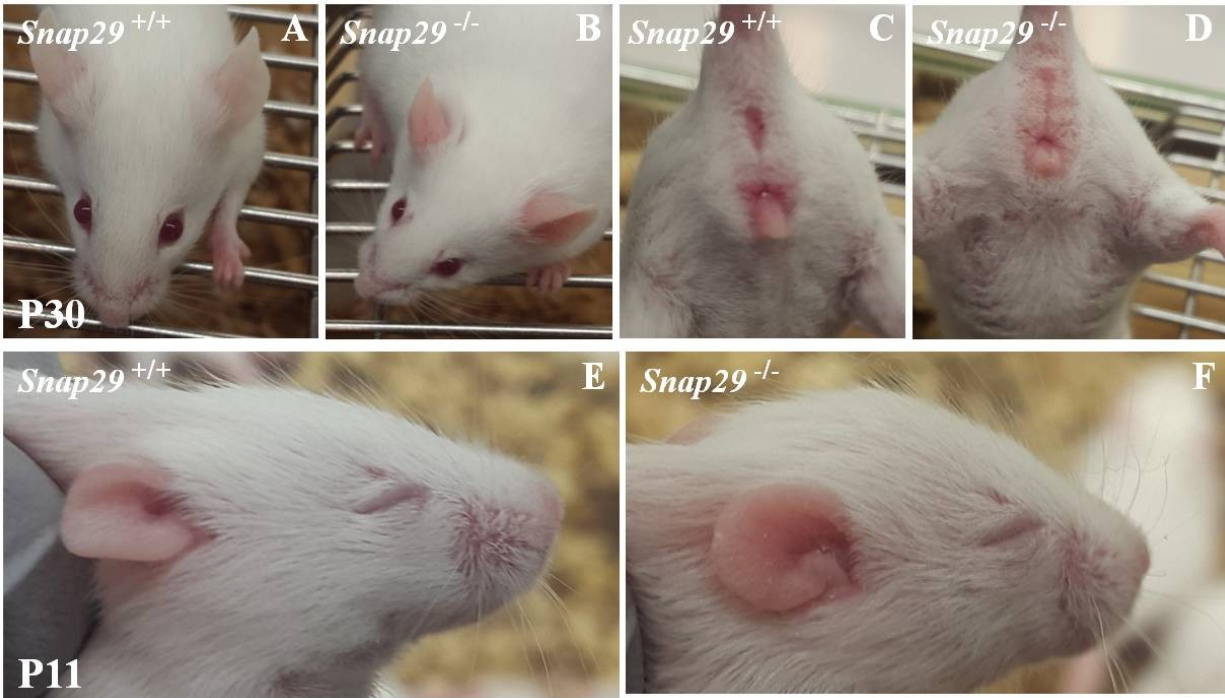


**Figure 23. Homozygous *Snap29* mice are morphologically different from their littermates and have a thicker epidermis.** (A and B) wild type and homozygous mutant mice can be distinguished from each other by reddish and thick ears, (C and D) as well as by reddish genitalia. E and F. differences in ear color and shape are noticeable before weaning (approximately at P11 stage).

Although *Snap29*<sup>lam1/+</sup> heterozygous mice were heavier when compared to *Snap29*<sup>lam1/lam1</sup> homozygous mutant littermates at P3 (Figure 21B), this weight difference is gone by weaning and they were not distinguishable from their wild type littermates in adulthood (Figure 21C). A small percentage of *Snap29*<sup>lam1/+</sup> heterozygous mice were slower in movements when compared to their wild type littermates at birth (n=8/113). These findings suggest that haploinsufficiency for *Snap29* can contribute to phenotypic abnormalities. Thus, the *Snap29* exon 2 deletion on a

mixed-genetic background results in dermatological abnormalities and survival with various penetrance and expressivity.

**3.2.4. Epidermal defects are present before the onset of skin abnormalities in *Snap29* homozygous mutant mice.** Previous knockout mouse models for *Snap29* showed an ichthyotic phenotype at birth, which resulted in death at birth due to severe epidermal barrier impairment (Schilleret *al.* 2016). Unlike these models, our *Snap29* hmz mutant mice exhibited severe skin scaling (Figure 24A and B) or dry skin starting from P2 and only 32.5% of them died between P1 and P7.

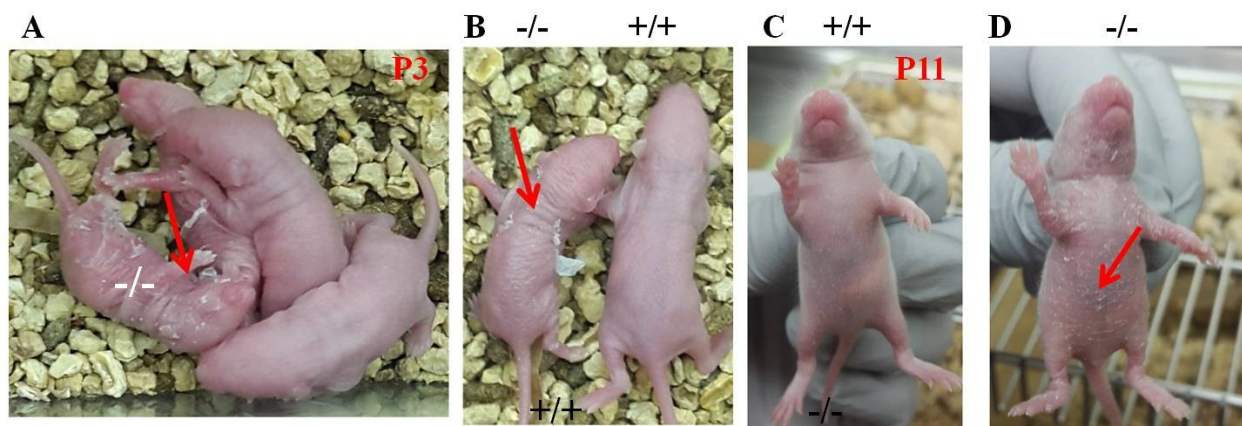


**Figure 24. Skin malformations in hmz mutant *Snap29* knockout mouse on a mixed genetic background (CD1/FvB).** A. Homozygous pups have severe skin scaling and B. are smaller than wild type littermates at P3; C and D. Skin shedding starts to recover slowly in hmz mutant pups at P11. Wild type littermate for comparison.

We have investigated whether the skin of *Snap29* hmz mutant mice shows the same abnormalities found in previous studies (Schilleret *al.*2016). Three different embryonic and

postnatal stages have been studied to determine the onset of dermatological defects in *Snap29<sup>lam1/lam1</sup>* homozygous mutants using H&E at E16.5, P1, and P3. No morphological differences were found between the skin samples of mutant and control littermates at E16.5. However, at both P1, prior to onset of skin abnormalities, and P3, when skin abnormalities are apparent, the epidermis of *Snap29<sup>lam1/lam1</sup>* homozygous mutant pups showed thicker and condensed stratum corneum when compared to control and heterozygous mutant littermates, as reported in previously established models (Schiller *et al.*, 2016) (Figure 25A-C). Thus, epidermal defects are found before the onset of skin abnormalities, as previously reported (Schiller *et al.*, 2016).

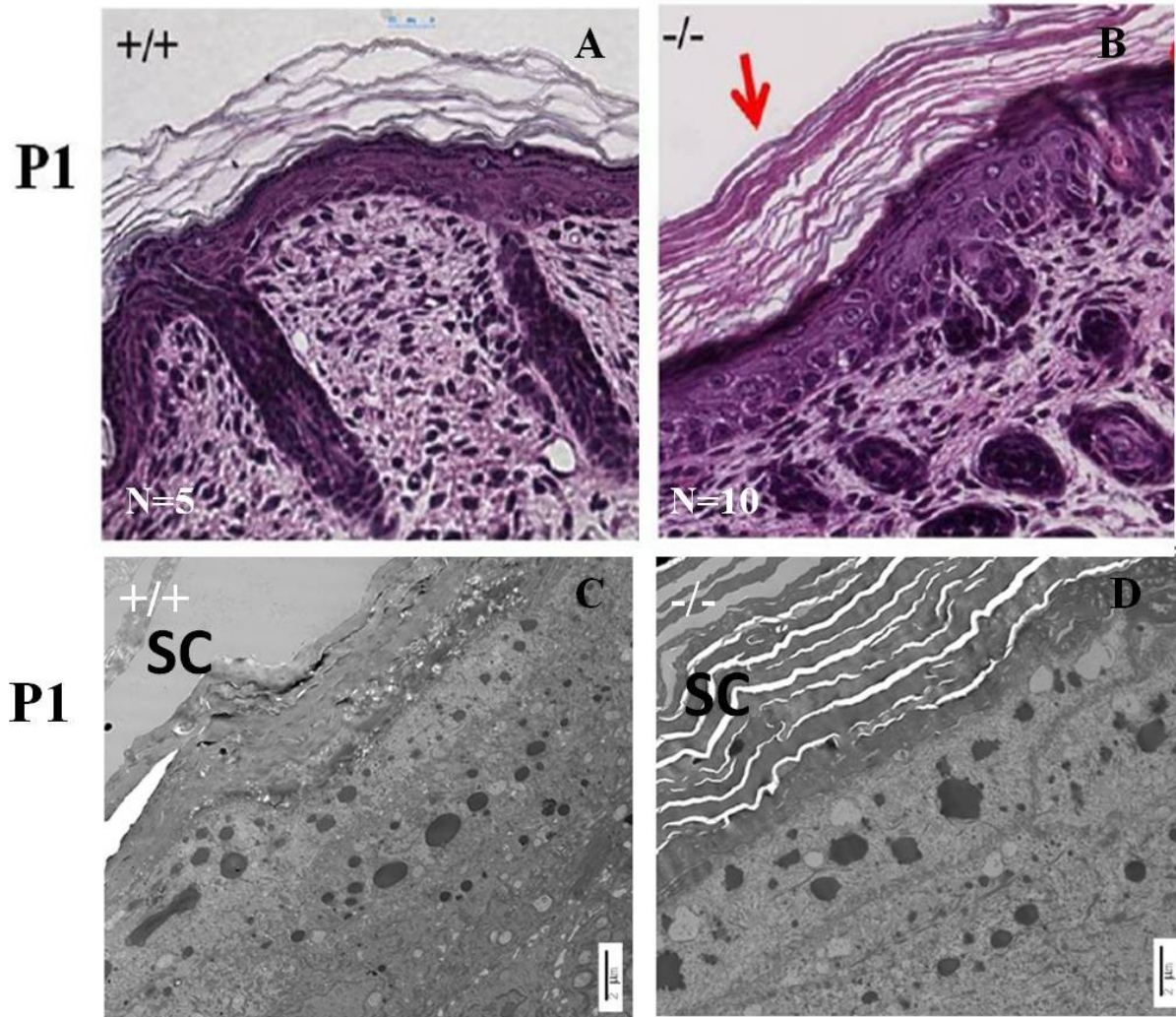


**Figure 25. H & E staining and TEM in dorsal skin of P1 pups.** A and B. H & E analysis showed thicker condensed stratum corneum in homozygous mutant pups compared to wild type littermates (red arrow, bars= 25  $\mu$ m), which was also observed by C and D. TEM

Next, we examined skin samples by TEM. It is been shown that skin biopsies of patients have many clear vesicles in epidermal layers that were not present in control epidermis (Sprecher *et al.* 2005). The lower layers of the thickened stratum corneum had vesicles of various sizes and contents, in parallel with normal looking lamellar granules that were released into the extracellular space between the superficial granular and cornified layers. Unlike previous findings (Sprecher *et al.*, 2005) we did not notice any of these changes (Figure 25E-F).

**3.2.5. Skeletal abnormalities in *Snap29* mice.** To determine if our mouse line models skeletal abnormalities seen in patients with mutations in *SNAP29* we analyzed 4 stages (E14.5, E16.5, P0 and P3) for skeletal abnormalities. Homozygous mutant pups presented with fused sutures at P3. Two different skeletal defects were observed in mutant embryos and pups. Both htz (n=8/17) and hmz mutant embryos and mice (n=13/32) had extra lumbar ribs (14 pairs of ribs) while only a single such case was seen in the tested wt embryos (1/12) as seen in patients with 22q11.2DS (Figure 26; Ming et al., 1997). Mineralization of some craniofacial bones, namely the frontal, parietal, occipital, and zygomatic maxillar bones, was either delayed (n=3/13) or advanced (n=6/13) in homozygous mutant mice (Figure 26B and C).



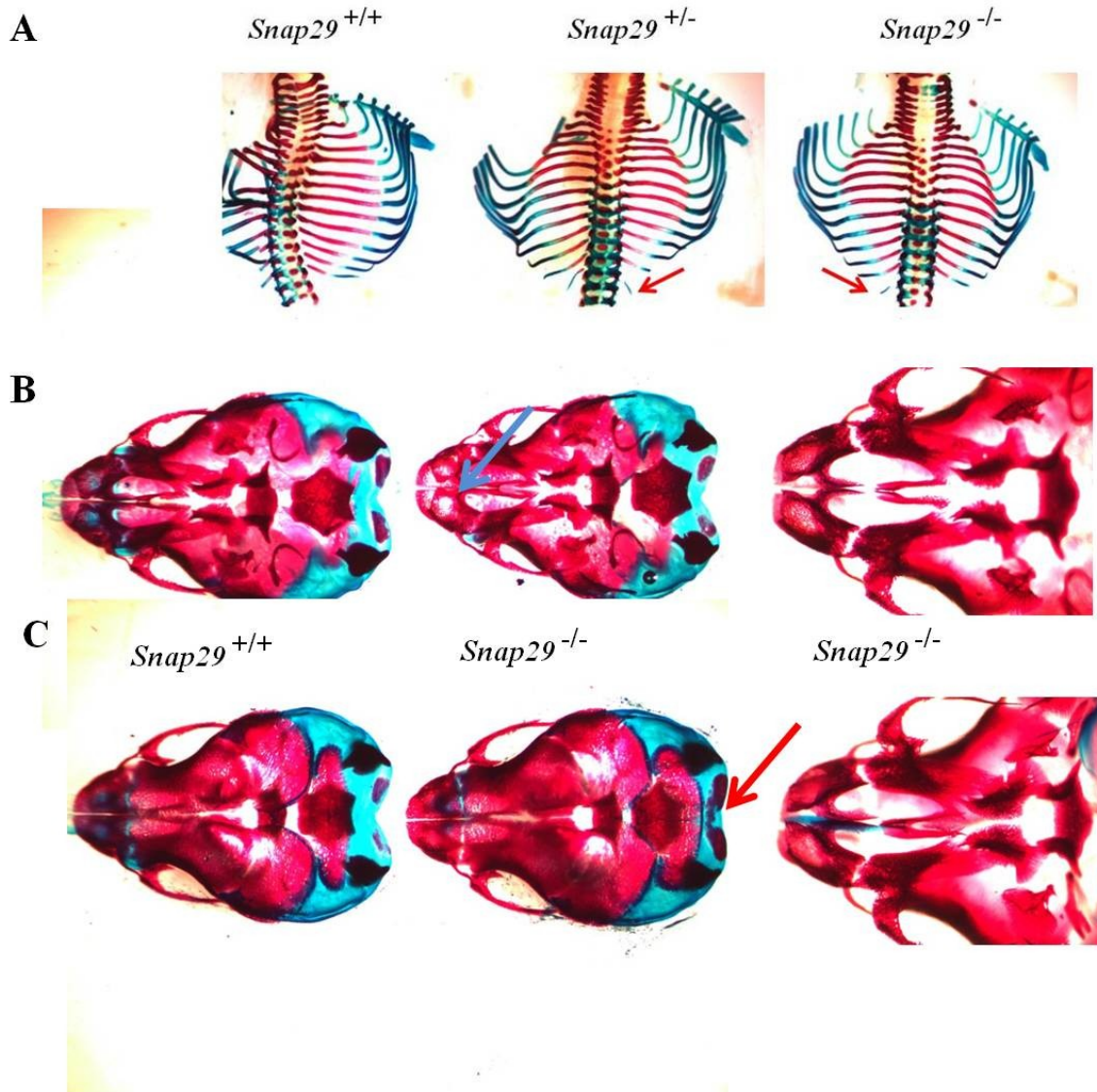


**Figure 26. Skeletal deformity in *Snap29* mice.** A. Heterozygous and homozygous mutant embryos had extra lumbar ribs (red arrows). B. Advanced and C. delayed abnormal mineralization in homozygous mutant embryos.

**3.2.6. Assessment of craniofacial abnormalities in *Snap29* mutant mice.** Since patients with mutations in *SNAP29* show dysmorphic features of the face, such as a long face, small anterior fontanelle; pointed, prominent nasal tip; and a small chin (Futch-Elemet *al.*, 2011) craniofacial dimorphism was assessed in *Snap29* mutants. The distances between the nose and eye, and

between the nose and the back of the head were measured at E17.5, P1, and P3 stages. No significant difference was found in these measurements when wild type and homozygous mutant pups were compared at E17.5 (Figure 27), P1 and P3 stages (Figure 22).

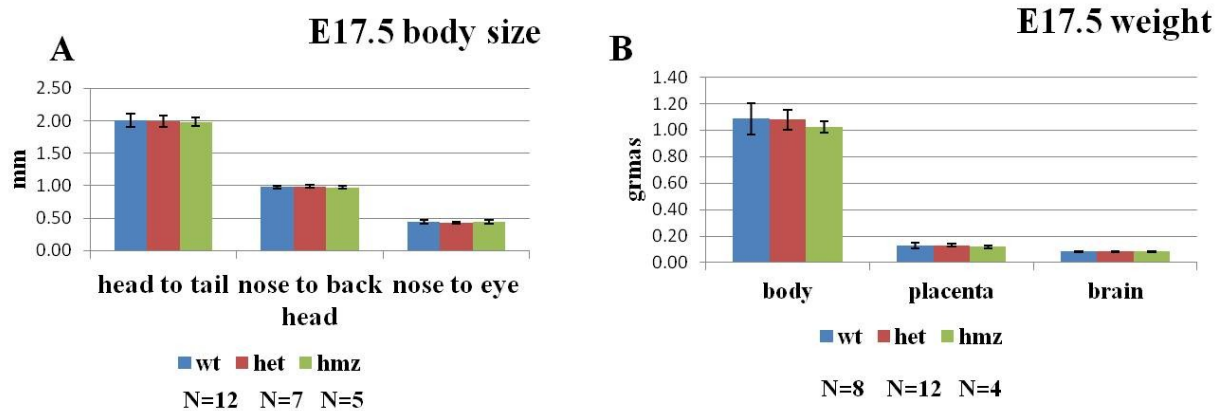


**Figure 27. E17.5 body weight and measurement analysis.** No significant differences were found in the body measurements or weight between wild type and mutant embryos at E17.5.

**3.2.7. Psychomotor retardation in *Snap29* heterozygous and homozygous mutant mice.** A subset of newborn *Snap29*<sup>lam1/lam1</sup> pups were unable to turn from supine to a prone position as quickly as their littermates. Furthermore, they were unable to stand on their feet as long as their littermates. Also, adult *Snap29*<sup>lam1/lam1</sup> mice presented with abnormal shaking while standing on an object (n=5/5) compared to wt animals (5/5). These observations showed that hmz mutant mice present with psychomotor retardation at birth.

To test for psychomotor impairment in newborn pups, P3 pups from the same litter (3 litters) were turned onto their back and the time taken for pups to go from the supine to a prone position onto their stomach was measured – each pup was turned 3 times and the average of their turn times was compared between genotypes. Although a subset of hmz mutant pups were unable to stand up on their feet after turning back onto their stomach (n=6/40 of followed hmz mutant pups, compared to N=13 wt, N=21 htz and N=5 hmz mutant littermates), no significant difference was found on the time it takes for pups of the three genotype to go from supine to a prone position at P3 (Figure 28).

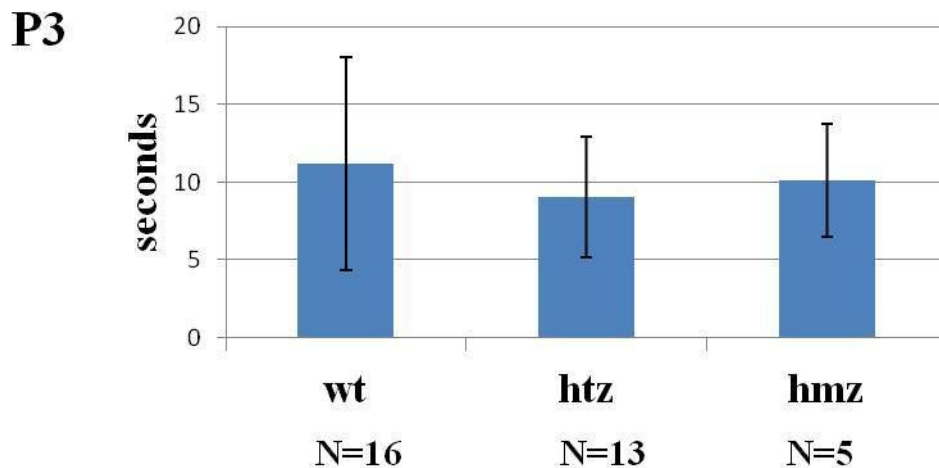


**Figure 28. Measurement of psychomotor retardation in *Snap29* P3 pups.** In the first step, 3 litters from P3 stages were turned onto their back and the time it takes for pups to go from the supine to a prone position onto their stomach was recorded. No significant difference was observed on the time it takes for pups of the three genotype to go from supine to a prone position.



To assess motor function further in *Snap29* mice, I used 3 types of test: rotarod, to evaluate neuromuscular coordination, balance and grip strength (Crawley *et al.*, 1999), catwalk, to assess gait, locomotion function and coordination (Hamers *et al.*, 2006) of the mice and grip strength meter, to study neuromuscular functions by measuring the maximum force displayed by the animals (Smithet *et al.*, 1995).

**3.2.7.1. Rotarod and grip strength assessment.** Rotarod assessment was done only for male mice at 5 weeks of age. It revealed a coordination defect in the *Snap29* null mice which had a significantly shorter latency to fall compared to wt and htz mice (Figure 29).

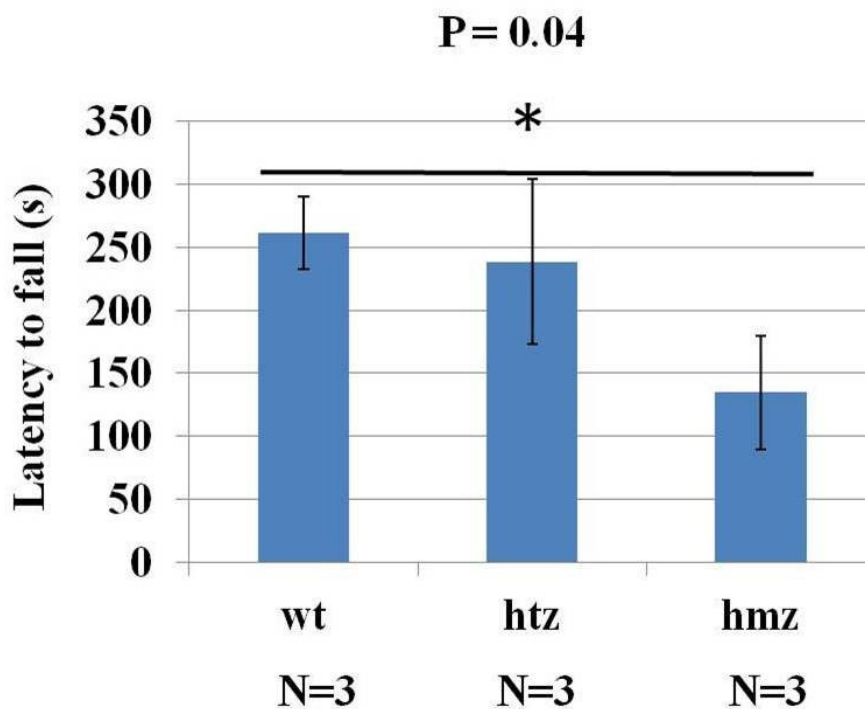


**Figure 29. Assessment of neuromuscular coordination in 5-weeks old mice by Rotarod.** Homozygous mutant *Snap29* male mice have significantly decreased latency to fall compared to wild type males.

In order to test if poor performances of *Snap29* mutant mice on the rotarod were due to abnormal muscle strength, they were assessed with the grip strength test. The grip strength test revealed that muscle strength of hmz mutant female mice at 7 weeks of age significantly decreased in hind limbs, while front limbs showed the same trend with no significance (Figure 30A and B). Repetition of the test using the same female mice at the age of 14 weeks revealed a significant decrease in muscle strength in both fore and hind limbs (Figure 30C and D). Muscle strength of hmz mutant male mice significantly decreased in both fore and hind limbs at 7 weeks of age (Figure 30E and F).

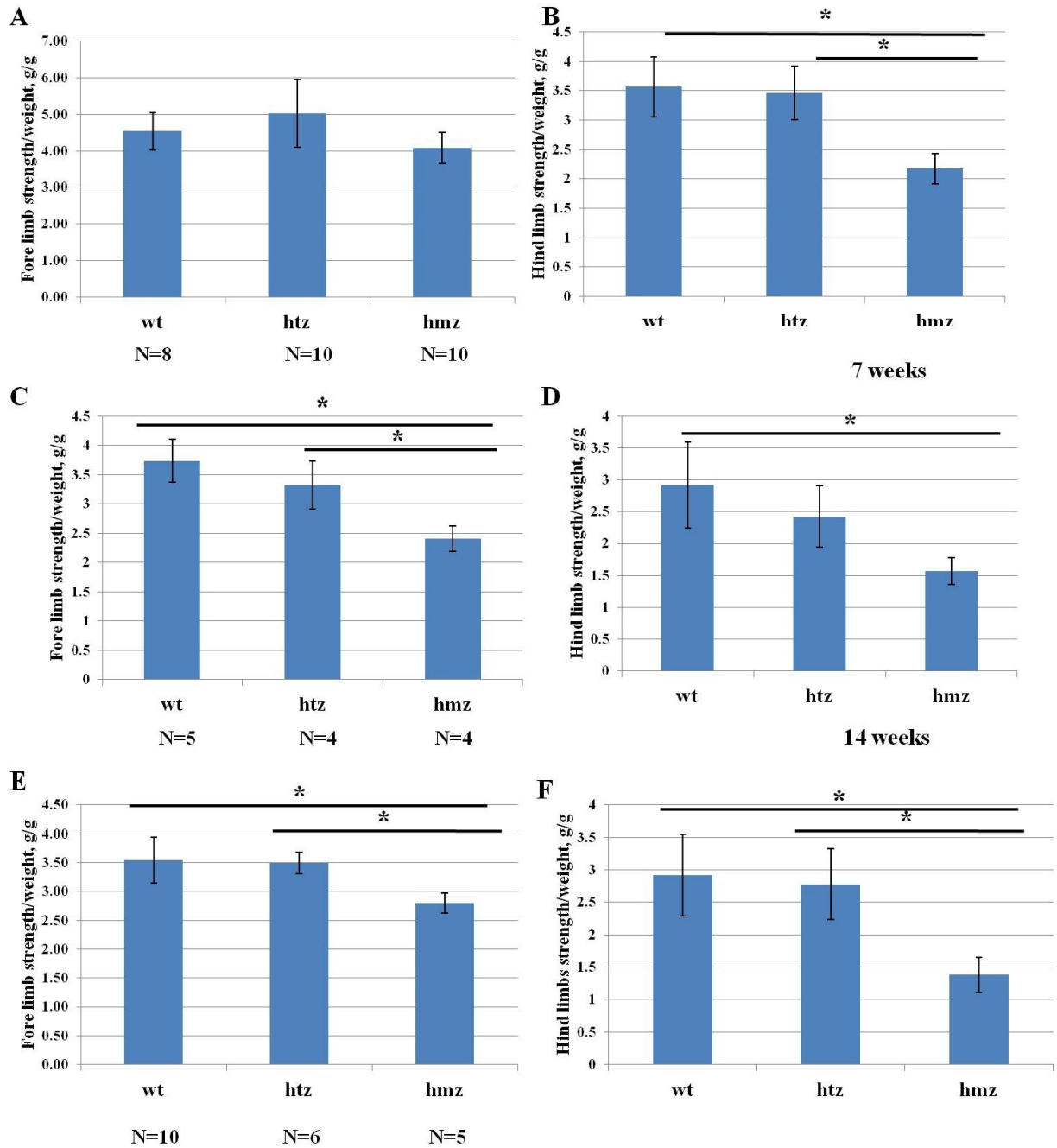


**Figure 30. Assessment of muscle strength by grip strength meter in 7 and 14-weeks old mice.** A. Muscle strength of fore limbs in 7 weeks old female mice. B. Grip strength meter revealed significantly decreased muscle strength in hind limbs of hmz mutant female mice in 7 weeks old mice. C and D. Significantly decreased muscle strength both in fore and hind limbs in

14 weeks old female mice. E and F. Muscle strength of hmz mutant male mice significantly decreased in both fore and hind limbs in at 7 weeks of age.

**3.2.7.2. Gait abnormalities in *Snap29* mutant mice.** To assess gait skills in adult mice, the CatWalk gait analysis was performed at 6 weeks of age. A number of parameters, as measured by the CatWalk gait program, were significantly different between genotypes in both sexes (Figure 31).

Increased stance phase (the duration in seconds of contact of a paw with the glass plate (Westin, J.E 2012), which is compliant with the typical "dragging of the body" seen in a Parkinson's mouse model (Westin,*et al.*, 2012) was observed in both front and hind limbs in hmz mutant females and was significantly different in both htz and hmz mutant males compared to WT (Figure 31A and B).

Single stance, the duration (in seconds) of ground contact for a single hind paw (Coulthard *et al.*, 2002, 2003), was elevated in both front paws and as well as in the right hind paw of *Snap29* homozygous mutant female animals, while it was significantly affected in all paws in hmz mutant males (Figure 31 C and D).

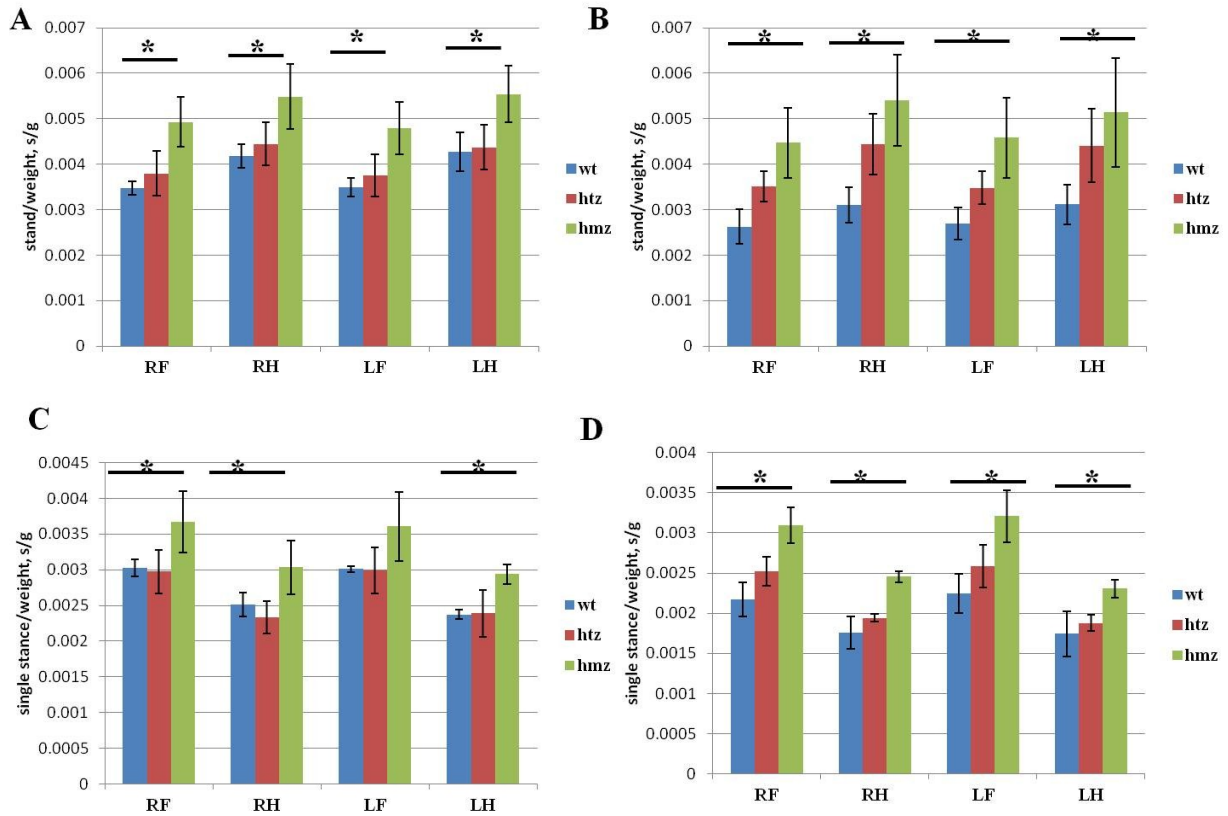


**Figure 31. Gait analysis of *Snap29* mice.** Catwalk automated gait analysis test of *Snap29* mutants and wild type littermates was performed on both sexes at 5-6 weeks of age. *Snap29* mutant mice exhibited motor dysfunction. Stand mean normalized by weight increased in both females (A) and males (B) in all limbs. C and D. Single stance mean normalized for females (C) and for males (D) increased compared to controls. RF, right front paw, RH, right hind paw, LF, left front paw, and LH, left hind paw.

Thus, both *Snap29* heterozygous and homozygous mutant mice display motor impairments when compared to their wild type littermates; hmz mutant mice showed defects in neuromuscular coordination, balance and grip strength by rotarod. Reduction in neuromuscular

function and motor coordination was confirmed by grip strength meter and catwalk respectively. Additionally, a number of different dynamic and static gait parameters have been found to be affected in both htz and hmz mutant mice. Taken together, these data show that *Snap29* mutated animals have motor dysfunction.

**3.2.8. Brain malformations in *Snap29*<sup>lam1/lam1</sup> homozygous mutant mice.** Patients with both CEDNIK and 22q11.2DS show severe structural and neurological abnormalities in the brain. Therefore, several parameters were used to assess the brains of wild type, *Snap29* heterozygous and homozygous mutant mice for structural abnormalities.

In one case, the brain of a *Snap29* homozygous mutant pup was abnormally shaped when compared to littermates (N=1/16; Figure 32). However, H&E and Nissl staining did not reveal any significant differences between genotypes in E17.5 (Figure 33 and 34).

E17.5

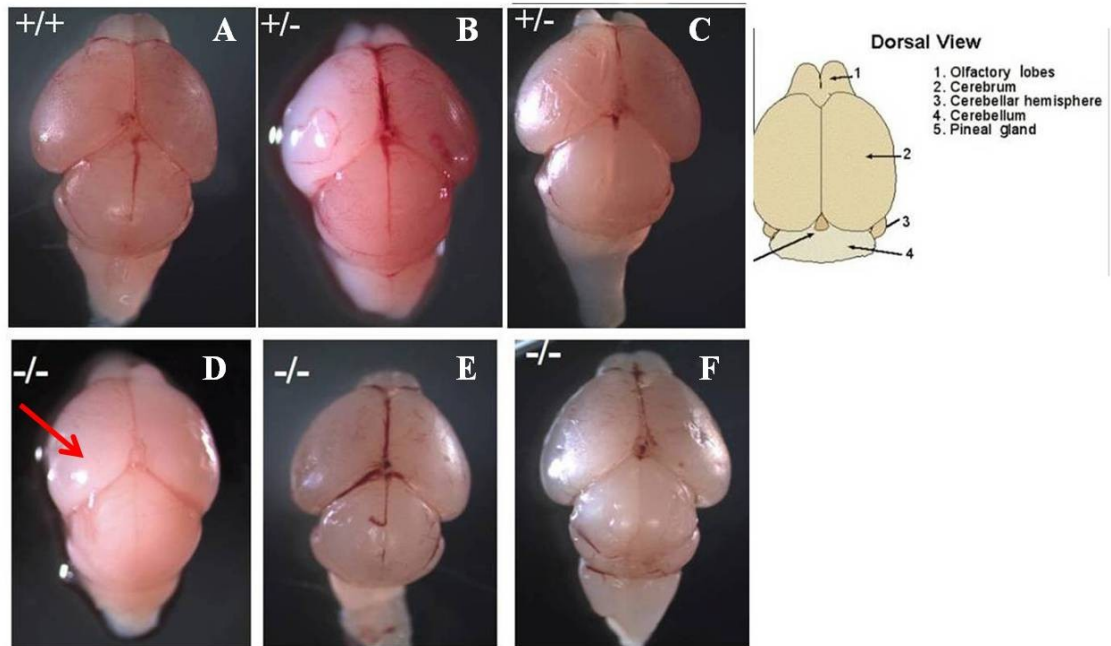


**Figure 32. Representative images of brains from E17.5.** Brain samples from *Snap29* wt and mutant embryos. Analysis of *Snap29* homozygous mutant embryos revealed abnormal brain shape (panel D, arrow showing abnormally shaped cerebrum) in E17.5 (1/11).

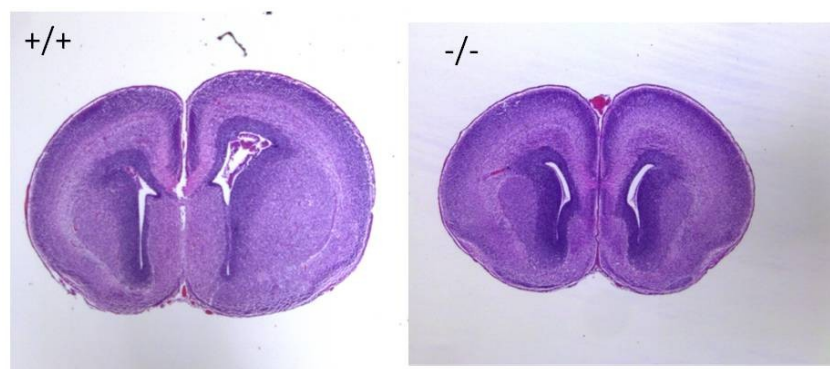


**Figure 33. Hematoxylin and Eosin staining of E17.5 brains.** H & E did not reveal any difference in staining of brains between different *Snap29* genotypes in E17.5



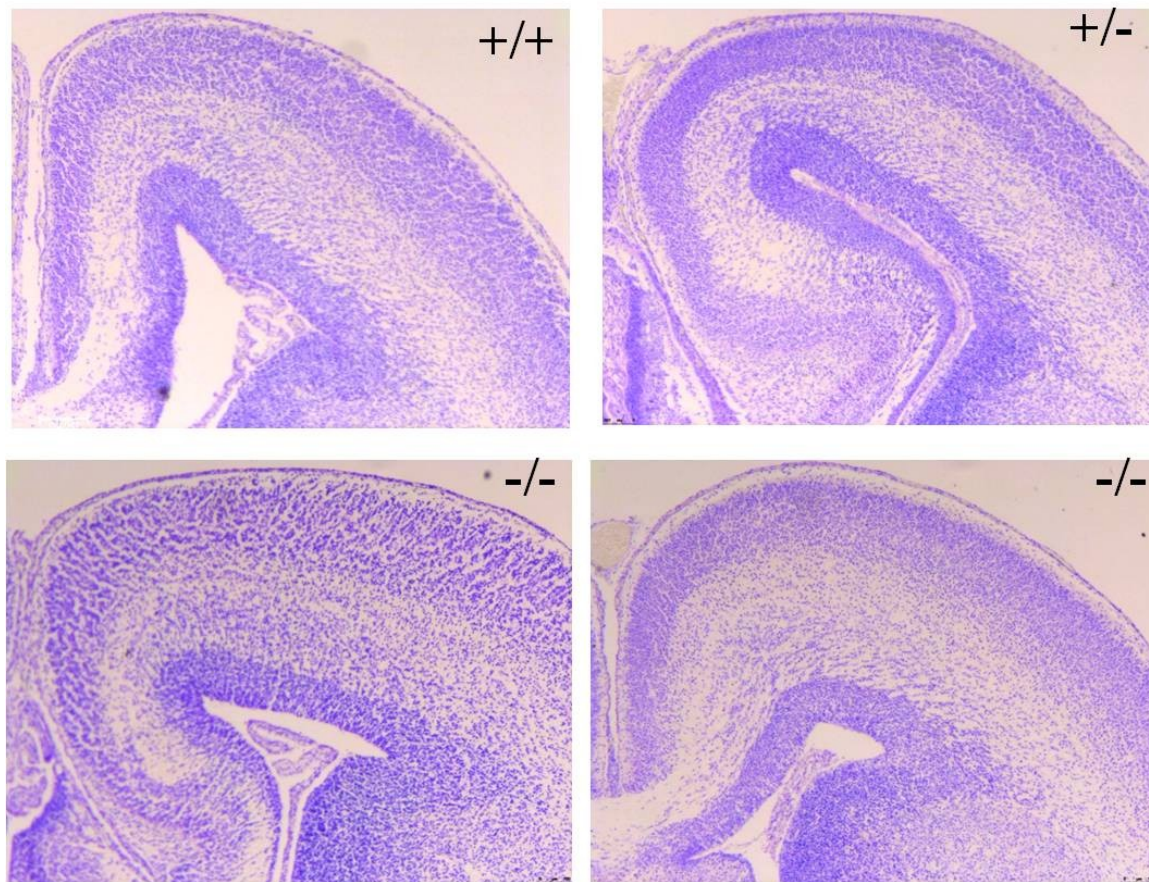
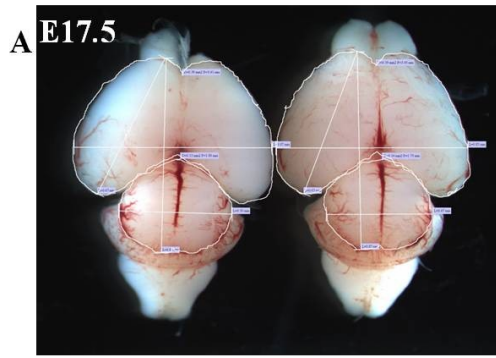


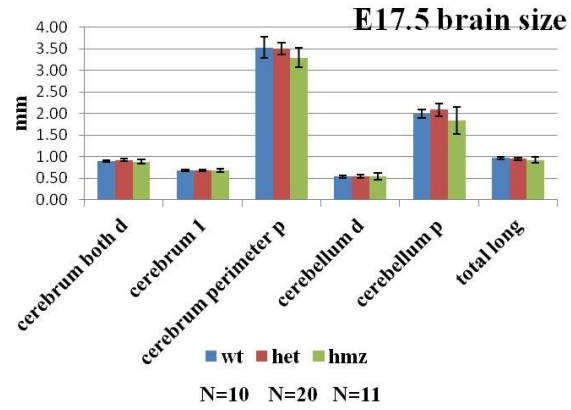
**Figure 34. Nissl staining in E17.5 brains.** Nissl staining did not reveal any difference in staining of brains between different *Snap29* genotypes in E17.5

Because we found abnormal brain shape in one homozygous pup next, we measured different parts of the brains in E17.5, P1 and P3. While brains from E17.5 pups did not show any difference in size (Figure 35B), cerebrum and cerebellum of homozygous mutants were significantly smaller compared to wild type animals in P1 (Figure 35C), though this was recovered in P3 (Figure 35D). Brain sizes (corrected to body weight) of heterozygous P3 pups were significantly bigger than WT and hmz mutant littermates (Figure 35D).

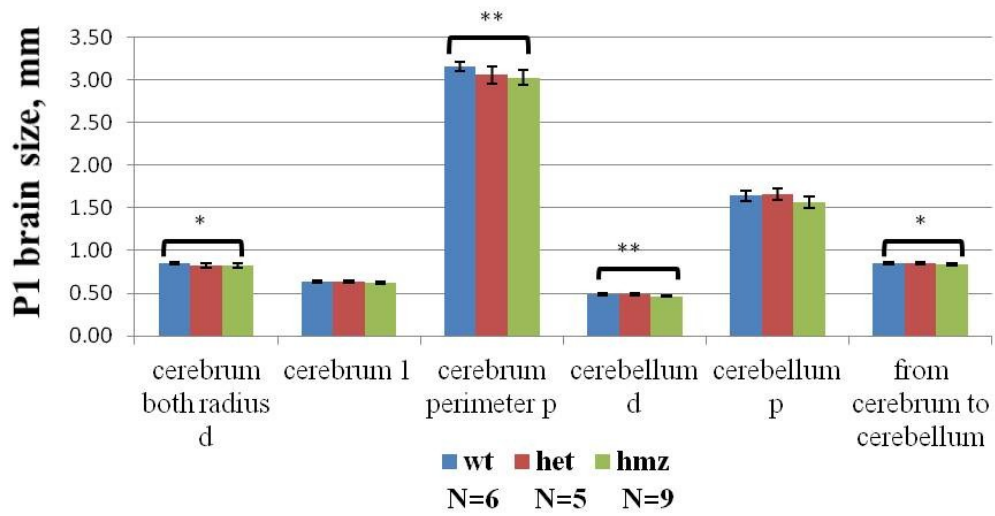




**B**



**C**



**D**

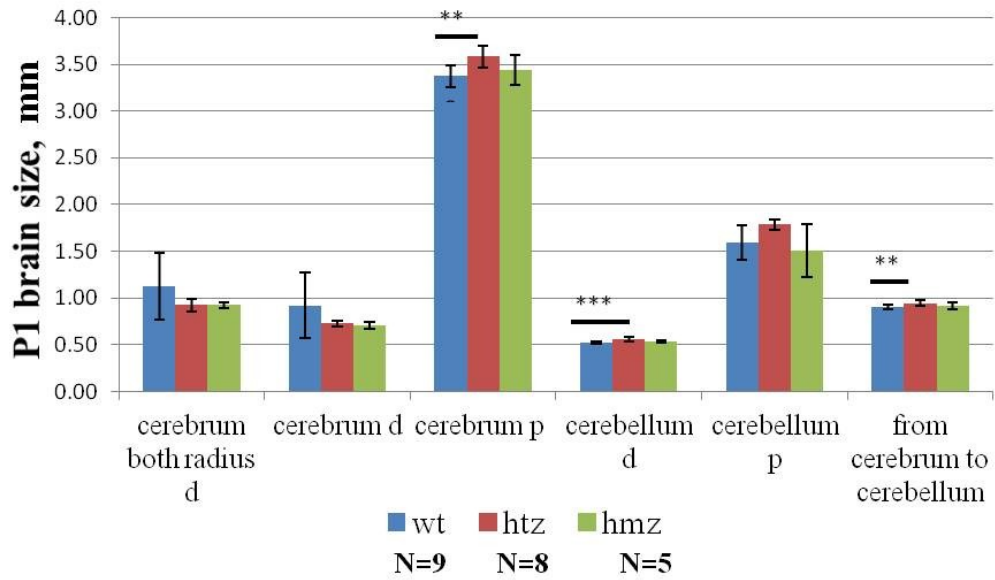


**Figure 35. Analysis of brain size in E17.5, P1, and P3 stages.** A. Representative images of measurements of different parts of the brain using brain images. B. Measurement of brain at E17.5; C. Measurements at postnatal day 1 (P1) show significant reduction in size of both cerebrum and cerebellum. D. Cerebrum and cerebellum size is recovered at P3.

We also performed MRIs in one cohort of 11-week old mice and found that hmz mutant mice have an abnormal bilaterally presenting spots in brain (Figure 36, red arrows).

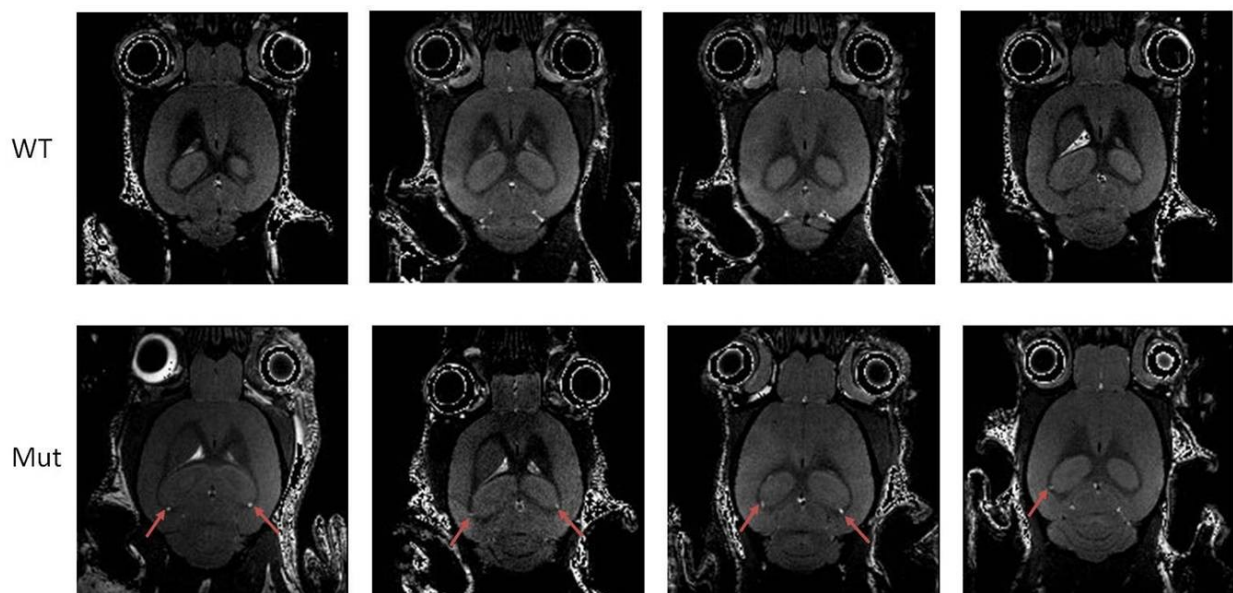


**Figure 36. Magnetic resonance imaging (MRI) of the heads of 11 week old *Snap29* mutant mice.** 11 week old hmz mutant mice have an bilateral abnormal spots in brain (red arrows).

Brains of *Snap29* E17.5 embryos were also analyzed for cortical organization using IHC and neuronal birth. Different cortical markers were used to characterize organization of different

layers of cortex: Reelin, an extracellular protein that is expressed in layer I and is important for the cortical layering and positioning of neurons (Fatemi *et al.*, 2008); CTIP2, which encodes zinc-finger transcription factors, is required for the development of layer 5 subcortical projection neurons, and is expressed by developing layer 5 and 6 neurons (Alcamo *et al.*, 2008); SatB2, a transcription factor that is expressed by the pyramidal and satellite neurons in layers II-V and determines the fate of cortical cells (Alcamo *et al.*, 2008); and TBR1, a transcription factor that regulates the differentiation of layer VI (Hevner *et al.*, 2001). Although we noticed disorganization of cells with Reelin, SATB2 and TBR1 staining in subset of hmz mutant brains (Figure 37), counting the number of neurons in these layers of the cortex in different genotypes did not reveal any difference (Figure 38).

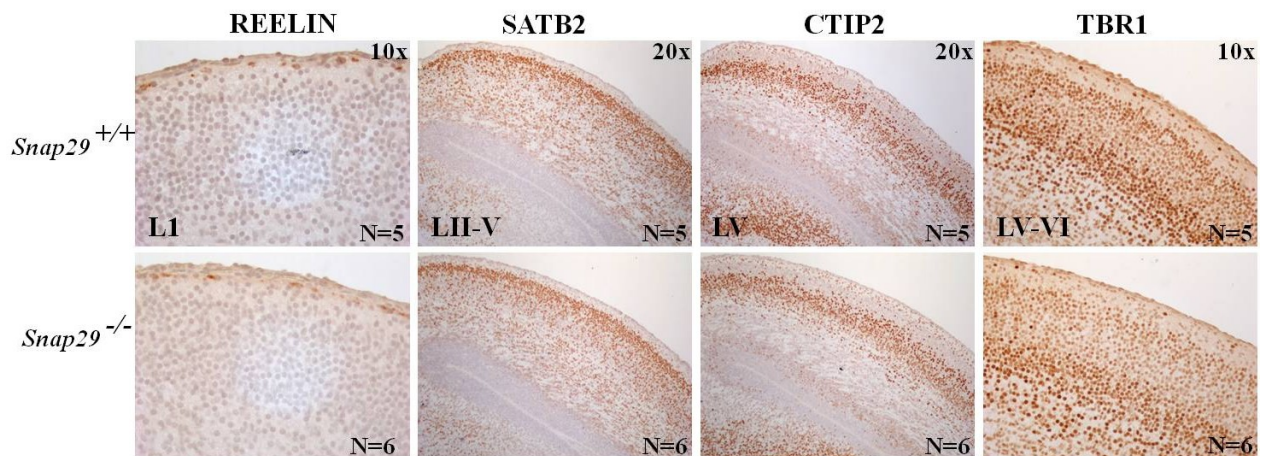


**Figure 37. Expression of cortical layer markers in E17.5 brains.** Expression of markers for cortical layers did not show differences between *Snap29* genotypes.

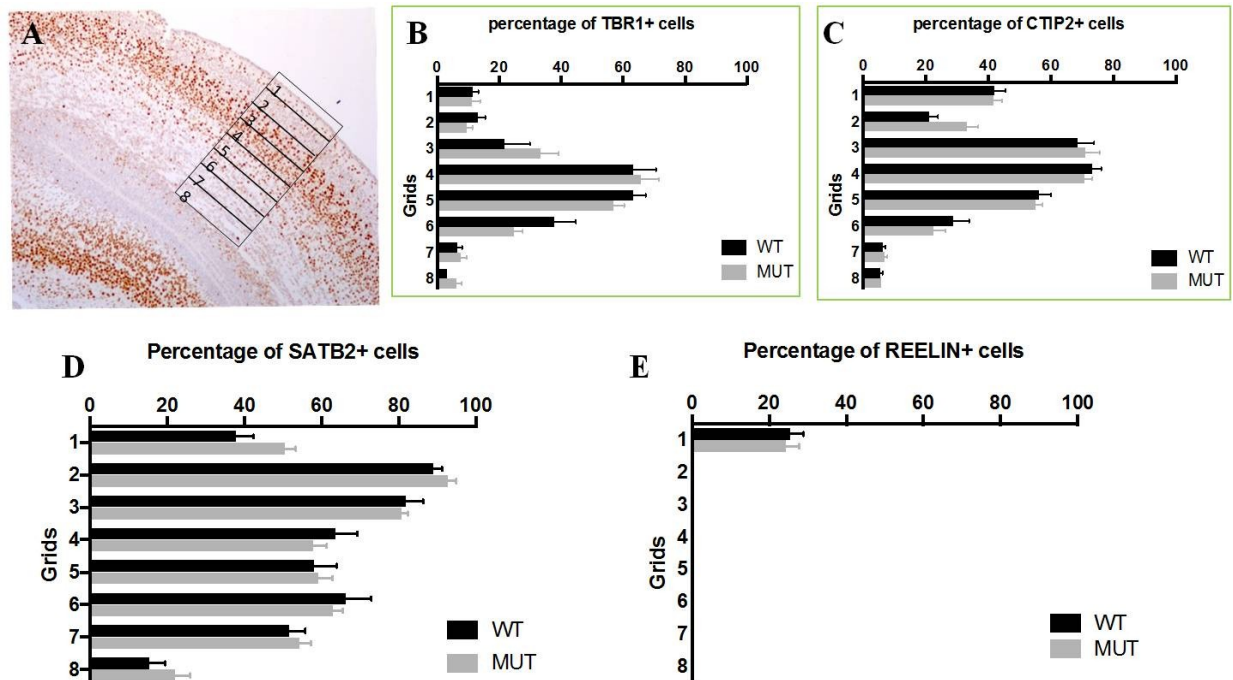


**Figure 38. Counting of cortical layer organization markers.** A. Representative cortical section that divided into 8 different layers spanning from the pial surface to the intermediate zone to count labeled neuronal cells (see methods for the details). B. Counting of TBR1; C. STIP2; D. SATB2; E. REELIN stained neurons did not show differences between *Snap29* genotypes. The total number of cells was counted using automatic local threshold (otsu, R:10).

BrdU and EdU were injected into 2 pregnant females at stages E12.5 and E14.5 or E13.5 and E15.5, respectively, in order to track neuronal birth. Embryos obtained from these pregnant females were analysed at E17.5. We observed an increased level of BrdU and EdU labeled cells around ventricles where the progenitor cells are born in the brains of a subset of hmz mutant mice, compared to WT animals (Figure 39). However, counting of the cells was not done for this experiment to determine if this increase significantly differs between genotypes.



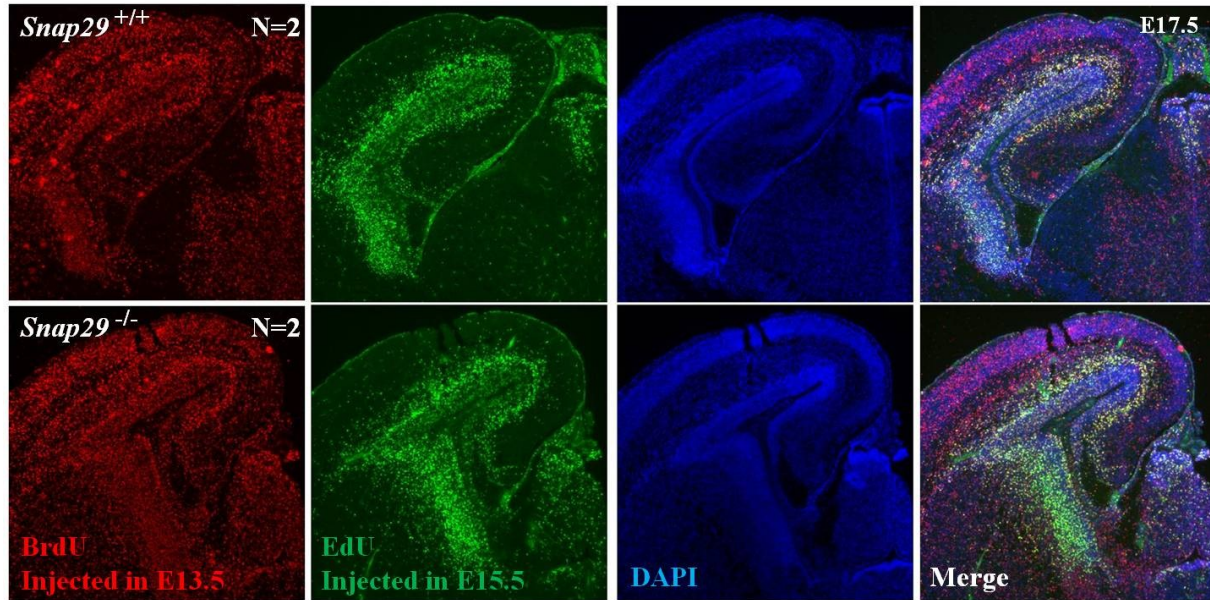


**Figure 39. Analysis of BrdU and EdU labeled E17.5 brains.** Pregnant female mice were injected with BrdU at E13.5 and EdU at E15.5 respectively. Pregnant females are dissected at E17.5 to analyse brains of embryos. Preliminary data showed increased BrdU and EdU labeled neurons in one hmz mutant brain (N=1/2).

**3.2.9. *Snap29* homozygous mutant male mice are infertile.** Since mating of *Snap29* homozygous mutant females (N=5) only resulted in live births after mating with *Snap29* heterozygous males and live births were not found when *Snap29* homozygous mutant male mice (N=4) were mated to wild type or homozygous mutant litter mates (Table 9), we assess the role of *Snap29* in male fertility.

**Table 9. Fertility assessment for *Snap29* knockout male mice**

mating #	male genotype	female genotype	duration of mating	# litter
1	+/- ♂	+/- ♀	5 months	13
		+/- ♀		
2	+/- ♂	+/- ♀	3 months	9
		+/- ♀		
3	+/- ♂	+/+ ♀	3 months	0
		-/- ♀		
4	-/- ♂	+/+ ♀	4 months	0
		-/- ♀		
5	-/- ♂	+/+ ♀	4 months	0
		-/- ♀		
6	-/- ♂	+/+ ♀	3 months	0
		-/- ♀		
7	-/- ♂	+/+ ♀	3 months	0
		-/- ♀		

One male and 2 females with various *Snap29* genotypes were mated in each mating. After 3-4 months of mating, no pups were born to hmz mutant *Snap29* males.

We found that there is a significant reduction in the testis weight (normalized to body weight) in *Snap29<sup>lam1/lam1</sup>* mice compared to htz mice and WT controls (Table 10), while the weight of the epididymis or other reproductive organs (prostate, seminal vesicles and coagulating glands) were not affected (Table 10).

**Table 10. Measurement of male reproductive organs.**

	WT	Htz	KO
Testis weight (x10 <sup>-2</sup> g/bw)	0.54±0.07 <sup>a</sup>	0.50±0.12 <sup>a</sup>	0.29±0.06 <sup>b</sup>
Epididymis weight (x10 <sup>-2</sup> g/bw)	0.20±0.03 <sup>a</sup>	0.23±0.02 <sup>a</sup>	0.22±0.01 <sup>a</sup>
Seminal vesicles (x10 <sup>-2</sup> g/bw)	0.79±0.06 <sup>a</sup>	0.98±0.17 <sup>a</sup>	0.72±0.08 <sup>a</sup>
Prostate (x10 <sup>-2</sup> g/bw)	0.19±0.05 <sup>a</sup>	0.19±0.00 <sup>a</sup>	0.17±0.03 <sup>a</sup>
Coagulating glands (x10 <sup>-2</sup> g/bw)	0.10±0.01 <sup>a</sup>	0.13±0.04 <sup>a</sup>	0.07±0.01 <sup>a</sup>
Abnormal seminiferous tubules (%)	0.15±0.10 <sup>a</sup>	2.23±1.06 <sup>a,b</sup>	10.31±3.67 <sup>b</sup>

Different parameters were measured for the organs of infertile hmz mutant *Snap29* mice organs along with males of other genotypes. Different letters denote significant differences for comparison of each organ among the three groups (Kruskal-Wallis ANOVA,  $p \leq 0.05$ ,  $n=6-8$ ).

In addition, all *Snap29*<sup>lam1/lam1</sup> testis have abnormal spermatogenesis with abnormal seminiferous tubules with degenerated germ cells, extensive vacuolization, loss of immature germ cells accumulated in the lumen, and giant multinucleated spermatids (Figure 40). Furthermore, the diameter of degenerated seminiferous tubules was reduced in *Snap29*<sup>lam1/lam1</sup> (D) compared to WT (C) testis, and few seminiferous tubules of *Snap29* homozygous mutant testis had spermatozoa in their lumen (Figure 40). We did not observe any abnormality in the scrotum or the presence of cryptorchidic testis in the *Snap29*<sup>lam1/lam1</sup> mice.

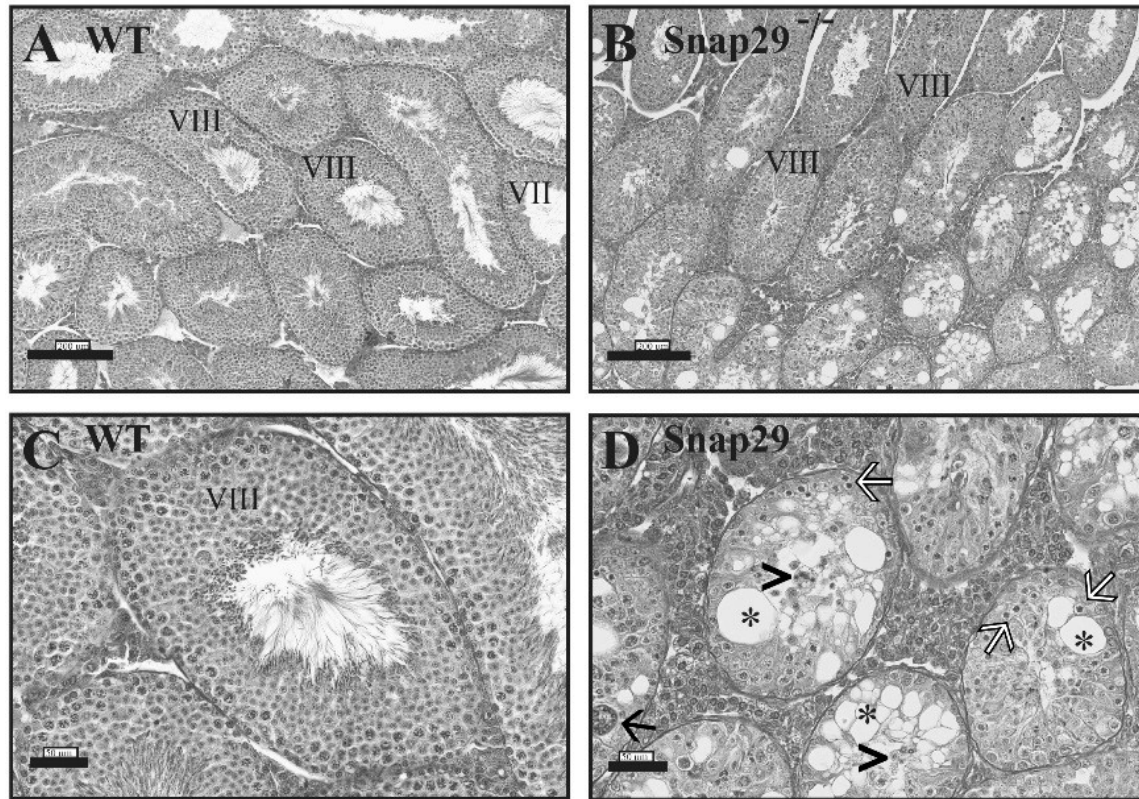


**Figure 40. Histological analysis of *Snap29*<sup>-/-</sup> testis.** Testis sections were stained with hematoxylin and eosin to evaluate spermatogenesis in WT (A and C) and *Snap29*<sup>-/-</sup> (B and D) mice. WT testis displayed normal spermatogenesis (Stages VII and VIII showing elongating spermatids and spermatozoa in the lumen). Seminiferous tubules in *Snap 29*<sup>-/-</sup> testis had degenerated germ cells (white arrows), loss of immature germ cells accumulated in the lumen (arrow heads), giant multinucleated spermatids (black arrow) and extensive vacuolization (\*). The diameter of degenerated seminiferous tubules was reduced in *Snap 29*<sup>-/-</sup> (D) compared to WT (C) testis.



**3.2.10. Clinical seizures.** In addition to the abnormalities described above, a subset of surviving *Snap29* homozygous mutant mice (n=2/25) exhibited seizures similar to subset of patients with mutation in *Snap29* (Lichao *et al. et al.*, 2017) and patients with 22q11.2DS (Mudigoudaret *al.*, 2017) at P10, which seemingly recovered in adulthood.

**3.2.11. Aim 2 summary.** Using CRISPR/Cas we successfully generated a novel constitutive knockout mouse model for *Snap29* gene which survived to adulthood. Viability of hmz mutant mice between birth and weaning is 67%. *Snap29* mutant allele segregated at expected Mendelian frequency. *Snap29* homozygous mutant mice model skin, and motor abnormalities similar to those found in CEDNIK patients and might be involved in fertility problems seen in 22q11.2DS patients.

## CHAPTER 4: DISCUSSION

**4.1. General overview.** In this study, *SCARF2* and *SNAP29*, two genes located in the region coinciding to the 22q11.2 deletion have been investigated as potential candidates for phenotypic variability seen in patients with 22q11.2DS. Most patients with 22q11.2DS are hemizygous for a 3 Mb region of chromosome 22 and have been reported to have a number of different birth defects in various combinations (including craniofacial dysmorphisms, and CNS and motor malformations) that could not previously be tied back to a specific gene in the region.

A number of mouse models have been generated for 22q11.2DS (Kimber *et al.*, 1999, Lindsay *et al.*, 1999, Puech *et al.*, 2000, Lindsay *et al.*, 2001). However, none of these models could replicate the spectrum of phenotypes seen in patients, suggesting the existence of candidate genes in the deleted region that had not yet been investigated. Alternatively, the differences observed in clinical manifestations may be caused by a modifier effect of the genes elsewhere in the genome or the effect of a contiguous gene deletion. Even though a subset of the phenotypes have been attributed to a deficiency of the *TBX1* gene (Jerome *et al.*, 2001), the exact roles of other genes located in the deleted region remain elusive. We were interested in *SCARF2* and *SNAP29* firstly because homozygous mutations in these genes were associated with congenital syndromes, showing their importance during development. Secondly, neither of the genes were included in the deleted region of existing 22q11.2DS mouse models, despite the majority of 22q11.2DS patients having a deletion that includes *SCARF2* and *SNAP29* (McDonald-McGinn *et al.*, 2013).

In the present study, we elucidated the possible contributions of the *SCARF2* and *SNAP29* genes to the phenotypic spectrum of 22q11.2DS and performed the first detailed mapping of *Scarf2* and *Snap29* mRNA expression before and during mouse organogenesis.

We found that the transcripts of both genes are present before and during mouse organogenesis in many tissues, including precursors of many tissues affected in patients. In the next part of the study, we concentrated on characterization of the novel *Snap29* knockout mouse line, which we generated using CRISPR/Cas9. The engineered *Snap29* mouse line survived to adulthood and reproduced a subset of phenotypes seen in patients with CEDNIK and 22q11.2DS. Homozygous mutant *Snap29* mice displayed skin, craniofacial, brain, motor, and skeletal abnormalities, as well as fertility problems similar to those found in 22q11.2DS and CEDNIK patients. Hence, we postulated that deletion of *SNAP29* contributes to the phenotypic spectrum of abnormalities found in a subset of 22q11.2DS patients.

**4.1.1. The possible role of *SCARF2* in 22q11.2DS.** *SCARF2* is a member of a family of scavenger proteins that has not been well characterized (Plüddemann *et al.*, 2007). It is reported that the gene has multiple EGF-like repeats in its extracellular domain, while the cytoplasmatic domain contains many serine and threonine phosphorylation sites. The ability to internalize modified low-density lipoproteins (LDLs), a function that is a hallmark of SRs, is significantly reduced in *SCARF2* compared to other family members. *SCARF2* transcripts have been found in many human tissues by northern blot analysis including the heart, eye, lung, liver, kidney, spleen, gastrointestinal tract, muscle, ovary, prostate, testis, colon, and stomach (Ishii *et al.*, 2002). Expression of *Scarf2* also has been reported in branchial arches, mandibular and maxillary components, and urogenital ridge tissues in E10.5 mouse embryos (Smith *et al.*, 2007). Consistent with the expression pattern found by others, our *in situ* data showed expression of the gene in multiple tissues before and during mouse organogenesis (including branchial arches) with higher expression in primordia of skeletal cartilages. Of note, we have found that expression

of *Scarf2* mRNA is quite broad starting from E10.5 (including primordia of facial structures) and ubiquitous at E13.5. Some of the regions with a strong signal observed by *in situ* RNA hybridization overlapped with the regions affected in VDEGS patients, such as limbs, digits, eye, pinna, and cartilage primordium of the ribs. Highly specific and restricted expression was observed in digits and pinnae at E14.5, which corresponds to the abnormal extremities and ears seen in patients. Our expression data shows the importance of the *Scarf2* gene in branchial arch and bone development, and indicates that *Scarf2* may also function in other tissues. We thus provide additional information for further analyses of the functional role of *SCARF2* during development.

Studies by different groups previously confirmed the association of hmz mutations in *SCARF2* with VDEGS (Anastasio *et al.*, 2010, Migliavacca *et al.*, 2014). Patients with VDEGS are known to have characteristic facial features and skeletal abnormalities, as listed in section 1.1.5 of this thesis. However, recent studies confirmed that *SCARF2* mutations in humans are associated with variable expressivity; additional phenotypes have been recorded in subset of patients with VDEGS, such as ambiguous genitalia (Bistrizter *et al.*, 1993), cerebellar enlargement and learning difficulties (Schweitzer *et al.*, 2003), laryngeal abnormalities (Carr *et al.*, 2007), sclerocornea (Migliavacca *et al.*, 2014), hydronephrosis (Patel *et al.*, 2014), thus increasing the spectrum of VDEGS phenotypes. In fact, most of these phenotypes are also observed in patients with 22q11.2DS. Bedeschi *et al.* (2010) described the first patient in whom a 22q11.2 deletion unmasked a recessive mutation in *SCARF2*, giving the patient a combination of typical characteristics of both 22q11.2DS and VDEGS syndromes. The expression of *Scarf2* mRNA in multiple tissues reported in this study, together with atypical findings in patients, highlights the importance of *SCARF2* and suggests that the gene functions not only in

craniofacial development and bone morphogenesis pathways but also in a number of other tissues that were not reported to be affected in patients with VDEGS. It is possible that hemizyosity of *SCARF2* alone or in combination with hemizyosity of other genes in the 22q11.2 deletion may contribute to some of the atypical phenotypes found in the patients with 22q11.2DS. To identify the precise role of the gene will require further study. Since *Scarf2* homozygous mutant mice are viable, (IKMC) detailed analysis of these mice during embryogenesis and after birth needs to be performed in order to determine whether they model phenotypic abnormalities found in VDEGS patients and to identify the exact contribution of *SCARF2* to 22q11.2DS.

**4.1.2. The possible role of *SNAP29* in 22q11.2DS.** *SNAP29* maps to the 22q11.2 region and has been shown to be essential for normal development (Sprecher *et al.*, 2005, Fuchs-Telemet *al.*, 2011). It encodes for a ubiquitous member of the t-SNARE protein family. *SNAP29* mediates membrane fusion in the intercellular secretory pathway and in recycling synaptic vesicles (Sprecher *et al.*, 2005, Qingninget *al.*, 2001, Ping-Yueet *al.*, 2005). In studies using primary neurons, *SNAP29* was reported to have an inhibitory role in synaptic vesicle recycling (Qingninget *al.*, 2001 and Ping-Yue *et al.*, 2005). The gene has been implicated in several other cellular processes, including autophagy (Morelli *et al.*, 2014). Studies conducted on *SNAP29* mutant fibroblasts identified abnormal migration and endocytosis of  $\beta$ 1-integrin, suggesting abnormal cell migration may contribute to polymicrogyria seen in CEDNIK patients (Rapaportet *al.*, 2010). However, none of these studies have established the embryological basis for CEDNIK syndrome or the contribution of *SNAP29* to 22q11.2DS.

Homozygous mutations in *SNAP29* are associated with the neurocutaneous syndrome CEDNIK, indicating the importance of *SNAP29* for neurogenesis. CEDNIK patients present with skin defects at birth or in the first few months of life, failure to thrive, cerebral malformations, developmental delays, severe mental retardation, roving eye movements during infancy, trunk hypotonia, and poor head control. MRI reveals corpus callosum abnormalities, pachygyria, and polymicrogyria in most patients (Ben-Salem *et al.*, 2015). Importantly, a subset of the phenotypes found in CEDNIK patients has also been described in 22q11.2DS patients.

Despite the fact that, multiple congenital anomalies are associated with *SNAP29*, the contribution of the gene to the traits of these disorders has not been examined, thus making this gene the focus of my thesis research. We postulated that hemizygosity for *SNAP29* alone or in combination with other genes in the 22q11.2DS region may be responsible for a subset of the abnormalities, including cortical malformations and neurological abnormalities, found in 22q11.2DS patients.

We analyzed *Snap29* mRNA expression before and during organogenesis in wild type CD1 embryos, in order to identify which tissues it is expressed in and whether these correspond to tissues affected in patients. Expression of *Snap29* has been reported in the developing nervous system of E14.5 mouse embryos (<http://www.informatics.jax.org/assay/MGI:4828343>). In addition, knock-in of a reporter construct into the *Snap29* locus has allowed visualization of *Snap29* expression in a number of organs, including the trachea, stomach, pituitary gland, brain, kidneys, bladder, testis, adrenal glands, and rib cartilages (<https://www.mousephenotype.org/data/genes/MGI:1914724>). Similar to *Scarf2*, we observed ubiquitous expression of *Snap29* at E10.5 and E12.5 by *in situ* hybridization. *In situ* hybridisation of embryo sections confirmed the ubiquitous expression in all tissues present at

both of these embryonic stages. In fact, different assays performed by Hohenstein A. C. and Roche P.A (2001) confirmed that SNAP29 has the capacity to bind to many different syntaxins that present on a variety of intracellular organelles and play a role in various intracellular protein trafficking pathways. Consistent with the data by Hohenstein A. C. and Roche P.A (2001), the ubiquitous expression that we observed suggests that *Snap29* is required in many tissues during mouse development.

Taking into consideration the intriguing expression data and extremely severe phenotypes that involve many of the same organs and tissues reportedly affected in CEDNIK patients, we decided to generate a novel, constitutive knockout *Snap29* mouse model in an outbred genetic background. The mouse model would allow us to rescue neonatal death. A mouse model with mutations in *Snap29* could shed insight into potential roles for this gene in the central and peripheral nervous system and enable us to study both neonatal and postnatal consequences of mutations in this gene.

Using CRISPR/Cas9, we generated the *lam1* mutant mouse line with a deletion of exon 2 in the *Snap29* gene (Figure 20). Heterozygous embryos and mice carrying the deletion on a mixed genetic background have reduced SNAP29 protein, are viable, and are fertile. Homozygous mutant mice and embryos have no detectable SNAP29 protein and recapitulate most of the abnormalities that have been reported in CEDNIK patients. Notably, the majority of hmz mutant mice in our outbred line survived to weaning, showing multiple congenital abnormalities.

We found that 67.5% of *Snap29*<sup>*lam1/lam1*</sup> mice survived to adulthood, unlike the previously reported *Snap29* knockout models on the C57BL/6 genetic background (Schiller *et al.* 2016). 50% (n = 9/18 of pups followed for skin defects) of surviving *Snap29*<sup>*lam1/lam1*</sup> mice developed

some type of skin abnormality within the first 4 days of life (Figure 24). We observed variable penetrance and expressivity of the phenotypes; the skin of some pups peeled and scaled, as was previously reported in *Snap29* pups on a C57BL/6 genetic background (Schiller *et al.*, 2016). However, skin abnormalities in *Snap29* homozygous mutant mice developed in different time point after birth (between P1 and P6) like human patients. This skin phenotype resembles that seen in CEDNIK syndrome patients. In fact, a subset of *Snap29*<sup>lam1/lam1</sup> mice displays peeling of large sheets of skin, which appears to be more severe than previously reported skin abnormalities in *Snap29* knockout mice (Schiller SA *et al.*, 2016). However, a few hmz mutant mice did not develop any noticeable skin phenotypes (N=4) similar to subset of patients reported; 2 patients with pathogenic mutations in *SNAP29* and hemizygous for 22q11.2 was shown not to have any skin abnormalities (McDonald-McGinn *et al.*, 2013). Furthermore, the skin phenotypes resolved in all surviving homozygous mutant mice by P10 (n=25). Thus, people with mutations in *SNAP29* show variable expressivity and/or penetrance, similar to what we observe in our mouse model.

TEM analysis of fibroblasts from patients with mutations in *SNAP29* and from a zebrafish model with knockdown of *Snap29* revealed delayed maturation and secretion of lamellar granules. Lamellar granules are involved in transport of lipids and proteases to the epidermis, thus showing a role for SNAP29 in lipid transport that could well be the basis of skin abnormalities in CEDNIK patients (Sprecher *et al.*, 2005). In addition, the outer layer of the skin, the stratum corneum (SC), is condensed in both human patients and *Snap29* knockout mice. Although *Snap29*<sup>lam1/lam1</sup> mice also have a condensed SC layer, skin condition was only severe in subset of *Snap29*<sup>lam1/lam1</sup> pups. We did not detect any clear vesicles in the epidermal layers by TEM in P1 pups (the stage before onset of skin shedding).



The *Snap29*<sup>lam1/lam1</sup> mice have other skin defects, including abnormally thick and red ears, and reddish skin around the genitalia (Figure 23). The latter may be due to late onset dermatitis affecting parts of body with less hair which needs further investigation.

CEDNIK and 22q11.2DS patients present with a number of skeletal problems, including scoliosis and clinodactyly. However, we did not observe any skeletal problems in mutant mice except extra lumbar ribs, which are seen in patients with 22q11.2DS (Minget *et al.*, 1997).

CEDNIK and 22q11.2DS patients are known to develop a number of different CNS malformations, which are listed in Table 4. However, it is unclear if the structural, anatomical or other defects (such as, myelination or synaptic properties) affected in 22q11.2DS contribute to neurological defects described 22q11.2DS patients. Furthermore, it is reported that 1/3 of 22q11.2DS patients develop schizophrenia or schizoaffective disorder and 22q11.2DS accounts for 1-2% of schizophrenia cases (Karayiorgou *et al.*, 2010). Indeed, polymorphism in the promoter region of the *SNAP29* gene has been proposed to be associated with schizophrenia and contribute to the mental health of a subgroup of 22q11.2DS patients with the common 3 Mb deletion, as well as patients with the 1.5 Mb deletion through a distal, *cis*-acting mechanism (Saito *et al.*, 2001).

*Snap29* mutant mice showed some phenotypes that might account for the CNS abnormalities found in patients. A subset of *Snap29*<sup>lam1/lam1</sup> mice presented with psychomotor delay, this was first observed pups during the first few days of life (n=18/32 hmz mutant pups) and confirmed with more comprehensive tests in adulthood (section 3.2.7 of this thesis). We also found that two homozygous mutant pups suffered from seizures. Seizures and psychomotor delay in *Snap29* homozygous mutant embryos are consistent with the neurological defects that

have been reported in CEDNIK and 22q11.2DS patients and suggest that this line of mice can be used to study neurological and psychopathology found in 22q11.2DS and CEDNIK patients.

It was previously reported that individuals carrying deletion in 22q11.2 region have significantly fewer children than their siblings. (Costain *et al.*, 2011). The study of 141 patients with 22q11.2DS showed that 85.8% of them were childless. Reduced reproductive fitness was higher among men compared women with the deletion, which could be partially due to the younger age and the neuropsychiatric conditions (Costain *et al.*, 2011)..

We provide evidence of abnormal testes morphology and defect in spermatogenesis in the male *Snap29*<sup>lam1/lam1</sup> mice. We also demonstrated reduced breeding success in *Snap29*<sup>lam1/lam1</sup> males, while females were not affected. In addition, one of our htz mutant control mice that was tested for fertility did not give rise to any offspring. Analysis of testis and spermatogenesis in that mouse gave similar results to the infertile hmz mutant male mice. Further analysis showed that htz mice also were affected, but not as severe as hmz mutant males. We thus postulate that hemizyosity for *SNAP29* might contribute to the reduced reproductive fitness observed in 22q11.2DS male patients.

We show that the novel *Snap29 lam1* mutant mouse line models skin malformations, as well as motor defects described in CEDNIK and in a subset of patients with 22q11.2DS. Furthermore, we reveal a novel requirement for *SNAP29* in male fertility. Our findings show strong evidence to support the contribution of *SNAP29* hemizyosity to the phenotypic spectrum of abnormalities found 22q11.2DS patients and a previously unknown role for *SNAP29* in male fertility. Thus, our results suggest that *Snap29* gene contributes to the abnormalities that cannot be explained by previously generated mouse models.

**4.1.3. 22q11.2DS unmasks rare variants in *SCARF2* and *SNAP29*.** Our lab and others have shown that the 22q11.2 deletion unmasks rare variants in the corresponding region of the intact chromosome, which results in manifestations of recessive disorders normally caused by the *SCARF2* and *SNAP29* genes (Figure 41; Anastasio *et al.*, 2010, McDonald-McGinn *et al.*, 2013, Bedeschi *et al.*, 2010).

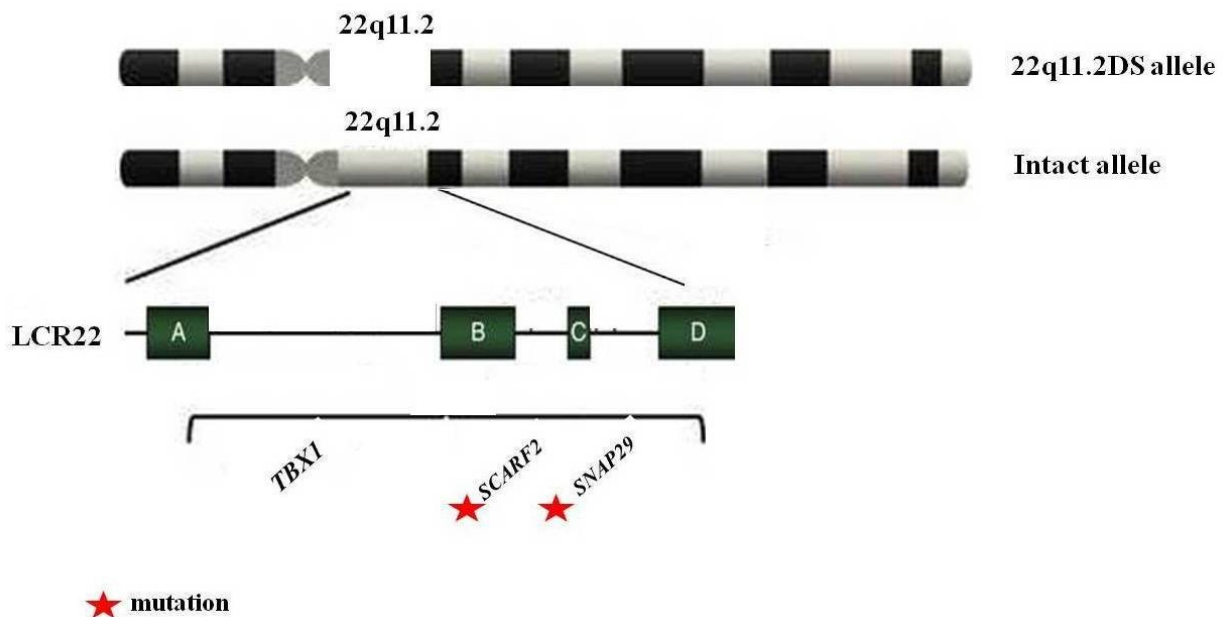


**Figure 41. 22q11.2DS unmasks rare variants in *SCARF2* and *SNAP29*.** The 22q11.2DS unmasks rare variants in two genes, *SCARF2* and *SNAP29*, in the 22q11.2 region of the intact chromosome, resulting in recessive disorders in a subset of hemizygous patients.

**4.1.4. Haploinsufficiency of *TBX1* explains some of the major phenotypes found in 22q11.2DS.** Up to 45 genes can be deleted in patients with 22q11.2DS. Mouse models with the smaller A-B deletion, affecting a subset of the 45 genes, support a strong role for haploinsufficiency of the T-box gene, *TBX1* in the disorder (Lindsay *et al.*, 2001). *Tbx1* is a transcription factor that is expressed in the developing pharyngeal region, specifically the

pharyngeal endoderm, core mesoderm of the pharyngeal arches and second heart field (Jerome, *et al.*, 2001). Our group and others have shown that mice with homozygous mutations in *Tbx1* (*Tbx1*<sup>-/-</sup>) phenocopied cardiac, palatal, thymic, and parathyroid abnormalities associated with 22q11.2DS; whereas heterozygous carriers (*Tbx1*<sup>+/-</sup>) showed a milder version of aortic arch abnormalities only (Jerome *et al.*, 2001). Since these initial studies in mice, numerous groups have confirmed the contribution of *TBX1* to congenital heart anomalies in humans (Merscher, *et al.*, 2001, Zweier *et al.*, 2007, Xu *et al.*, 2014). However, several additional malformations found in 22q11.2DS patients, for example skin, brain, motor, and genitourinary anomalies, occur in tissues that do not express nor require *Tbx1* during development. This observation is consistent with the contribution of additional gene(s) in the 22q11.2 region to abnormalities found in 22q11.2DS patients.

**4.1.5. Haploinsufficiency for *TBX1* and one or both of *SNAP29* and *SCARF2* might explain phenotypic variability found in 22q11.2DS.** We postulate that haploinsufficiency for *TBX1* along with that of *SNAP29* and/or *SCARF2* might explain the phenotypic variability found in 22q11.2DS patients. This effect would be expected in those patients harbouring A-C or A-D mutations, which result in deletion of *TBX1* along with one or both of *SCARF2* and *SNAP29* (Figure 42).

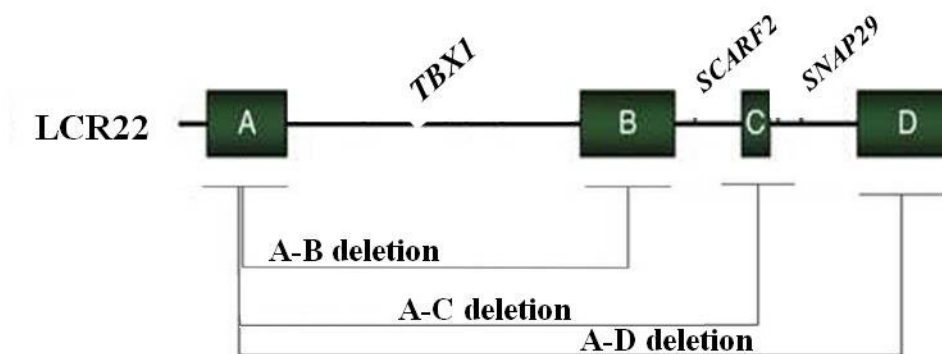


**Figure 42. Different size of deletions encompassing *TBX1*, *SCARF2*, and *SNAP29* genes within the 3 Mb region of 22q11.2.** Schematic diagram showing the A-B deletion, affecting *TBX1*; the A-C deletion, affecting *TBX1* and *SCARF2*; and the A-D deletion, affecting *TBX1*, *SCARF2*, and *SNAP29*.

In studies by Guris *et al.* (2006), genetic interactions between *Tbx1* and *Crkl* were used to model variable penetrance of heart defects in 22q11.2DS. This work provided an important molecular basis for cardiac abnormalities found in patients with A-D deletions. Similar interactions might exist between *TBX1* and *SCARF2* and/or *SNAP29*. Of note, patients with 22q11.2DS and patients carrying single mutation in *TBX1*, *SCARF2*, or *SNAP29* share subset of abnormalities (Table 11).

**Table 11. Phenotypic abnormalities shared between patients with 22q11.2DS, and patients with a single mutation in *TBX1*, *SNAP29* and *SCARF2***

<b>22q11.2DS</b>	<b><i>TBX1</i><sup>-/-</sup></b>	<b><i>SCARF2</i><sup>-/-</sup></b>	<b><i>SNAP29</i><sup>-/-</sup></b>
<b>CNS</b>	<b>NR</b>	<b>YES</b>	<b>YES</b>
<b>craniofacial</b>	<b>YES</b>	<b>YES</b>	<b>YES</b>
<b>hearing loss</b>	<b>YES</b>	<b>NR</b>	<b>YES</b>
<b>ophthalmological</b>	<b>NR</b>	<b>YES</b>	<b>YES</b>
<b>parathyroid</b>	<b>YES</b>	<b>NR</b>	<b>NR</b>
<b>thymus</b>	<b>YES</b>	<b>NR</b>	<b>NR</b>
<b>cardiac</b>	<b>YES</b>	<b>NR</b>	<b>NR</b>
<b>motor</b>	<b>NR</b>	<b>YES</b>	<b>YES</b>
<b>developmental delay</b>	<b>NR</b>	<b>NR</b>	<b>YES</b>
<b>feeding</b>	<b>NR</b>	<b>NR</b>	<b>YES</b>
<b>skeletal</b>	<b>NR</b>	<b>YES</b>	<b>YES</b>
<b>dental</b>	<b>NR</b>	<b>YES</b>	<b>NR</b>
<b>renal</b>	<b>NR</b>	<b>YES</b>	<b>NR</b>
<b>respiratory</b>	<b>NR</b>	<b>YES</b>	<b>YES</b>
<b>skin</b>	<b>NR</b>	<b>NR</b>	<b>YES</b>

Thus, we propose that a combinatory effect of heterozygosity in the 3 genes together might cause the majority of phenotypes in patients with the 3 Mb deletion of 22q11.2DS. The phenotypes could arise through three possible mechanisms (Figure 43):

1. *TBX1* might be the main causal gene generating differential phenotypes by regulating *SCARF2* and *SNAP29* genes.
2. Heterozygosity of *TBX1*, *SCARF2*, and *SNAP29* independently, or their interaction, might cause 22q11.2DS phenotypes.
3. There might be a common factor downstream of these genes that cause the phenotypes.

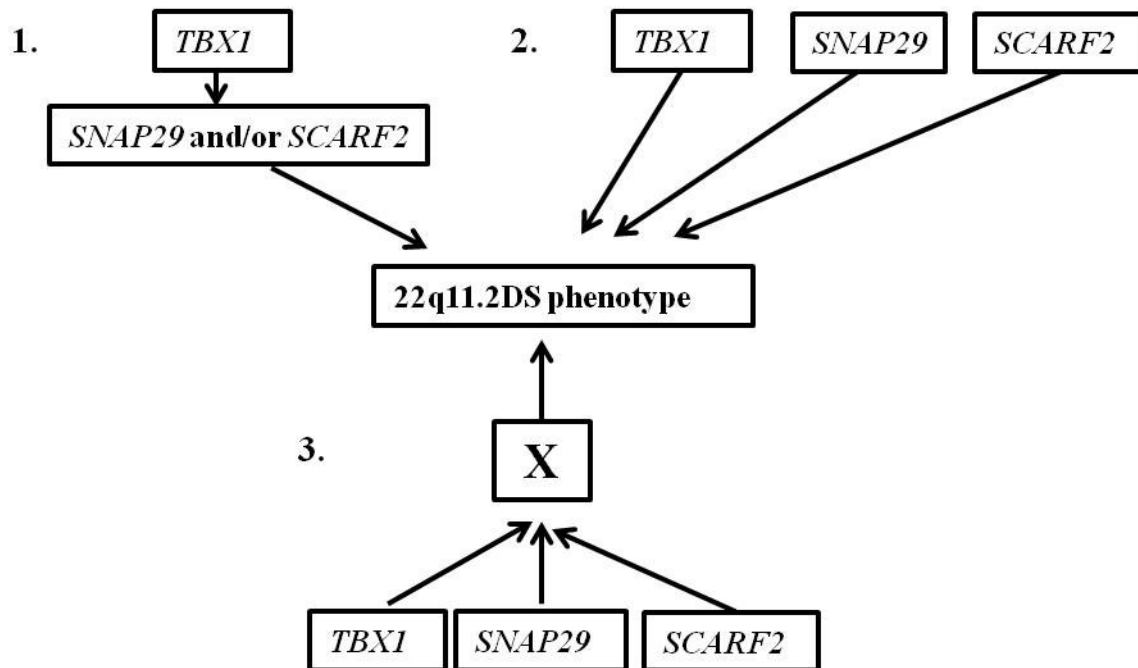


**Figure 43. Three possible different mechanisms leading to 22q11.2DS phenotype.**

Mouse models with mutations in *Tbx1* combined with mutations in *Snap29* and/or *Scarf2* could help identify the tissues in which interaction between these developmentally important genes contribute to the abnormalities found in 22q11.2DS.

**4.2. Contiguous gene syndromes.** Contiguous gene syndromes (CGSs), also known as microdeletion or microduplication syndromes (MMSs), arise from a deletion or duplication of a cluster of genetic features containing a number of genes physically linked together in a subchromosomal region (Tan *et al.*, 2009, Weise *et al.*, 2012, Pereira and Marion, 2018). Highly variable clinical manifestations involving many organs and systems are the main characteristics

of CGS. The variability in clinical phenotypes depends on the identity and number of genes involved in the CGS (Homefray *et al.*, 2015). Miller–Dieker syndrome, Angelman syndrome, and Williams syndrome are examples of CGSs. It is very difficult to correlate specific phenotypes with deleted genes in most CGSs. In some of these syndromes, many genes are deleted or duplicated but only one of them is gene-dosage sensitive and thus responsible for the particular clinical symptoms (Weise *et al.*, 2012). CGSs are usually caused by non-allelic homologous recombination between multiple LCRs that exist in human genome. To date, 211 microdeletion and 79 microduplication syndromes have been reported and generally microduplications show a milder clinical phenotype compared to microdeletions (Weise *et al.*, 2012).

22q11.2DS has recently been added to the list of CGS because it results from the loss of many genes that are close together (Pereira E. and Marion R., 2018). Most of the genes deleted in the syndrome have not been well characterized. A number of 22q11.2 mouse models strongly suggest that *TBX1* is a major determinant of the syndrome (Figure 5; Lindsay *et al.*, 1999, Lindsay *et al.*, 2001, Kimber *et al.*, 1999, Puech *et al.*, 2000, Merscher *et al.*, 2001, Yagi *et al.*, 2003).

*Tbx1* homozygous mutant mice have cardiac, palatal, thymic and parathyroid abnormalities similar to those found in 22q11.2DS (Jerome *et al.*, 2001). Mutational analysis of *TBX1* in patients with phenotypes consistent with 22q11.2DS proved that mutations in *TBX1* are responsible for five of the major phenotypes found in 22q11.2DS: facial anomalies, cardiac abnormalities, thymic hypoplasia, velopharyngeal insufficiency with cleft palate, and parathyroid dysfunction with hypocalcaemia (Yagi *et al.*, 2003). However, since a number of additional abnormalities found in 22q11.2DS are not observed when *TBX1* is mutated or deleted, and



patients with nested deletions of 22q11.2 not including *TBX1* show a similar range of abnormalities as patients with deletions of *TBX1*, other genes in the 22q11.2 region must contribute to the disease manifestations (Yagi *et al.*, 2003).

**4.3. Mouse models in human disease.** 22q11.2DS is associated with significant morbidity and, in some cases, premature mortality. The disease involves multiple organs and systems at birth and late-onset conditions including cognitive deficits and psychiatric illness (McDonald-McGinn *et al.*, 2015). Similar to most CGSs, correlations between deleted genes and specific phenotypes remain elusive. Because multiple organs and systems can be affected, the quality of the life can be significantly affected for patients and their families.

Animal models have played a critical role in the investigation and characterization of disease pathophysiology, and in the evaluation of new therapeutic agents and treatments. To understand the molecular basis of 22q11.2DS, studies focused on mouse models with hemizygous deletions in regions of chromosome 16 that are syntenic to the human 22q11.2DS locus (Botta *et al.*, 1997, Lund *et al.*, 2000). Although several animal models of 22q11.2DS have been reported, none could replicate the features of the syndrome completely (Kimber *et al.*, 1999, Lindsay, *et al.*, 1999 and Puech *et al.*, 2000, Lindsay,*et al.*, 2001). Nonetheless, mouse models provided a basis for identification and characterization of the developmental basis of a subset of phenotypes and help to improve diagnosis. Moreover, mouse models were also useful to understand that not all genes located in the 22q11.2 region contribute to phenotypes.

In our case, the novel mouse model for *Snap29* that we generated has helped us with the following statements:

1. Using a relatively new strategy with 4 sgRNAs, we completely deleted exon 2 in the gene.

2. Using an outbred genetic background, we could rescue the homozygous lethal phenotype in pups, which on an inbred C57BL/6 background did not survive.
3. We showed that heterozygosity for the *Snap29* mutation might cause craniofacial and motor abnormalities
4. Homozygous mice can present with skin, motor, and fertility problems with variable penetrance.
5. Homozygous male mice have reduced fertility.
6. Survival of *Snap29*<sup>lam1/lam1</sup> pups renders our mouse model useful for more detailed analysis of later-onset phenotypes seen in patients.
7. *Snap29* mutant mice develop neurological abnormalities and thus can be used for further assessment of the neurological defects observed in patients.
8. A subset of mice died before developing a skin phenotype, suggesting other possible causes of death.
9. This model will be helpful to elucidate the contribution of *SNAP29* to the 22q11.2 DS.

## CHAPTER 5. CONCLUSION AND FUTURE DIRECTIONS

### 5. 1. Conclusions

- *Scarf2* and *Snap29* are expressed in precursors of tissues affected in VDEGS, CEDNIK, and 22q11.2DS, as well as in many other tissues.
- CRISPR/Cas technology was used to successfully generate a new constitutive knockout mouse model for *Snap29*.
- Unlike existing models, the majority of *Snap29* homozygous mice survived to weaning.
- *Snap29* homozygous mutant mice show skin, motor, and skeletal abnormalities similar to those found in 22q11.2DS and CEDNIK patients.
- *Snap29* haplosufficiency causes infertility in mice, which might accounts for reduced reproductive fitness in males carrying 22q11.2DS.

## 5.2. Future directions

### 5.2.1. Determine whether the *Snap29* knockout line models brain abnormalities seen in the patients.

Brain malformations in CEDNIK patients may be due to several different causes: abnormal patterning, abnormal neuronal proliferation or survival, and/or abnormal migration. We assessed cortical markers and the number of cells present in different layers of the cortex, in order to evaluate cortical organization. We did not find any differences in number of the cells within different layers nor in cortical marker expression. We also assessed neuronal proliferation by BrdU and EdU labeling. Although preliminary results showed a visible difference in BrdU labeling between wt and a subset of hmz mutant brains, we did not quantify the labeled cells. In the future, BrdU labelled cells will be counted in order to evaluate neuronal proliferation. In addition, aberrant neuronal migrations were proposed to cause polymicrogyria in patients. Our lab will thus assess the existence of neuronal migration defects in the brains of hmz mutant mice. Additionally, using MRI, we have found that there are abnormal bilateral spots in the brains of adult mice, which look like CSF leakage. We will section and look the structure of these brains to identify the cause and exact location of the spots. Since abnormalities in the secretory pathway may also contribute to neuronal defects, we will collect brain samples for TEM to characterize abnormalities in the secretory pathway. Using TEM, we will examine organelle morphology and accumulation of autophagosomes in neurons from wild type and *Snap29* homozygous mutant pups. These experiments will allow us to confirm whether our mouse line models the brain abnormalities seen in patients.

### 5.2.2. Investigating possible causes of motor defect in mutant mice

We observed that homozygous mutant pups were slower and unable to stand on their feet for as long as their littermates in the first few days of their life, while adult *Snap29* homozygous mutant mice presented with abnormal shaking while standing on an object. These observations lead us to hypothesis that our hmz mutant mice have motor problem. To evaluate motor dysfunction in adult mice we used several techniques; neuromuscular coordination was assessed by rotarod, gate of mice was analysed by catwalk, and muscle strength by grip strength meter. We found that both *Snap29* heterozygous and homozygous mutant mice displayed motor impairments when compared to their wild type littermates. In the next step, we will evaluate possible mechanisms causing the motor dysfunction in our mice. To do so, we will section the spinal cord and limbs from P0 pups. The histology of the spinal cord will be assessed by Nissl staining. We will look at the shape of muscle fibers, assess branching of neurons, and count neuron number in the sections. We can use different antibodies, such as Islet-1 and Tuj-1, to distinguish motor neurons from other cells for counting, and investigate motor neuron death using the TUNEL assay. We could also check for autophagy markers, such as microtubule-associated protein 1 LC3, because motor neuron diseases have been linked with autophagy and *Snap29* has been shown to play an important role in autophagy (Tarabal *et al.*, 2005). These experiments will allow us to identify possible causes of motor dysfunction in mutant mice.

### 5.2.3. Evaluation of possible behavioural abnormalities in *Snap29*<sup>lam1/lam1</sup> mice.

60% of 22q11.2DS patients exhibit a number of psychiatric disorders, including anxiety, attention-deficit, autism, schizophrenia, mood disorders, cognitive deficits, visual spatial

abnormalities, impaired executive function and depression (Tang *et al.*, 2015). It is reported that 1/3 of 22q11.2DS patients develop schizoaffective disorder (Karayiorgou *et al.*, 2010) and mutations in *SNAP29* are predicted to contribute to schizophrenia and to the mental health of a subgroup of 22q11.2DS patients with the common 3 Mb deletion (Saito *et al.*, 2001). To determine if *Snap29* homozygous mice exhibit behavioural disturbances and cognitive impairment characteristics (such as vision, olfaction and balance, memory) wild type and *Snap29* homozygous mutant mice will be assessed for behavioural abnormalities using standard methods (Craig M. Powell and Tsuyoshi Miyakawa, 2006, Rodriguiz *et al.*, 2006). Open Field test will be performed according to standard conditions to measure anxiety (Rodriguiz RM and Wetsel WC, 2006). Y-maze test will be used to assess short term and spatial memory, respectively (Vorhees CV and Williams MT, 2014). Prepulse inhibition of the startle (PPI) will be assessed using a four startle chambers apparatus as previously described (Brody *et al.*, 2004, Rodriguiz and Wetsel WC, 2006). Brains will be collected from mice after the experiments and processed for structural examination.

#### **5.2.4. Examine possible ophthalmological problems in *Snap29*<sup>lam1/lam1</sup> mice.**

CEDNIK and 22q11.2DS patients present with a number of ophthalmological and eye abnormalities listed in Table 4. In order to identify if *Snap29*<sup>lam1/lam1</sup> line models eye problems existing in patients we will perform electroretinography (ERG) test on mice in collaboration with Dr. Pierre Lachapelle (McGill University). ERG test helps to measure the electrical response of mice retinal cells (Chang *et al.*, 2013). If ERG results are abnormal then we will determine if the mouse has the abnormal rod response (dark-adapted ERG) or abnormal cone ERG response (light-adapted ERG) or abnormal rod and cone ERG. In the next step eyes will be removed and sectioned to examine for the structural changes. Retinal vessel attenuation and

retinal pigment epithelial perturbation are signs of retinal degenerations and diseases (Chang *et al.*, 2013). To evaluate internal ocular health we can do mouse fundus examination. Mouse fundus examination is a useful test to find hemorrhages, exudates, cotton wool spots, blood vessel abnormalities (tortuosity, pulsation and new vessels) and pigmentation. Retinal degeneration, optic disc coloboma, or vascular problems can be easily detected by fundus exam.

## CHAPTER 6. REFERENCES

Adolph and Franchak. The development of motor behavior. Wiley Interdiscip Rev Cogn Sci. 8(1-2), 2017.

Adolph and Scott Robinson. Motor Development. NYU Psychology, 2015.

Adolph & Berger Motor development. In D. Kuhn & R. S. Siegler (Eds.), Cognition, perception, and language. Volume 2 of the Handbook of child psychology, 6th ed., pp. 161–213, 2006.

Alcamo *et al.*, Satb2 regulates callosal projection neuron identity in the developing cerebral cortex. Neuron. 57(3):364-77, 2008.

Anastasio *et al.* Mutations in SCARF2 Are Responsible for Van Den Ende-Gupta Syndrome The American Journal of Human Genetics 87, 553–559, 2010.

Anthwal and Thompson The development of the mammalian outer and middle ear. J. Anat. (2016) 228, pp217--232

Baldini *et al.*, The 22q11.2 Deletion Syndrome: A Gene Dosage Perspective. TheScientificWorld Journal. 6, 1881–1887, 2006.

Bassett *et al.*, Clinical features of 78 adults with 22q11 Deletion Syndrome. Am J Med Genet A. 138:307–13, 2005.

Bassett *et al.* International 22q11.2 Deletion Syndrome Consortium Practical guidelines for managing patients with 22q11.2 deletion syndrome. J Pediatr. 159(2):332-9, 2011.



Bassett *et al.*, Catechol-O-methyl transferase and expression of schizophrenia in 73 adults with 22q11 deletion syndrome. *Biol. Psychiatry* 61, 1135–1140, 2007.

Bearden *et al.*, Regional brain abnormalities in 22q11.2 deletion syndrome: association with cognitive abilities and behavioral symptoms. *Neurocase*. 10(3):198-206, 2004.

Bedeschi *et al.* Unmasking of a Recessive SCARF2 Mutation by a 22q11.12 de novo Deletion in a Patient with Van den Ende-Gupta Syndrome *Mol Syndromol*. 1(5): 239–245, 2010.

Pansky. Review of Medical embryology. Embryome Sciences, Inc 1301 Harbor Bay Parkway, Alameda, CA, 94502, 1982.

Ben-Salem *et al.*, A new Arab family with CEDNIK syndrome suggests a possible founder effect for the c.223delG mutation. *The Journal of dermatology*. 42(8):821-822, 2015.

Berthier & Keen. Development of reaching in infancy. *Experimental Brain Research*, 169, 507–518, 2006

Bish *et al.* Thalamic reductions in children with chromosome 22q11.2 deletion syndrome. *Developmental Neuroscience* Vol 15 No 9 28, 2004.

Bistrizter *et al.*, Congenital contractural arachnodactyly in two double second cousins: possible homozygosity. *Clin. Genet*. 44: 15-19, 1993.

Bollag *et al.*, An ancient family of embryonically expressed mouse genes sharing a conserved protein motif with the T locus. *Nat Genet*. 7:383–389, 1994.

Bonifacino and Glick . The Mechanisms of Vesicle Budding and Fusion. *Cell*, Vol. 116, 153–166, January 23, 2004.

Boot *et al.*, Movement disorders and other motor abnormalities in adults with 22q11.2 deletion syndrome. *AJMG*. Volume167, Issue3, Pages 639-645, 2015.

Bosse *et al.*, Malignant rhabdoid tumor of the bladder and ganglioglioma in a 14 year-old male with a germline 22q11.2 deletion. *Cancer Genetics*, 207 (9), 415 – 419, 2014

Bottaet *al.*, Causes of the phenotype–genotype dissociation in DiGeorge syndrome: clues from mouse models. *TRENDS in Genetics* Vol.17 No.10, 2001.

Bottaet *al.*, Comparative mapping of the DiGeorge syndrome region in mouse shows inconsistent gene order and differential degree of gene conservation. *Mamm. Genome*. 8, 890–895, 1997.

Bretelle *et al.*, Prenatal and postnatal diagnosis of 22q11.2 deletion syndrome. *European Journal of Medical Genetics* 53, 367e370, 2010.

Brody *et al.*, Assessment of a prepulse inhibition deficit in a mutant mouse lacking mGlu5 receptors. *Mol Psychiatry*. 9(1):35-41, 2004.

Burnet *al.*, Conotruncal anomaly face syndrome is associated with a deletion within chromosome 22q11. *J. Med. Genet.* 30, 822–824, 1993.

Canton *et al.* Scavenger receptors in homeostasis and immunity. *Nature Reviews. Immunology* volume 13. 2013.

Cardiff *et al.* Manual hematoxylin and eosin staining of mouse tissue sections, Cold Spring Harb. Protoc. 2014.

Carlson B Human Embryology and Developmental Biology, 5th edn. Philadelphia, PA: Saunders. 2014.

Carr *et al.*, Van Den Ende-Gupta syndrome: laryngeal abnormalities in two siblings. *Am. J. Med. Genet.* 143A: 2706-2711, 2007.

Carroll. *Female Reproductive System*. Elsevier's Integrated Physiology. Pages 177-187, 2007.

Chang. Mouse models for studies of retinal degeneration and diseases. *Methods Mol Biol.* 935, 2013.

Sellier *et al.*, Decreased DGCR8 Expression and miRNA Dysregulation in Individuals with 22q11.2 Deletion Syndrome. *PLoS One.* 9(8): e103884, 2014.

Chen, *et al.* Case-control study and transmission disequilibrium test provide consistent evidence for association between schizophrenia and genetic variation in the 22q11 gene ZDHHHC8. *Hum. Molec. Genet.* 13: 2991-2995, 2004.

Chih-Ping and Shu-Chin. Prenatal Sonographic Features of 22q11.2 Microdeletion Syndrome. *Journal of Medical Ultrasound*, Volume 16, Issue 2, Pages 123-129, 2008.

Cheung, *et al.* Neonatal hypocalcemia, neonatal seizures, and intellectual disability in 22q11.2 deletion syndrome. *Genet. Med.* 16, 40–44, 2014.

ChiDooling, *et al.* Gyral development of the human brain. *Annals of Neurology*, 1(1), 86–93, 1977.

Clancy, B. *et al.* Translating developmental time across mammalian species. *Neuroscience*, 105(1), 7–17, 2001.

Conrad *et al.* Mitochondrial and cytosolic thioredoxin reductase knockout mice. In: Hatfield D.L., Berry M.J., Gladyshev V.N. (eds) *Selenium*. Springer, Boston, MA, 2006.

Cooper. A mechanism for inside-out lamination in the neocortex. *Trends in Neurosciences*, 31(3), 113–119, 2008.

Copp, Greene et al. The genetic basis of mammalian neurulation. *Nature Reviews. Genetics*, 4(10), 784–793, 2003.

Corradini *et al.* SNAP-25 in Neuropsychiatric Disorders Mechanisms of Exocytosis: *Ann. N.Y. Acad. Sci.* 1152: 93–99, 2009.

Costain *et al.* Sex differences in reproductive fitness contribute to preferential maternal transmission of 22q11.2 deletions. *J Med Genet*, 2011.

Coulthard *et al.* Gait analysis as an objective measure in a chronic pain model. *J Neurosci Methods*. 116: 197- 213, 2002

Coulthard *et al.* Gait analysis as a correlate of pain induced by carrageenan intraplantar injection. *J Neurosci Methods*.128: 95-102, 2003.

Powell and Miyakawa. Schizophrenia-Relevant Behavioral Testing in Rodent Models: A Uniquely Human Disorder? *Biol Psychiatry*. 59(12): 1198–1207. 2006

Crawley JN. Behavioral phenotyping of transgenic and knockout mice: experimental design and evaluation of general health, sensory functions, motor abilities, and specific behavioral tests. *Brain Res*. 835(1):18-26, 1999.

Dastjerdi *et al.*, Tbx1 regulation of myogenic differentiation in the limb and cranial mesoderm. *Dev Dyn*. 236(2):353-63, 2007.

Roalf *et al.* White matter microstructural deficits in 22q11.2 deletion syndrome. *Psychiatry Research: Neuroimaging Volume 268*, 30, Pages 35-44, 2017.

Daw *et al.* A common region of 10p deleted in DiGeorge and velocardiofacial syndromes. *Nat. Genet.* 13, 458–460, 1996.

de Vries, Hopkins. Fetal movements and postures what do they mean for postnatal development? In Unknown Westport, UK: Greenwood.

de Vries *et al.* The emergence of fetal behaviour. I. Qualitative aspects. *Early Hum Dev* 7, 301–322, 1982.

Delorme *et al.* Search for copy number variants in chromosomes 15q11-q13 and 22q11.2 in obsessive compulsive disorder. *BMC Medical Genetics* 2010, 11:100 *BMC Medical Genetics*, 11:100, 2010.

Dorninger *et al.* Reduced muscle strength in ether lipid-deficient mice is accompanied by altered development and function of the neuromuscular junction. *Journal of Neurochemistry*. 29 May 2017.

Driscollet *al.* Prevalence of 22q11 microdeletions in DiGeorge and velocardiofacial syndromes: implications for genetic counselling and prenatal diagnosis. *J. Med. Genet.* 30, 813–817, 1993.

Dunham *et al.* The DNA sequence of human chromosome 22. *Nature*, 402: 489–95, 1999.

Edelmannet *al.* A common molecular basis for rearrangement disorders on chromosome 22q11. *Hum. Mol. Genet.*, 8, 1157–1167, 1999.

Eicheret *al.* Dysphagia in children with a 22q11.2 deletion: unusual pattern found on modified barium swallow. *J. Pediatr.* 137:158–164, 2000.

Emanuel. *et al.* Blocks of duplicated sequence define the endpoints of DGS/VCFS 22q11.2 deletions, 1999.

Farrell *et al.* HIRA, a DiGeorge syndrome candidate gene, is required for cardiac outflow tract septation. *Circ Res.* 84(2):127-35, 1999.

Fasshauer *et al.* Conserved structural features of the synaptic fusion complex: SNARE proteins reclassified as Q- and R-SNAREs. *Proc. Natl Acad. Sci. USA* 95, 1998

Fatemi . Reelin Glycoprotein, Structure, Biology and Roles in Health and Disease. Springer 2008.

Fenelon *et al.* Deficiency of Dgcr8, a gene disrupted by the 22q11.2 microdeletion, results in altered short-term plasticity in the prefrontal cortex. *Proc Natl Acad Sci U S A* 108, 4447–4452, 2011.

Fuchs-Telem *et al.* CEDNIK syndrome results from loss-of-function mutations in SNAP29. *Br J Dermatol.* 2011 Mar;164(3):610-6. Epub 2011.

Fung *et al.* Practical guidelines for managing adults with 22q11.2 deletion syndrome. *Genet Med.* (8):599-609, 2015.

Gary . Wright. Development of the Human External Ear. *J Am Acad Audiol* 8: 379-382, 1997.

Gennery. Immunological aspects of 22q11.2 deletion syndrome. *Cell Mol Life Sci.* 69(1):17–27, 2012.

Gerdes *et al.* Cognitive and behavior profile of preschool children with chromosome 22q11.2 deletion. *Am J Med Genet.* 85(2):127-33, 1999.

Ghariani *et al.* Polymicrogyria in chromosome 22q11 deletion syndrome. *Eur J Paediatr Neurol.* 6(1):73-7, 2002.

Giannottiet *al.* Cayler cardiofacial syndrome and del 22q11: part of the CATCH22 phenotype. *Am. J. Med. Genet.* 53, 303–304, 1994.

Gilbert. *Developmental Biology*. 6th edition. Sunderland (MA): Sinauer Associates; Spermatogenesis. Available from: <https://www.ncbi.nlm.nih.gov/books/NBK10095/> 2000.

Gilbert . *Developmental Biology*. 6th edition. Sunderland (MA): Sinauer Associates; 2000. Paraxial Mesoderm: The Somites and Their Derivatives. Available from: <https://www.ncbi.nlm.nih.gov/books/NBK10085/>

Gilbert. *Developmental Biology*. 6th edition. Sunderland (MA): Sinauer Associates; Oogenesis. Available from: <https://www.ncbi.nlm.nih.gov/books/NBK10008/2000>.

Gogos *et al.* Catechol-O-methyltransferase-deficient mice exhibit sexually dimorphic changes in catecholamine levels and behavior. *Proc. Nat. Acad. Sci.* 95: 9991-9996, 1998.

Gogoset *al.* The gene encoding proline dehydrogenase modulates sensorimotor gating in mice. *Nature Genet.* 21: 434-439, 1999.

Goodman *et al.* Hyperprolinaemia in patients with deletion (22)(q11.2) syndrome. *J. Inherit. Metab. Dis.* 23, 847–848, 2000.

Greber *et al.* Decreased levels of synaptosomal associated protein 25 in the brain of patients with Down Syndrome and Alzheimer's disease. *Electrophoresis*. 20 , 928±934, 1999.

Gripp *et al.* Nasal dimple as part of the 22q11.2 deletion syndrome. *Am J Med Genet.* 69:290–2, 1997.

Grosse *et al.* Synaptosome-associated protein of 25 kilodaltons in oocytes and steroid-producing cells of rat and human ovary: molecular analysis and regulation by gonadotropins. *Biol Reprod* 63, 643–650, 2000.

Grossfeld *et al.* The 11q terminal deletion disorder: a prospective study of 110 cases. *Am. J. Med. Genet. A* 129A, 51–61, 2004.

Guna *et al.* Comparative mapping of the 22q11.2 deletion region and the potential of simple model organisms. *Journal of Neurodevelopmental Disorders*, 7:18, 2015.

Guo *et al.* O-GlcNAc-modification of SNAP-29 regulates autophagosome maturation. *Nature Cell Biology* Vol. 16, No 12, 2014.

Guris *et al.* Dose-dependent interaction of Tbx1 and Crkl and locally aberrant RA signaling in a model of del22q11 syndrome. *Dev Cell*. 10(1):81-92, 2006.

Hacıhamdioğlu *et al.* 22q11 deletion syndrome: current perspective. *The Application of Clinical Genetics*, 2015.

Hamers *et al.* CatWalk-assisted gait analysis in the assessment of spinal cord injury. *J Neurotrauma*. 23(3-4):537-48, 2006.

Henao-Mejia *et al.* Generation of Genetically Modified Mice Using the CRISPR–Cas9 Genome-Editing System. *Cold Spring Harb Protoc*, 2016.

Hepp and Langley. SNAREs during development. *Cell Tissue Res*. 305:247–253, 2001.

Hepper. Prenatal psychological and behavioral development. In J. Valsiner & K. J. Connolly (Eds.), *Handbook of developmental psychology*. pp. 91–113. 2003.



Hevner *et al.* Tbr1 regulates differentiation of the preplate and layer 6. *Neuron* 29, 353–36, 2001.

Hogan *et al.* Manipulating the Mouse Embryo. A Laboratory Manual (Cold Spring Harbor Laboratory Press, Cold Spring Harbor, 1994.

Hohenstein and Roche. SNAP-29 Is a Promiscuous Syntaxin-Binding SNARE. *Biochemical and Biophysical Research Communications* 285, 167–171, 2001.

Homfray, Farndon. Twining's Textbook of Fetal Abnormalities (Third Edition), 2015

Honer *et al.* Abnormalities of prefrontal cortex SNARE complex proteins in bipolar disorder *Bipolar Disorders*. 4(Suppl. 1): 50, 2002.

Ikebuchi *et al.* SNAP-25 is essential for cortical granule exocytosis in mouse eggs. *Am J Physiol* 274, C1496–C1500, 1998.

In Clark *et al.* Etiology and Morphogenesis of Congenital Heart Disease. Futura, Armonk, NY.

Ishii *et al.* SREC-II, a new member of the scavenger receptor type F family, trans-interacts with SREC-I through its extracellular domain. *J. Biol. Chem.* 277, 39696–39702, 2002.

Itakura *et al.* ,The hairpin-type tail-anchored SNARE syntaxin 17 targets to autophagosomes for fusion with endosomes/lysosomes, *Cell* 151 (6), 1256–1269, 2012.

Itakura The hairpin-type tail-anchored SNARE syntaxin 17 targets to autophagosomes for fusion with endosomes/lysosomes. *Cell.*;151(6):1256-69, 2012.

Jahn , Scheller . SNAREs--engines for membrane fusion. *Nat Rev Mol Cell Biol.* 7(9):631-43, 2006.

Jalbrzikowski *et al.* Structural abnormalities in cortical volume, thickness, and surface area in 22q11.2 microdeletion syndrome: Relationship with psychotic symptoms. *NeuroImage: Clinical* 3, 405–415, 2013.

Jaouadi *et al.* A novel TBX1 missense mutation in patients with syndromic congenital heart defects. *Biochem Biophys Res Commun.* 2018...

Jerome *et al.* DiGeorge syndrome phenotype in mice mutant for the T-box gene, *Tbx1*. *Nat. Genet.*, 27, 286–291, 2001.

Jerome-Majewska *et al.* The trafficking protein Tmed2/p24 $\beta$ 1 is required for morphogenesis of the mouse embryo and placenta. *Dev Biol*, 341: 154–166, 2010.

Jianyu *et al.* The SREC-I and SREC-II associated with epidermal growth factor in scavenger receptor family are the potential regulative transmembrane receptors in *Larimichthys crocea*. *Fish & Shellfish Immunology* 47, 182e195, 2015.

Jyonouchi . *et al.* CHARGE (coloboma, heart defect, atresia choanae, retarded growth and development, genital hypoplasia, ear anomalies/ deafness) syndrome and chromosome 22q11.2 deletion syndrome: a comparison of immunologic and nonimmunologic phenotypic features. *Pediatrics* 123, e871–e877, 2009.

Kaplan *et al.* Human chromosome 22. *J. Med. Genet.*, 24, 65–78, 1987.

Karas *et al.* Perceived burden and neuropsychiatric morbidities in adults with 22q11.2 deletion syndrome. *J. Intellect. Disabil. Res.* 58, 198–210, 2014.

Karayiorgou *et al.* 22q11.2 microdeletions: linking DNA structural variation to brain dysfunction and schizophrenia. *Nature Reviews Neuroscience* volume11, pages402–416, 2010.

Kavoussi and Burnett Development of the Male Reproductive System. In: Kavoussi P., Costabile R., Salonia A. (eds) Clinical Urologic Endocrinology. Springer, London, 2013.

Khatchadourian *et al.* Structural abnormalities in spermatids together with reduced sperm counts and motility underlie the reproductive defect in HIP1<sup>-/-</sup> mice. Molecular Reproduction and Development, 74:341–359, 2007.

Kimber *et al.* Deletion of 150 kb in the minimal DiGeorge/velocardiofacial syndrome critical region in mouse. Hum Mol Genet. ;8(12):2229-37, 1999.

Kimberly *et al.* Altered brain microRNA biogenesis contributes to phenotypic deficits in a 22q11-deletion mouse model. Nature Genetics, Vol. 40, NUo 6, 2008.

Kobrynski. *et al.* Velocardiofacial syndrome, DiGeorge syndrome: the chromosome 22q11.2 deletion syndromes. www.thelancet.com Vol 370, 2007.

Konczak and Dichgans The development toward stereotypic arm kinematics during reaching in the first 3 years of life. Experimental Brain Research, 117, 346–354, 1997.

Kostovic, and Jovanov-Milosevic, N. The development of cerebral connections during the first 20–45 weeks' gestation. Seminars in Fetal & Neonatal Medicine, 11(6), 415–422, 2006.

Kurahashi *et al.* Another critical region for deletion of 22q11: a study of 100 patients. Am. J. Med. Genet., 72, (1997) 180–185, 1997.

Lambert *et al.*, The 22q11.2 deletion syndrome: Cancer predisposition, platelet abnormalities and cytopenias. American Journal of Medical Genetics Part A 176(4), 2017.

Lichao *et al.* Case Report Identification of a novel SNAP29 mutation in a patient with nocturnal frontal lobe epilepsy with long interictal and ictal phases: a case report. *Int J Clin Exp Med.*;10(2):3912-3917, 2017.

Lim *et al.* Forebrain Overexpression of Alpha-Synuclein Leads to Early Postnatal Hippocampal Neuron Loss and Synaptic Disruption. *Exp Neurology*, 221 (1):86-97. 2010.

Lin & Scheller. Structural organization of the synaptic exocytosis core complex. *Neuron* 19, 1087–1094, 1997.

Lindsay *et al.* Congenital heart disease in mice deficient for the DiGeorge syndrome region. *Nature* , 401, 379–383, 1999.

Lindsay *et al.* Tbx1 haploinsufficiency in the DiGeorge syndrome region causes aortic arch defects in mice. *Nature*, 410, 97–101, 2001.

Liu *et al.* Genetic variation in the 22q11 locus and susceptibility to schizophrenia. *Proc. Nat. Acad. Sci.* 99: 16859-16864, 2002.

Lund *et al.* Comparative sequence analysis of 634-kb of the mouse chromosome 16 region of conserved synteny with the human velocardiofacial syndrome region on chromosome, 2000.

Luo . *et al.* Systematic Prioritization and Integrative Analysis of Copy Number Variations in Schizophrenia Reveal Key Schizophrenia Susceptibility Genes. *Schizophrenia Bulletin* vol. 40 no. 6 pp. 1285–1299, 2014.

Malina. Motor Development during Infancy and Early Childhood: Overview and Suggested Directions for Research. *International journal of sport and heat science*. Volume 2 Pages 50-66, 2004.

Malloand Brändlin, I. Segmental identity can change independently in the hindbrain and rhombencephalic neural crest. *Dev. Dyn.* 210, 146–156, 1997.

Matsuoka *et al.* Confirmation that the conotruncal anomaly face syndrome is associated with a deletion within 22q11.2. *Am. J. Med. Genet.* 53, 285–289, 1994.

McDonald-McGinn *et al.* Hemizygous mutations in SNAP29 unmask autosomal recessive conditions and contribute to atypical findings in patients with 22q11.2DS. *J Med Genet.*, ;50(2):80-90, 2013.

McDonald-McGinn *et al.* Chromosome 22q11.2 deletion syndrome (DiGeorge syndrome/velocardiofacial syndrome). *Medicine (Baltimore)*. 90(1):1-18, 2011.

McDonald-McGinn *et al.* The Philadelphia story: the 22q11.2 deletion: report on 250 patients. *Genet Couns.* 10:11Y24, 1999.

McDonald-McGinn *et al.* 22q11.2 deletion syndrome. *Nat Rev Dis Prim.* 2015.

McDonald-McGinn. and SullivanChromosome 22q11.2 deletion syndrome (DiGeorge syndrome/ velocardiofacial syndrome). *Medicine* 90, 1–18, 2011.

McDonald-McGinn *et al.* The 22q11.2 deletion syndrome: Cancer predisposition, platelet abnormalities and cytopenias. *American Journal of Medical Genetics Part A*, 140 (8), 906 -909, 2006.

McDonald-McGinn *et al.* The 22q11.2 deletion in African-American patients: an underdiagnosed population? *Am. J. Med. Genet. A* 134, 242–246, 2005.

McDonald-McGinn *et al.* The 22q11.2 deletion in African-American patients: an underdiagnosed population? *Am. J. Med. Genet. A* 134, 242–246, 2005.

McDonald-McGinn, Autosomal dominant ‘Opitz’ GBBB syndrome due to a 22q11.2 deletion. Am. J. Med. Genet. 59, 103–113, 1995.

McDonald-McGinn, *et al.* Malignancy in chromosome 22q11.2 deletion syndrome (DiGeorge syndrome/velocardiofacial syndrome). Am. J. Med. Genet. A 140, 906–909, 2006.

McDonald-McGinn *et al.* The 22q11.2 deletion: screening, diagnostic workup, and outcome of results; report on 181 patients. Genet. Test. 1, 99–108, 1997.

Merscher *et al.* TBX1 is responsible for cardiovascular defects in velo-cardio-facial/DiGeorge syndrome. Cell, 104, 619–629, 2001.

Migliavacca *et al.* Sclerocornea in a patient with van den Ende-Gupta syndrome homozygous for a SCARF2 microdeletion. Am J Med Genet A. ;164A(5):1170-4, 2014.

Ming *et al.* Skeletal anomalies and deformities in patients with deletions of 22q11. Am J Med Genet 72: 210–215, 1997.

Monteiro *et al.* Defining new guidelines for screening the 22q11.2 deletion based on a clinical and dysmorphologic evaluation of 194 individuals and review of the literature. Eur J Pediatr 172: 927–945, 2013.

Morelli *et al.* An essential step of kinetochore formation controlled by the SNARE protein Snap29. EMBO J. 2016 Oct 17;35(20):2223-2237. 2016.

Morton *et al.* Abnormalities in the synaptic vesicle fusion machinery in Huntington’s disease. Brain Research Bulletin Volume 56, Issue 2, Pages 111-117, 2001.

Mudigoudar *et al.* Epilepsy in 22q11.2 Deletion Syndrome: A Case Series and Literature Review. *Pediatr Neurol.* 76:86-90, 2017.

Mukai *et al.* Molecular substrates of altered axonal growth and brain connectivity in a mouse model of schizophrenia. *Neuron* 86, 680–695, 2015.

Nadarajahand Parnavelas . Modes of neuronal migration in the developing cerebral cortex. *Nature Reviews. Neuroscience*, 3(6), 423–432, 2002.

Nagamatsu *et al.* Decreased expression of t-SNARE, syntaxin 1, and SNAP-25 in pancreatic beta-cells is involved in impaired insulin secretion from diabetic GK rat islets: restoration of decreased t SNARE proteins improves impaired insulin secretion. *Diabetes*,; 48(12): 2367-2373, 1999.

Nair *et al.*, SNARE proteins are required for macroautophagy, *Cell* 146 (2), 290–302, 2011.

Napoli *et al.* Mitochondrial Citrate Transporter-dependent Metabolic Signature in the 22q11.2 Deletion Syndrome. *J Biol Chem.* 290(38): 23240–23253, 2015.

Neher and Sakaba . Multiple roles of calcium ions in the regulation of neurotransmitter release. *Neuron*.59(6):861-72, 2008.

OpenStax, *Anatomy & Physiology*. Chapter 27. The Reproductive System. OpenStax CNX.<http://cnx.org/contents/14fb4ad7-39a1-4eee-ab6e-3ef2482e3e22@8.24>, 2016.

Osen-Sand *et al.* Common and distinct fusion proteins in axonal growth and transmitter release. *J Comp Neurol* 367, 222–234, 1996.

Osen-Sand *et al.* Inhibition of axonal growth by SNAP-25 antisense oligonucleotides in vitro and in vivo. *Nature* 364, 1993.

Oskarsdottir *et al.* Incidence and prevalence of the 22q11 deletion syndrome: a population-based study in Western Sweden. *Arch. Dis. Child.* 89, 148–151, 2004.

Parke *et al.* Cardiovascular and craniofacial defects in Crk-null mice. *Mol. Cell. Biol.* 26.. 6272–6282, 2006.

Paronetto *et al.* Ranbp1, deleted in DiGeorge/22q11.2 deletion syndrome, is a microcephaly gene that selectively disrupts layer 2/3 cortical projection neuron generation. *Cereb. Cortex* 25, 3977–3993, 2015.

Patel, Salih *et al.* Expanding the clinical spectrum and allelic heterogeneity in van den Ende-Gupta syndrome. (Letter) *Clin. Genet.* 85: 492-494, 2014.

Payloret *et al.* Mice deleted for the DiGeorge/velocardiofacial syndrome region show abnormal sensorimotor gating and learning and memory impairments. *Hum. Mol. Genet.* 10, 2645–2650, 2001.

Pellegrini and Smith. Physical activity play: The nature and function of a neglected aspect of play. *Child Development*, 69, 577–598, 1998.

Pereira and Marion R. Contiguous Gene Syndromes. *Pediatrics in Review*. Vol. 39 No. 1, 2018.

Pereira and Marion Contiguous Gene Syndromes. *Pediatrics in Review*, Vol. 39, Issue1, 2018.

Philip and Bassett . Cognitive, behavioural and psychiatric phenotype in 22q11.2 deletion syndrome. *Behav Genet.* 41(3):403-12, 2011.

Ping-Yue *et al.* SNAP29-mediated Modulation of Synaptic Transmission in Cultured Hippocampal Neurons. *The Journal of Biological Chemistry*, Vol. 280, No. 27, Issue of July 8, pp. 25769–25779, 2005.



Pinkerton *et al.* . Development of the human ovary: A study using histochemical techniques. *Obstet. Gynecol.* 18:152–181, 1961.

Plüddemann, Neyen C, Gordon S. Macrophage scavenger receptors and host-derived ligands. *Methods.* 43:207–217, 2007.

PrabhuDas *et al.* Standardizing Scavenger Receptor Nomenclature. *J Immunol* March 1, 192 (5), 2014.

Prasad *et al.* Thioredoxin Reductase 2 (TXNRD2) Mutation Associated With Familial Glucocorticoid Deficiency (FGD). *J Clin Endocrinol Metab.* 99(8): E1556–E1563, 2014.

Puech *et al.* Normal cardiovascular development in mice deficient for 16 genes in 550 kb of the velocardiofacial/ DiGeorge syndrome region. *PNAS,* . 97 (18), 2000.

Qingning *et al.* SNAP-29: A general SNARE protein that inhibits SNARE disassembly and is implicated in synaptic transmission. *PNAS* November 20, vol. 98 no. 24, 14038–14043, 2001.

Racedo *et al.* Mouse and human CRKL is dosage sensitive for cardiac outflow tract formation. *Am J Hum Genet.* ;96(2):235-44, 2015.

Ramalho-Santos *et al.* SNAREs in mammalian sperm: possible implications for fertilization. *Dev Biol* 223: 54–69, 2000.

Rapaport *et al.* Loss of SNAP29 Impairs Endocytic Recycling and Cell Motility. *PLoS ONE* 5(3): e9759, 2010.

Raux . *et al.* Involvement of hyperprolinemia in cognitive and psychiatric features of the 22q11 deletion syndrome. *Hum. Mol. Genet.* 16, 83–91, 2007.

Revil and Jerome-Majewska. During embryogenesis, *esrp1* expression is restricted to a subset of epithelial cells and is associated with splicing of a number of developmentally important genes. *Dev Dyn* 242, 281-290, 2013.

Roberts *et al.* Targeted mutagenesis of the Hira gene results in gastrulation defects and patterning abnormalities of mesoendodermal derivatives prior to early embryonic lethality. *Mol Cell Biol.* 22(7):2318-28, 2002.

Rodriguez and Wetsel . Assessments of Cognitive Deficits in Mutant Mice. In: Levin ED, Buccafusco JJ, editors. *Animal Models of Cognitive Impairment*. Boca Raton (FL): CRC Press/Taylor & Francis; Chapter 12. Available from: <https://www.ncbi.nlm.nih.gov/books/NBK2527>, 2006.

Roizen *et al.* 22q11.2 Deletion Syndrome: Are Motor Deficits More Than Expected for IQ Level? *J Pediatr.* 2010 October ; 157(4): 658–661. 2010.

Rubinsztein . *et al.* Mechanisms of Autophagosome Biogenesis *Current Biology* Volume 22, Issue 1, Pages R29-R34, 2012.

Saito T *et al.* Polymorphism in SNAP29 gene promoter region associated with schizophrenia. *Mol Psychiatry.* 6(2):193-201, 2001.

Sandell . Chapter 9 - Neural Crest Cells in Ear Development. *Evolution, Development and Disease*, ScienceDirect. Pages 167-187, 2014.

Scambler . The 22q11 deletion syndromes. *Human Molecular Genetics*, Volume 9, Issue 16, 1, Pages 2421–2426, 2000.

Schiller *et al.* Establishment of Two Mouse Models for CEDNIK Syndrome Reveals the Pivotal Role of SNAP29 in Epidermal Differentiation. *J Invest Dermatol.* 2016.

Schweitzer *et al.* van den Ende-Gupta syndrome of blepharophimosis, arachnodactyly, and congenital contractures: clinical delineation and recurrence in brothers. *Am J Med Genet A*. 118A(3):267-73, 2003.

Schwerin. The anatomy of movement. *Anatomy, Brain Basics*. 2013.

Sellier C *et al.*, Decreased DGCR8 Expression and miRNA Dysregulation in Individuals with 22q11.2 Deletion Syndrome. *PLoS One*. 9(8): e103884, 2014.

Sgardioli *et al.* Diagnostic Approach to Microdeletion Syndromes Based on 22q11.2 Investigation: Challenges in Four Cases. *Mol Syndromol*. 8:244-252, 2017.

Sgardioli *et al.* 22q11.2 Deletion Syndrome: Laboratory Diagnosis and TBX1 and FGF8 Mutation Screening. *J Pediatr Genet*. 4(1):17-22, 2015.

Shaikh *et al.* Chromosome 22-specific low copy repeats and the 22q11.2 deletion syndrome: Genomic organization and deletion endpoint analysis. *Human Molecular Genetics*, Vol. 9, No. 4, 2000.

Shaikh *et al.* Evolutionarily conserved low copy repeats (LCRs) in 22q11 mediate deletions, duplications, translocations, and genomic instability: An update and literature review. *Genetics IN Medicine*, z Vol. 3 z No. 16, 2001.

Sharma. *et al.* Proteasome Inhibition Alleviates SNARE-Dependent Neurodegeneration. *Science Translational Medicine*. Vol. 4, Issue 147, pp. 147ra113, 2012.

Shashi *et al.* Evidence of gray matter reduction and dysfunction in chromosome 22q11.2 deletion syndrome. *Psychiatry Res*. 181(1):1-8, 2010.

Smith *et al.* The mouse Gene Expression Database (GXD): 2007 update.

Smith *et al.* Quantitative measurement of muscle strength in the mouse. *Journal of Neuroscience Methods* Volume 62, Issues 1–2, Pages 15-19, 1995.

Sobin *et al.* Neuromotor deficits in children with the 22q11 deletion syndrome. *Movement disorders*. *Movement Disorders* Vol. 21, No. 12, pp. 2082–2089, 2006.

Sobin. *et al.* Neuropsychological Characteristics of Children with the 22q11 Deletion Syndrome : A Descriptive Analysis. *Child Neuropsychol.* 11(1): 39–53, 2005.

Söllner *et al.* SNAP receptors implicated in vesicle targeting and fusion. *Nature.* 25;362(6418):318-24, 1993.

Som and Naidich. Illustrated Review of the Embryology and Development of the Facial Region, Part 1: Early Face and Lateral Nasal Cavities. *American Journal of Neuroradiology*, 2013.

Som and Naidich. Illustrated Review of the Embryology and Development of the Facial Region, Part 2: Late Development of the Fetal Face and Changes in the Face from the Newborn to Adulthood. *American Journal of Neuroradiology.* 35 (1) 10-18, 2014.

Sprecher *et al.* A Mutation in SNAP29, Coding for a SNARE Protein Involved in Intracellular Trafficking, Causes a Novel Neurocutaneous Syndrome Characterized by Cerebral Dysgenesis, Neuropathy, Ichthyosis, and Palmoplantar Keratoderma. *Am. J. Hum. Genet.* 77:242–251, 2005.

Stankiewicz and Lupski. Genome architecture, rearrangements and genomic disorders *Trends Genet.* 18: . 74–82, 2002.

Stark KL *et al.* Altered brain microRNA biogenesis contributes to phenotypic deficits in a 22q11-deletion mouse model. *Nat Genet.* 40(6):751-60, 2008.

Stark *et al.* Altered brain microRNA biogenesis contributes to phenotypic deficits in a 22q11-deletion mouse model. *Nat Genet* 40: 751–760, 2008.

Stevens *et al.* Risk of malignancy in 22q11.2 deletion syndrome. *Clin Case Rep.* 5(4): 486–490, 2017.

Stiles and Terry Jernigan. The Basics of Brain Development. *Neuropsychol Rev.* 20(4): 327–348, 2010.

Stiles. The fundamentals of brain development: Integrating nature and nurture. Cambridge: MA, Harvard University Press. 2008.

Streeter. Development of the auricle in the human embryo. *Contrib Embryol.* 69:111, 1922.

Südhof. Neurotransmitter Release: The Last Millisecond in the Life of a Synaptic Vesicle. *Neuron* Volume 80, Issue 3, 30, , Pages 675-690, 2013.

Sudhof . The synaptic vesicle cycle. *Annu Rev Neurosci.* 27:509-47, 2004.

Sullivan. The clinical, immunological, and molecular spectrum of chromosome 22q11.2 deletion syndrome and DiGeorge syndrome. *Curr Opin Allergy Clin Immunol.* 4:505–12, 2004.

Swati Gupta *et al.* Somatic overgrowth associated with homozygous mutations in both MAN1B1 and SEC23A . *Cold Spring Harb Mol Case*, 2016.

Swillen *et al.* Chromosome 22q11 deletion syndrome: update and review of the clinical features, cognitive-behavioral spectrum, and psychiatric complications. *Am J Med Genet* 97(2): 128–135, 2000.

Swillen *et al.* Early motor development in young children with 22q.11 deletion syndrome and a conotruncal heart defect. *Dev Med Child Neurol.* 47(12):797-802, 2005.

Swillen *et al.* Neuropsychological, learning and psychosocial profile of primary school aged children with the velo-cardio-facial syndrome (22q11 deletion): evidence for a nonverbal learning disability? *Child Neuropsychol.* 5:230–241, 1999.

Swillen *et al.* The behavioural phenotype in velo-cardio-facial syndrome (VCFS): from infancy to adolescence. *Genet Couns.* 10(1):79-88, 1999.

Taddei *et al.* Genetic factors are major determinants of phenotypic variability in a mouse model of the DiGeorge/del22q11 syndromes. *Proc. Natl. Acad. Sci. U. S. A.* 98, 11428–11431, 2001.

Takamori, Synaptic Vesicles. *Encyclopedia of Neuroscience*, 2009.

Tan and Rodriguez . *Molecular Pathology of the Cardiovascular System. Cell and Tissue Based Molecular Pathology.*Pages 214-240, 2009.

Tan *et al.* Meta-analysis of magnetic resonance imaging studies in chromosome 22q11.2 deletion syndrome (velocardiofacial syndrome). *Schizophr Res.*115(2-3):173-81, 2009.

Tanaka. *et al.* FAM210A is a novel determinant of bone and muscle structure and strength, *PNAS Latest Articles*, 2017.

Tang *et al.* Psychiatric disorders in 22q11.2 deletion syndrome are prevalent but undertreated. *Psychological Medicine.*44, 1267–1277, 2014.

Tanget *al.* Behavioral and Psychiatric Phenotypes in 22q11.2 Deletion Syndrome. *Journal of Developmental & Behavioral Pediatrics:* Vol. 36, Issue 8, p 639–650, 2015.

Tarabal *et al.* Protein retention in the endoplasmic reticulum, blockade of programmed cell death and autophagy selectively occur in spinal cord motoneurons after glutamate receptor-mediated injury. *Mol Cell Neurosci.*, 29: 283–298, 2005.

Bartzela *et al.* Update on 13 Syndromes Affecting Craniofacial and Dental Structures. *Front. Physiol.*, 2017.

*et al.* Structural brain abnormalities associated with deletion at chromosome 22q11: Quantitative neuroimaging study of adults with velo-cardio-facial syndrome. *The British Journal of Psychiatry*. Volume 178, , pp. 412-419, 2001.

Tobias *et al.* Towards earlier diagnosis of 22q11 deletions. *Arch Dis Child.* 1999 Dec; 81(6): 513–514, 1999.

Tokarev *et al.* Overview of Intracellular Compartments and Trafficking Pathways NCBI Bookshelf Austin (TX): Landes Bioscience; 2000-2013.

Valiente, and Mari. Neuronal migration mechanisms in development and disease. *Current Opinion in Neurobiology*, 20 (1), 68–78, 2010.

Vorhees and Williams. Assessing Spatial Learning and Memory in Rodents. *ILAR Journal* 55(2):310-32, 2014.

Wang. *et al.* SNARE-mediated membrane fusion in autophagy. *Seminars in Cell & Developmental Biology* 60, 97–104, 2016.

Wang, *et al.* Onestep generation of mice carrying mutations in multiple genes by CRISPR/Cas-mediated genome engineering. *Cell*, 153:910–918, 2013.

Weise . *et al.* Microdeletion and Microduplication Syndromes. J\_Histochem Cytochem; 60(5): 346–358, 2012.

Westin. *et al.* Automatic gait analysis in bilateral Parkinsonian rats and the role of L-DOPA therapy. Behavioural Brain Research, 226, 519-528, 2012.

Wodarz and Huttner. Asymmetric cell division during neurogenesis in *Drosophila* and vertebrates. Mechanisms of Development, 120(11). 1297–1309, 2003.

Wonodiet *al.* Association between polymorphism of the SNAP29 gene promoter region and schizophrenia. Schizophr Res. 78(2-3):339-41, 2005.

Wu *et al.* Genitourinary malformations in chromosome 22q11.2 deletion. J Urol.168(6):2564-5, 2002.

Han. *et al.* Sequence determinants of improved CRISPR sgRNA design. Genome Research. 2015.

Xu *et al.* Novel TBX1 loss-of-function mutation causes isolated conotruncal heart defects in Chinese patients without 22q11.2 deletion. BMC Med Genet. 15:78, 2014.

Yagi *et al.* Role of TBX1 in human del22q11.2 syndrome. Lancet 362, 1366–1373, 2003.

Yang *et al.* Amyloid- $\beta$  Oligomers May Impair SNARE-Mediated Exocytosis by Direct Binding to Syntaxin 1a. Cell Rep. 12(8):1244-51, 2015.

Yap and Winckler. Vesicular Sorting to Axons and Dendrites Reference Module in Biomedical Sciences Encyclopedia of Neuroscience.Pages 115–120, 2009.



Yoshida *et al.* Genetic mutation analysis in Japanese patients with non-syndromic congenital heart disease. J Hum Genet. 2016 Feb;61(2):157-62. Epub 2015.

Yu *et al.* Chapter Nine - Scavenger Receptors: Emerging Roles in Cancer Biology and Immunology. Advances in Cancer Research Volume 128, Pages 309-364, 2015.

Zani *et al.* Scavenger Receptor Structure and Function in Health and Disease. Cells, 4, 178-201, 2015.

Zweier. *et al.* Human TBX1 missense mutations cause gain of function resulting in the same phenotype as 22q11.2 deletions. Am. J. Hum. Genet. 80, 510–517, 2007.

## COPYRIGHT PERMISSIONS

**Figure 1.** Delorme *et al.* Search for copy number variants in chromosomes 15q11-q13 and 22q11.2 in obsessive compulsive disorder. BMC Medical Genetics 2010, 11:100

**Figure 1.** © Delorme *et. al*; licensee BioMed Central Ltd. 2010

This article is published under license to BioMed Central Ltd. This is an Open Access article distributed under the terms of the Creative Commons Attribution License (<http://creativecommons.org/licenses/by/2.0>), which permits unrestricted use, distribution, and reproduction in any medium, provided the original work is properly cited.

**Figure 2.** Shaikh *et al.* Evolutionarily conserved low copy repeats (LCRs) in 22q11 mediate deletions, duplications, translocations, and genomic instability: An update and literature review. Genetics in Medicine January/February 2001 z Vol. 3 z No. 16

**Figure 3.** Migliavacca *et al.* Sclerocornea in a patient with van den Ende-Gupta syndrome homozygous for a SCARF2 microdeletion. Am J Med Genet A. 2014;164A(5):1170-4

**Figure 4.** Sprecher *et al.* A Mutation in SNAP29, Coding for a SNARE Protein Involved in Intracellular Trafficking, Causes a Novel Neurocutaneous Syndrome Characterized by Cerebral Dysgenesis, Neuropathy, Ichthyosis, and Palmoplantar Keratoderma. Am. J. Hum. Genet. 77:242–251, 2005

**Figure 5.** Bottaet *al*, Causes of the phenotype–genotype dissociation in DiGeorge syndrome: clues from mouse models. *TRENDS in Genetics* Vol.17 No.10 October 2001

**Figure 6.** Stiles and Jernigan. The Basics of Brain Development. *Neuropsychol Rev.* 2010 Dec; 20(4): 327–348.

Figure 9. © The Author(s) 2010

Stiles. & Jernigan. *Neuropsychol Rev* (2010) 20: 327. <https://doi.org/10.1007/s11065-010-9148-4>

Publisher NameSpringer US

Print ISSN1040-7308

Online ISSN1573-6660

Open Access

This article is distributed under the terms of the Creative Commons Attribution Noncommercial License which permits any noncommercial use, distribution, and reproduction in any medium, provided the original author(s) and source are credited.

**Figure 8, Figure 9 and Figure 10.** Juan S. Bonifacino and Benjamin S. Glick. The Mechanisms of Vesicle Budding and Fusion. *Cell*, Vol. 116, 153–166, January 23, 2004

## SPRINGER NATURE LICENSE TERMS AND CONDITIONS

Jun 25, 2018

This Agreement between McGill University -- Vafa Keser ("You") and Springer Nature ("Springer Nature") consists of your license details and the terms and conditions provided by Springer Nature and Copyright Clearance Center.

License Number	4376130808110
License date	Jun 25, 2018
Licensed Content Publisher	Springer Nature
Licensed Content Publication	Genetics in Medicine
Licensed Content Title	Evolutionarily conserved low copy repeats (LCRs) in 22q11 mediate deletions, duplications, translocations, and genomic instability: An update and literature review
Licensed Content Author	Tamim H Shaikh, Hiroki Kurahashi, Beverly S Emanuel
Licensed Content Date	Jan 1, 2001
Licensed Content Volume	3
Licensed Content Issue	1
Type of Use	Thesis/Dissertation
Requestor type	non-commercial (non-profit)
Format	print and electronic
Portion	figures/tables/illustrations
Number of figures/tables/illustrations	1
High-res required	no
Will you be translating?	no
Circulation/distribution	<501
Author of this Springer Nature content	no
Title	Candidate genes implicated in the generation of phenotypic variability in 22q11.2 deletion syndrome; Snap29 and Scarf2
Instructor name	n/a
Institution name	n/a
Expected presentation date	Feb 2019
Portions	Figure 3
Requestor Location	McGill University 1225 SUSSEX

Montreal, QC H3H2A2  
Canada  
Attn: McGill University

## JOHN WILEY AND SONS LICENSE TERMS AND CONDITIONS

Jun 28, 2018

This Agreement between McGill University -- Vafa Keser ("You") and John Wiley and Sons ("John Wiley and Sons") consists of your license details and the terms and conditions provided by John Wiley and Sons and Copyright Clearance Center.

License Number	4377801067584
License date	Jun 28, 2018
Licensed Content Publisher	John Wiley and Sons
Licensed Content Publication	American Journal of Medical Genetics Part A
Licensed Content Title	Sclerocornea in a patient with van den Ende–Gupta syndrome homozygous for a SCARF2 microdeletion
Licensed Content Author	Michele P. Migliavacca, Nara L. M. Sobreira, Graziela P.M. Antonialli, et al
Licensed Content Date	Jan 29, 2014
Licensed Content Volume	164
Licensed Content Issue	5
Licensed Content Pages	5
Type of use	Dissertation/Thesis
Requestor type	University/Academic
Format	Print and electronic
Portion	Figure/table
Number of figures/tables	2
Original Wiley figure/table number(s)	Figure 1 and Figure 2
Will you be translating?	No
Title of your thesis / dissertation	Candidate genes implicated in the generation of phenotypic variability in 22q11.2 deletion syndrome; Snap29 and Scarf2
Expected completion date	Feb 2019
Expected size (number of pages)	150
Requestor Location	McGill University 1225 SUSSEX  Montreal, QC H3H2A2 Canada Attn: McGill University
Publisher Tax ID	EU826007151
Total	0.00 CAD
Terms and Conditions	

## ELSEVIER LICENSE TERMS AND CONDITIONS

Jun 28, 2018

This Agreement between McGill University -- Vafa Keser ("You") and Elsevier ("Elsevier") consists of your license details and the terms and conditions provided by Elsevier and Copyright Clearance Center.

License Number	4377810821064
License date	Jun 28, 2018
Licensed Content Publisher	Elsevier
Licensed Content Publication	The American Journal of Human Genetics
Licensed Content Title	A Mutation in SNAP29, Coding for a SNARE Protein Involved in Intracellular Trafficking, Causes a Novel Neurocutaneous Syndrome Characterized by Cerebral Dysgenesis, Neuropathy, Ichthyosis, and Palmoplantar Keratoderma
Licensed Content Author	Eli Sprecher,Akemi Ishida-Yamamoto,Mordechai Mizrahi-Koren,Debora Rapaport,Dorit Goldsher,Margarita Indelman,Orit Topaz,Ilana Chefetz,Hanni Keren,Timothy J. O'Brien,Dani Bercovich,Stavit Shalev,Dan Geiger,Reuven Bergman,Mia Horowitz,Hanna Mandel
Licensed Content Date	Aug 1, 2005
Licensed Content Volume	77
Licensed Content Issue	2
Licensed Content Pages	10
Start Page	242
End Page	251
Type of Use	reuse in a thesis/dissertation
Intended publisher of new work	other
Portion	figures/tables/illustrations
Number of figures/tables/illustrations	1
Format	both print and electronic
Are you the author of this Elsevier article?	No
Will you be translating?	No
Original figure numbers	Figure 1
Title of your thesis/dissertation	Candidate genes implicated in the generation of phenotypic variability in 22q11.2 deletion syndrome; Snap29 and Scarf2
Expected completion date	Feb 2019
Estimated size (number of pages)	150
Requestor Location	McGill University 1225 SUSSEX

## ELSEVIER LICENSE TERMS AND CONDITIONS

Jun 25, 2018

This Agreement between McGill University -- Vafa Keser ("You") and Elsevier ("Elsevier") consists of your license details and the terms and conditions provided by Elsevier and Copyright Clearance Center.

License Number	4376120023120
License date	Jun 25, 2018
Licensed Content Publisher	Elsevier
Licensed Content Publication	Trends in Genetics
Licensed Content Title	Causes of the phenotype-genotype dissociation in DiGeorge syndrome: clues from mouse models
Licensed Content Author	Annalisa Botta,Francesca Amati,Giuseppe Novelli
Licensed Content Date	Oct 1, 2001
Licensed Content Volume	17
Licensed Content Issue	10
Licensed Content Pages	4
Start Page	551
End Page	554
Type of Use	reuse in a thesis/dissertation
Portion	figures/tables/illustrations
Number of figures/tables/illustrations	1
Format	both print and electronic
Are you the author of this Elsevier article?	No
Will you be translating?	No
Original figure numbers	Figure 1
Title of your thesis/dissertation	Candidate genes implicated in the generation of phenotypic variability in 22q11.2 deletion syndrome; Snap29 and Scarf2
Expected completion date	Feb 2019
Estimated size (number of pages)	150
Requestor Location	Vafa Keser 1225 SUSSEX#1205  Montreal, QC H3H2A2 Canada Attn: Vafa Keser
Publisher Tax ID	GB 494 6272 12
Total	0.00 CAD

## SPRINGER NATURE LICENSE TERMS AND CONDITIONS

Dec 13, 2018

This Agreement between McGill University -- Vafa Keser ("You") and Springer Nature ("Springer Nature") consists of your license details and the terms and conditions provided by Springer Nature and Copyright Clearance Center.

License Number	4487371450065
License date	Dec 13, 2018
Licensed Content Publisher	Springer Nature
Licensed Content Publication	Nature Reviews Disease Primers
Licensed Content Title	22q11.2 deletion syndrome
Licensed Content Author	Donna M. McDonald-McGinn, Kathleen E. Sullivan, Bruno Marino, Nicole Philip, Ann Swillen et al.
Licensed Content Date	Nov 19, 2015
Licensed Content Volume	1
Type of Use	Thesis/Dissertation
Requestor type	academic/university or research institute
Format	print and electronic
Portion	figures/tables/illustrations
Number of figures/tables/illustrations	1
High-res required	no
Will you be translating?	no
Circulation/distribution	<501
Author of this Springer Nature content	no
Title	Candidate genes implicated in the generation of phenotypic variability in 22q11.2 deletion syndrome; Snap29 and Scarf2
Institution name	n/a
Expected presentation date	Feb 2019
Portions	Figure 2: Low copy repeats and genes within the 22q11.2 deletion.
Requestor Location	McGill University 1225 SUSSEX  Montreal, QC H3H2A2 Canada Attn: McGill University
Billing Type	Invoice
Billing Address	McGill University 1225 SUSSEX



**ELSEVIER LICENSE  
TERMS AND CONDITIONS**

Jul 22, 2018

This Agreement between McGill University -- Vafa Keser ("You") and Elsevier ("Elsevier") consists of your license details and the terms and conditions provided by Elsevier and Copyright Clearance Center.

License Number	4394501509595
License date	Jul 22, 2018
Licensed Content Publisher	Elsevier
Licensed Content Publication	Cell
Licensed Content Title	The Mechanisms of Vesicle Budding and Fusion
Licensed Content Author	Juan S Bonifacino,Benjamin S Glick
Licensed Content Date	Jan 23, 2004
Licensed Content Volume	116
Licensed Content Issue	2
Licensed Content Pages	14
Start Page	153
End Page	166
Type of Use	reuse in a thesis/dissertation
Portion	figures/tables/illustrations
Number of figures/tables/illustrations	1
Format	both print and electronic
Are you the author of this Elsevier article?	No
Will you be translating?	No
Original figure numbers	Figure 1, Figure 2, Figure 3
Title of your thesis/dissertation	Candidate genes implicated in the generation of phenotypic variability in 22q11.2 deletion syndrome; Snap29 and Scarf2
Expected completion date	Feb 2019
Estimated size (number of pages)	150
Requestor Location	McGill University 1225 SUSSEX  Montreal, QC H3H2A2 Canada Attn: McGill University
Publisher Tax ID	GB 494 6272 12
Total	0.00 CAD
Terms and Conditions	